



Universitat Autònoma de Barcelona

**Ruthenium Complexes with N/C-donor Ligands: Redox Catalysts for
Water Oxidation and the Epoxidation of Alkenes**

JOAN AGUILÓ CARRERAS

Tesi doctoral

Programa de doctorat de “Catàlisis Homogènea”

Dr. Lluís Escriche Martínez i Dr. Xavier Sala Román

Departament de Química

Facultat de Ciències

2013

Memòria presentada per aspirar al Grau de Doctor per Joan Aguiló Carreras.

Joan Aguiló Carreras

Vist i plau

Dr. Lluís Escriche Martínez

Departament de Química

Facultat de Ciències

Universitat Autònoma de Barcelona

Dr. Xavier Sala Román

Departament de Química

Facultat de Ciències

Universitat Autònoma de Barcelona

Bellaterra, 22 de gener de 2013

A na Mercè i a ses nines.

Sa llum de sa meva vida

ACKNOWLEDGEMENTS

In this section I express in my tong language my acknowledgement to all people who has walked with me during this long period.

La Traviata (Giuseppe Verdi, cors de l'Scala de Milan). Voldria un gin tonic de Bombay, però és massa d'hora. Tremolen les mans, sa panxa i sobretot el cor. Això no serà fàcil. (Un clinex, per favor!)

En primer lloc he d'agrair als meus directors de tesi que m'hagin fet costat durant 5 anys, 2 mesos i setze dies (fins avui) en aquest camí. Sona com si res, però M'HAN FET COSTAT. Lluís i Xavi gràcies per deixar-me caure i així aprendre i per ajudar-me a aixecar-me quan les forces ja fallaven. Els vostres consells químics, però sobretot vosaltres com a persones, han fet que el camí hagi sigut més bo de dur. Lluís, gràcies per l'oportunitat d'entrar al grup i gràcies per ser com ets, una persona excel·lent, culta, riallera, pessimista i racional a la vegada. Xavi, gràcies per ser-hi SEMPRE, a totes hores, en qualsevol moment, per sms, per whatsapp, per correu o al despatx. Gràcies per fer-me sentir que tenia alguna cosa així com un Big Brother a Barcelona. Aquesta tesi porta el teu nom i no de bades. En el paràgraf dels directors de tesi, sense ser-ho de manera oficial, hi ha en Toni Llobet. Aquell que sense voler molestar, des de el primer dia, com qui és a darrera el teló, va xiulant "Joan, el que necessitis, d'acord?". Això no ho pot explicar tothom, jo SI. Gràcies Toni. Sempre (menys els dimecres) has tengut la porta oberta del despatx i la millor de les predisposicions a discutir qualsevol cosa. En definitiva puc dir que he treballat amb tres genis. Cadascú amb la seva làmpada màgica, però els tres uns autèntics genis. (Segon clinex)

A la reraguarda, el nostre "avi", el Profesor Jaume Casabó. Ai Jaume! m'enduc una quantitat innumerable de moments divertits amb tu on els problemes deixaven de ser-ho. Gràcies per despendre alegria només caminant, mirant o parlant. D'en Jordi García-Antón i d'en Roger Bofill he après, entre moltes altres coses, el que és la lluita constant per fer-se un lloc en el món de la recerca, que no és poc! Gràcies als dos. Gràcies Roger pel teu toc extra-picant extra-repetitiu a les converses, massa die avorrides dels migdies. En aquest apartat també vull recordar a na Montse Rodríguez i a na Isabel Romero per la seva disponibilitat constant. Montse, gràcies per la companyia en el *patiment* de l'EuChem de Granada, però també gràcies pels moments de festa, disbauxa i alegria amb les tapes i els vinets. I would like to remember now Prof. Martin Albrecht. Thank you Martin for all your advices, thank you for having the door open from 06.00 a.m. till 08.00 p.m. and thank you for giving to me the oportunitat of being part of your group for four months. Together with him I would like to thank all the friendliness from Seva, Puia, Vivienne, Sabinne and Anneke. I felt like I was one of you (Pinte, please!) Finalment als meus professors de química (Pilar i Tomeu) i de la UIB, especialment a n'Àngel García Raso i a en Joan Jesús Fiol per ensenyar-me a entrar a un laboratori de recerca (i a tu Kika per ensenyar-me a estar dedins i per ser "*llum i sac d'experiència en tantes coses!*" en els moments de tenebra)

Vull agrair als serveis d'anàlisi química i de RMN de la UAB i al servei de suport a la recerca de l'ICIQ la seva disponibilitat i bon fer durant aquest temps. Vull fer una menció especial per a en Pau Nolis, na María Jesús Ibarz i na Laura i na Maria de GC per tots els moments que m'han aguantat i han fet que les mostres anessin més aviat a canvi d'ensaïmades que mai han arribat. (Sa corrupció és inherent a la sang dels illencs). Així mateix vull enrecordar-me de la paciència de les secretàries: na Dolors (secretària de la Unitat de Q.Inorgànica molts anys), de na Ceci, de na Maria José (ICIQ) i de na Toñi en aquests darrers dies de depòsit. Sense tota aquesta gent les tesis no serien les tesis que son. GRÀCIES!

He tengut una companya de laboratori. Una. Per lo bo i per lo dolent, però només una. És la meva companya de laboratori i mai ningú te podrà substituir. Amb na Laia he après moltes coses, MOLTES. Crec que ella també alguna més que d'altra... Gràcies Laia per fer de germana gran i anar davant, davant; darrera teu les coses han estat molt més senzilles. Gràcies pels moments de riure i pels moments de més enfado. La barreja de tots ells han fet que avui siguem el que som, i això no és poc! El grup ara ha crescut i és ple de *bitxos* que treballen (fins i tot peixos), però sobretot grans al.lots que fan que quan arribis a la UAB et sentis com a casa. Fernando, home introvertit i tímid com una mala cosa, però que fa aquella mitja rialla de la qual entens que li va bé el que li dius. Hai-Jie, un dels meus "fillets" al laboratori, un exemple de paciència i de bona feina. Escolta com ningú, fa el que vol! Jonathan, Selene i Rosa gràcies per ser l'ànima del grup. Sense vosaltres tres el grup Sala-Escriche-Bofill-GarcíaAntón-Casabó no seria res, seria buit, no tendria rialla, no tendria bon humor, no tendria Gaga style, no tendria *xixa*...

Gràcies a tota la gent de la planta de inorgànica (Lecina, Sílvia, Cata, Katia, Spin, Adaris, Leo, Edu, Alba, Miquel, Herrera, Merche, Adu, MaDolores,..) els orgànics, la Susi d'analítica i als teòrics den Sergi, per ser un autèntic refugi en els moments de desesperació al laboratori. Un autèntic electró, Francàs. (tercer)

Aquest darrer any he tengut la sort de fer feina a l'ICIQ i compartir moments amb un grup de gent extremadament heterogeni, però sobretot excepcional. Pau, Carolina, Lorenzo (succa!), Takashi, MarieCurie guy, Rocco, Isidora, Carlo i de rebot Lidia i Arianna, gràcies a tots per la vostra acollida i per l'ajuda. He après moltíssim aquest any i sempre gràcies a que algú de vosaltres m'ha donat una mà. Somnath thank you for being one of the best person I have ever known. (Hauríem d'aprendre més dels indis!). Als del bus, gràcies pel *pressing*, HE ACABAT!

Aquests son els agraïments d'una tesi, però per jo son els agraïments d'alguna cosa més. Són els agraïments d'una part important de la meva vida. Són els agraïments del que ha estat la meva vida a Barcelona. Tenir un peu aquí i un allà té moltes coses bones, però també implica tenir el cor dividit. Mai ets al 100% a cap dels dos llocs. Durant aquests cinc anys he estat lluny de casa, lluny de sa meva família i dels que eren els meus amics de sempre. He vist néixer, gairebé sense adonar-me'n una altra família. La meva família de Barcelona. En aquesta família han entrat i han sortit molts membres, és impossible

que hi càpiguen tots en aquest trosset de paper tant petit; així que anomenaré els imprescindibles, els que fan que cada vegada que anam a Mallorca deixi un trosset de cor a Barcelona i cada vegada que aterri a el Prat pensi, “ai ja hi som una altra vegada, que bé!”

Gràcies Sergi per ser com ets. Amb això n’hi ha prou. Gràcies per no ser el típic barceloní. Gràcies per ser de Gràcia (quart). Gràcies per fer que una conversa amb tu sapiguem on comença i mai on acabarà. Gràcies per ser amic, per jugar a squash dos anys amb jo, per no fer ni una mala cara en cinc anys i per fer que tinguem en Fígols un refugi protector d’aquesta ciutat de vegades massa gran per aquells que venim d’una illeta tant petiteta. Gràcies Dani perquè una birra, unes patates i unes olives i un gin tonic i unes quelys i un poc de formatge a qualsevol hora, qualsevol dia, en qualsevol moment tenen un gust diferent si tu hi ets. Gràcies pels camins a la UAB i pels camins a Barcelona, gràcies per, ser un dels amics més fidels que mai es trobaran! (Fi del primer acte, cinquè). Gràcies Grandaddy, gràcies Luca, per fer que qualsevol sopar es converteixi en un “fiesta loca” com diria na Mercè. Luca ets com un pot de Nutella, sempre en vols més!. Gràcies Laura per ser la més antiga d’aquest grup. Gràcies per ser de les poques que me planten cara i me diuen el que m’han de dir. Gràcies per fer que qualsevol conversa intrascendental se converteixi en un tema de debat acarnissat (genèrics, cremes, ...) Sobretot gràcies per mai voler sortir de marxa, però sempre ser la darrera en tornar (a peu, of course!). Finalment gràcies als membres més recents d’aquesta família: Josep i Càrol, Esther i David i Aloa i Lores. Gràcies per haver-nos acollit com si fóssim uns més de la vostra família. Sobretot gràcies Aloa per ser una lliçó de vida, lluita i esperança. Nins, TOTS, feis que faci tantes ganes que vengui es cap de setmana!

Ara toca el torn de la planta (la planta d’inorgànica, si, dels que ja no hi son). Heu estat els companys de camí durant molt de temps i m’enduc la maleta plena de records de tots vosaltres. Oriol, Sònia i ara Max, sou amics, sou exemple i sou els companys ideals d’aquell dies de primavera i estiu que enyores tant Es Trenc i vosaltres i Mataró se converteixen en el millor remei contra la melancolia. Nacho, Aldonza i ara Sílvia, companeros de viatge, ¡os echamos tanto de menos!. Nuestra pareja favorita. Meri i Albert, dels records més dolços és el vostre. Els vostres nuvis diuen bon dia cada dia i fan esbossar una rialla abans d’anar a fer feina. Gemma, Jordi, Miguel, Mònica i Ruben també formau part de la UAB-family i sou protagonistes d’infinat de moments de diversió, de balls, de videos, de festes,...

I la gent de Mallorca? Aquells que me fan sentir com si mai hagués partit. Aquells que han demostrat ser els vertaders amics, aquells que mai posen traves de dies ni hores per quedar, els que sempre tenen ses portes de casa seva obertes de bat a bat. Gràcies Cata, JC, Pilar i Aurora per tants i tants sopars de bon menjar i millor companyia i comprensió. Un dia tendrem sa nostra caseta a Alaró i els compensarem. Gràcies Maria i Bernat, doncs venir a casa vostra és el nostre petit oasi. Passar el segon aigovés d’aquella casa de sa padrina és deixar ses preocupacions lluny i permetre que els rellotges s’aturin mirant es foc. Sou una fotografia en blanc i negre, un exemple de

senzillesa i humilitat i elegància i amor a la vegada. GRÀCIES Laura, Àlex, Maria i Guillem. Sou amics. Sempre hi sou, a qualsevol hora per fer qualsevol cosa. Mos feis sentir tant especials i valorats. Costa expressar el que se sent un divendres horabaixa quan arribes amb dues hores de retràs a un sopar a les 23.00 i veus que t'esperen amb una rialla i un "no passis pena!" I te faran una aferrada per es coll. I en aquells moments un mes semblarà que sigui un segon. (Sisè i segon disc)

El cercle vital se va tancant i arribam a sa gent important, els que mai fallen. Mon pare i ma mare gràcies per es vostre suport i estima incondicional. Per donar-me valors i fer-me sa persona que som. Sense vosaltres, sa vostra estima i sa vostra educació no seria aquí. M'heu ensenyat que des de la humilitat i la senzillesa amb esforç i seny se pot ser GRAN. Aquesta és sa vostra tesi. Gaspar, gràcies. Ets es millor germà que mai podria tenir, tot un exemple a sa vida, un referent, el que qualsevol voldria ser quan fos gran! Qui té un germà amb una llicenciatura acabada mentre es pare de dues filles? Carmen, ho he fet "me he ido y he hecho algo que no se hacía aquí", què faig ara?, gràcies a tu també per sa s'empenta que vares pegar. Núria i Rita un dia llegireu això. Heu de saber que ses vostres rialles, sa vostra innocència, sa vostra il.lusió i ses vostres aferrades pes coll i besades son un dels motius pels quals jo he acabat el que teniu entre mans. Als Pujol-Nicolau-Pellicer-Ribas gràcies per tot es vostre suport i lliçons de vida que també vosaltres anau donant. Kika i Pepita gràcies per aquells tappers que han salvat tants i tants migdies i sobretot per esser padrines, per ser experiència i amor constant. Carme i Joan, gràcies pel suport incondicional, pel saber anar per la vida i per deixar-me ser part de sa vostra família i especialment per "deixar-me" sa joia més valuosa que qualsevol persona voldria tenir a la seva vida.

Mercè si tu no hi fossis no hi hauria res de res. Gràcies per sa companyia en el dia a dia; sa paciència i els silencis en els moments de nirvis i crits; ses caminades quan feia falta respirar aire pur; ses renyades a es quarto d'escriure; els encoratjaments en els moments mes difícils; les correccions, l'ajudar-me a retorbar-me amb mi mateix quan estava perdut. En definitiva, gràcies per voler compartir sa teva vida amb aquest ogro-mú barbut!

A tots aquells que haurien de ser aquí i que m'he oblidat d'ells. A aquells que varen pronosticar que no hi hauria tesi. A els que ja no hi son i a els que han de venir!

*Me sobren paraules (agulla, fil de cosir, tisoires, estufa),
me sobren paraules (vermut, patates, olives),
paraules molt curtes (pi),
paraules molt llargues (esternoclestmastoideu),
paraules molt fàcils (mamà),
paraules difícils (obliquïtat)... i jo què sé.
Me falten paraules per explicar què significa per jo,
me falten paraules ...
es diccionaris són plens de paraules gratis i certes,
paraules d'amor senzilles i tendres...*

A. Font
(final)

The work performed in the present doctoral thesis has been possible thanks to the funding of:

Institut Català d'Investigació Química (ICIQ).

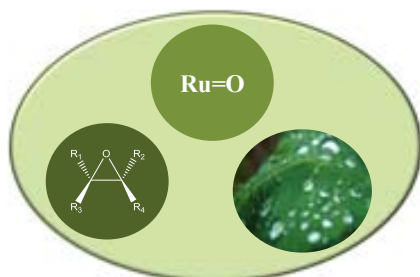
Ministerio de Economía y Competitividad. Secretaría de Estado de Investigación, Desarrollo e Innovación.

Finally I would also like to thank Universitat Autònoma de Barcelona for the pre-doctoral PIF-UAB grant and the ICIQ for a one-year contract.



GRAPHICAL ABSTRACTS

Chapter I. General Introduction

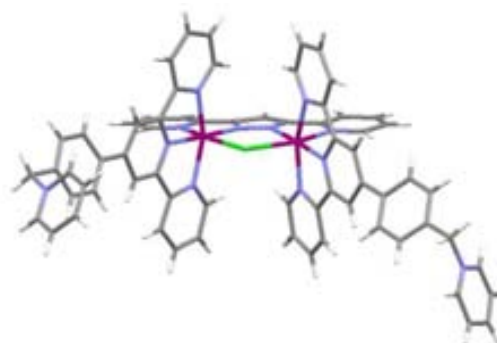


Introduction to the Ruthenium chemistry, especially focused in the Ru-H₂O/Ru=O systems and its properties. Special interest is also paid in the water oxidation catalysis as well as the epoxidation of alkenes.

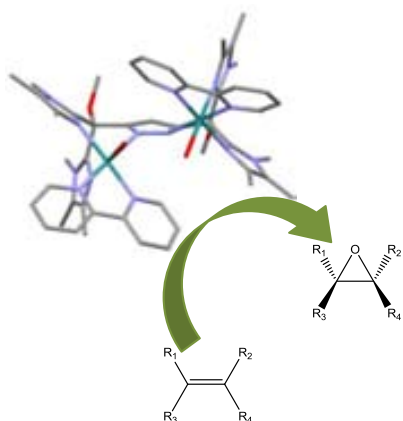
Chapter II. Objectives

Chapter III. "*Ru-Hbpp*" Complexes Containing the *TrpyPyr* Scaffold: Heterogenization and Water Oxidation Catalysis

In this chapter we present the immobilization of two new "*Ru-Hbpp*" complexes on the surface of Silica, FTO-TiO₂ films and Nafion polymer. The catalytic performance of these new hybrid materials towards the oxidation of water will be discussed and compared with their homogeneous counterparts and other related systems previously reported.



Chapter IV. Bis-facially Bridged Ru Dinuclear Complexes: Powerful Catalyst for the Epoxidation of Alkenes



In this chapter we report the synthesis and characterization of a novel diruthenium complex containing the bis-facial hexadentate bridging ligand Hbimp. Its reactivity towards the oxidation of water and olefins and the comparative discussion with the already reported family of related dinuclear complexes is reported herein.

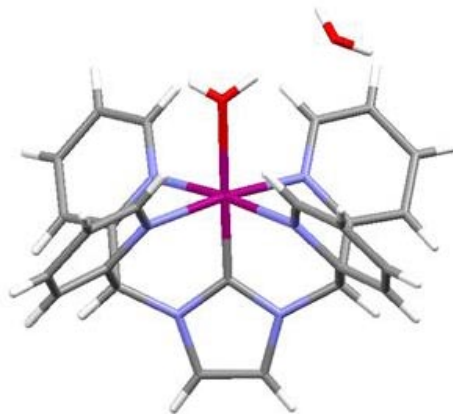
Chapter V. Towards new Phthalazine-Triazole N/C-hybrid Ligands: Synthesis, Coordination Chemistry and Future Prospects



The synthesis of a new family of tetradentate bridging phthalazine-triazole ligands capable to coordinate a metal centre *via* both N and C atoms has been planned and attempted. The synthesis and characterization of a new dinuclear Ru complex containing one of these ligands is here reported and further discussed in this chapter. The work herein described was initially designed and performed in Prof. Martin Albrecht's laboratory at UCD (University College Dublin) during a four months stage of the candidate.

Chapter VI. Mononuclear Ru(II) Complexes Containing the PY4Im Ligand: Synthesis, Characterization and Oxidative Catalysis

In this chapter we present the synthesis and the spectroscopical and electrochemical characterization of a new family of complexes with general formula $[\text{Ru}^{\text{II}}(\text{PY4Im})(\text{X})]^{n+}$ ($\text{X} = \text{Cl}$, $n = 1$ or $\text{X} = \text{H}_2\text{O}$, $n = 2$), where PY4Im is the pentadentate 1,3-bis(bis(2-pyridyl)methyl)imidazol-2-ylidene ligand. These results together with the performance of the new species towards the oxidation of water and alkenes will be thoroughly discussed in the present chapter.



Chapter VII. Conclusions and Future Prospects

TABLE OF CONTENTS

Graphical Abstracts

Table of Contents

Glossary of Terms and Abbreviations

CHAPTER I. General Introduction	1
I.1. Ruthenium Chemistry	5
I.1.1. Ruthenium properties	5
I.1.2. Polypyridyl based Ruthenium aqua complexes	7
I.1.3. RuIV=O a catalytically active group	9
I.2. Water Oxidation Catalysis	13
I.2.1. World Energy Outlook	13
I.2.2. Natural and Artificial Photosynthesis	15
I.2.3. Dinuclear and Polynuclear Ruthenium WOCs	17
I.2.4. Ru-based mononuclear WOCs	19
I.2.5. Mechanistic studies on Ru-based WOCs	21
I.2.6. Other Metals as WOCs	23
I.2.6.1. Iridium	23
I.2.6.2. Cobalt	24
I.2.6.3. Iron	25
I.3. Epoxidation Catalysis	25
I.3.1. Alkenes epoxidation catalyzed by Ru-based complexes	26
I.3.2. Mechanism for the epoxidation of alkenes <i>via</i> Ru(IV)=O	27
I.4. References	31
 CHAPTER II. Objectives	 41
 CHAPTER III. "Ru-Hbpp" Complexes Containing the TrpyPyr Scaffold: Heterogenization and Water Oxidation Catalysis	 47
III.1. Introduction	51

III.2.	Results & Discussion	53
III.2.1.	Ligand synthesis	53
III.2.2.	Synthesis of complexes	53
III.2.3.	Characterization of 4(PF₆) , 5(PF₆)₄ , 7(PF₆)₄ and 8⁵⁺	57
III.2.3.1.	NMR spectroscopy	57
III.2.3.2.	X-ray Crystal Structures	59
III.2.3.3.	Electrochemistry	62
III.2.3.4.	UV-vis	66
III.2.4.	Synthesis and characterization of supported systems	67
III.2.4.1.	Silica- 7⁴⁺	67
III.2.4.2.	FTO-TiO ₂ - 5⁴⁺	68
III.2.4.3.	Nafion®	72
III.2.5.	Water Oxidation Catalysis	78
III.2.5.1.	Chemically triggered materials	79
III.2.5.2.	Electrochemically triggered materials	83
III.3.	Conclusions	86
III.4.	Experimental Section	87
III.5.	References	92
III.6.	Supporting Information	95

CHAPTER IV. Bis-facially Bridged Ru Dinuclear Complexes:

Powerful Catalyst for the Epoxidation of Alkenes	115	
IV.1.	Introduction	119
IV.2.	Results & Discussion	121
IV.2.1.	Synthesis and characterization of 1 , 2(PF₆)₂ and 3³⁺	121
IV.2.1.1.	Electrochemistry	125
IV.2.1.2.	UV-vis	129
IV.2.2.	Water Oxidation Catalysis	130
IV.2.3.	Epoxidation Catalysis	131
IV.3.	Conclusions	137
IV.4.	Experimental Section	138
IV.5.	References	141
IV.6.	Supporting Information	145

CHAPTER V. Towards new Phthalazine-Triazole N/C-hybrid	
Ligands: Synthesis, Coordination Chemistry and Future Prospects	155
V.1. Introduction	159
V.2. Results & Discussion	161
V.2.1. Ligand Synthesis	161
V.2.2. Characterization of 5 , 3a-b , 7⁺ and 8²⁺	166
V.2.2.1. NMR spectroscopy	166
V.2.2.2. X-ray Crystal Structures	169
V.2.3. Synthesis and characterization of 9(PF₆)₃ and 10(PF₆)	171
V.2.3.1. NMR spectroscopy	172
V.2.3.2. X-ray Crystal Structures	174
V.2.3.3. Electrochemistry	177
V.3. Conclusions and Future Prospects	178
V.4. Experimental Section	179
V.5. References	183
V.6. Supporting Information	185
CHAPTER VI. Mononuclear Ru(II) Complexes Containing the	
PY4Im Ligand: Synthesis, Characterization and Oxidative Catalysis	209
VI.1. Introduction	213
VI.2. Results & Discussion	215
VI.2.1. Synthesis of PY4Im ligand	215
VI.2.2. Synthesis and characterization of 3(Cl) and 4(BF₄)₂	215
VI.2.2.1. NMR spectroscopy	216
VI.2.2.2. X-ray Crystal Structures	218
VI.2.2.3. Electrochemistry and UV-vis features	221
VI.2.3. Water Oxidation Catalysis	227
VI.2.4. Epoxidation Catalysis	232
VI.3. Conclusions	234
VI.4. Experimental Section	235
VI.5. References	238
VI.6. Supporting Information	241
CHAPTER VII. Conclusions and Future Work	253

GLOSSARY OF TERMS AND ABBREVIATIONS

1D	Monodimensional
2D	Bidimensional
AcO ⁻	Acetate
ATP	Adenosine Triphosphate
bpea	bis(2-pyridyl)ethylamine
bpy	2,2'-bipyridine
COSY	Correlation Spectroscopy
CPE	Controlled Potential Electrolysis
CV	Cyclic Voltammetry
d	doublet
d	Chemical shift
DCE	1,2-dichloroethane
DCM	Dichloromethane
DFT	Density Functional Theory
dmsO	Dimethyl sulfoxide
DPV	Differential Pulse Voltammetry
E	Potential
ϵ	Extinction Coefficient
E _{1/2}	Half wave potential
ESI-MS	Electrospray Ionization Mass Spectroscopy
ET	Electron transfer
FTO	Fluorinated-doped Tin Oxide
GC	Gas chromatography
hbimp	3,5-bis[bis(1,4,5-trimethylimidazol-2-yl)-methoxymethyl]pyrazole)
hbpp	3,5-bis(2-pyridyl)pyrazole
hpbl	1,1'-(4-methyl-1H-pyrazole-3,5-diyl)bis(1-(pyridin-2-yl)ethanol)
ITO	Indium Tin Oxide
J	Coupling constant
λ	wavelength
M	Molar
μ	ionic force
m/z	Mass-to-Charge ratio
MLCT	Metal to Ligand Charge Transfer
MS	Mass Spectroscopy
NADPH	Nicotinamide Adenine Dinucleotide Phosphate
NHE	Normal Hydrogen Electrode
NMR	Nuclear Magnetic Resonance

NOESY	Nuclear Overhousser Spectroscopy
OEC	Oxygen Evolving Center
PCET	Proton Coupled Electron Transfer
PEM	Proton Exchange Membrane
Ph	Phenyl
POM	Polyoxometalate
ppm	Parts per million
PSI	Photosystem I
PSII	Photosystem II
PT	Proton Transfer
py	Pyridine
PY4Im	1,3-bis(bis(2-pyridyl)methyl)imidazol-2-ylidene
pyr-dc3-	3,5-bis(dicarboxylate)pyrazolate
Pz	Pyrazole
RT	Room Temperature
s	Singlet
SSCE	Sodium Saturated Calomel Electrode
t	Triplet
TBAH	Tetra(N-butyl)ammonium hexafluorophosphate
TOF	Turn Over Frequency
TON	Turn Over Number
tpym	tris-(2-pyridyl)methane
trpy	2,2':6',2''-terpyridine
trpyPyr	4'-(- <i>p</i> -(Pyridin-1-ylmethyl)phenyl)-2,2':6',2''-terpyridine
UV-vis	Ultraviolet-visible spectroscopy
vs.	versus
WOC	Water Oxidation Catalyst

CHAPTER I

General Introduction

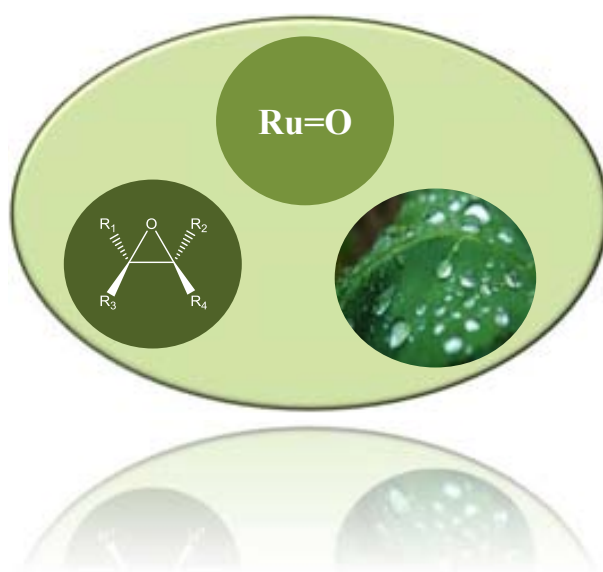


TABLE OF CONTENTS

CHAPTER I. General Introduction

- I.1. Ruthenium Chemistry
 - I.1.1. Ruthenium properties
 - I.1.2. Polypyridyl based Ruthenium aqua complexes
 - I.1.3. RuIV=O a catalytically active group
- I.2. Water Oxidation Catalysis
 - I.2.1. World Energy Outlook
 - I.2.2. Natural and Artificial Photosynthesis
 - I.2.3. Dinuclear and Polynuclear Ruthenium WOCs
 - I.2.4. Ru-based mononuclear WOCs
 - I.2.5. Mechanistic studies on Ru-based WOCs
 - I.2.6. Other Metals as WOCs
 - I.2.6.1. Iridium
 - I.2.6.2. Cobalt
 - I.2.6.3. Iron
- I.3. Epoxidation Catalysis
 - I.3.1. Alkenes epoxidation catalyzed by Ru-based complexes
 - I.3.2. Mechanism for the epoxidation of alkenes *via* Ru(IV)=O
- I.4. References

I.1. Ruthenium Chemistry

I.1.1. Ruthenium properties

Ruthenium, initially called Ruthenia, from the Latin word for Rus' (ancient Russia) was discovered more than 150 years ago in Siberia by Karl Klaus. It is one of the rarest elements on the Earth's crust with an abundance of $10^{-7}\%$. Nevertheless, this element generates high interest in between the scientist thanks to the widest, together with Osmium, range of accessible oxidation states (from -2 in $[\text{Ru}(\text{CO})_2]^{2-}$ to +8 in RuO_4) covering the total of 11 oxidation states theoretically possible for a transition metal, all of them with different coordination geometries.¹ Consequently, Ruthenium complexes are redox-active and their application as redox reagents in many different chemical reactions is a topic of much current interest. The kinetic stability of Ruthenium complexes in those different oxidation states and the often reversible nature of the redox pairs make these complexes particularly interesting for scientist. The application of Ruthenium complexes is outstanding wide, being clearly correlated to the nature of the coordinated ligands.

It is interesting to see how one single metal such as Ruthenium can give a wide variety of products from a single substrate, simply by changing its coordination environment. For instance, styrene yields all the substrates shown in Figure 1 when reacted catalyzed by differently tuned Ruthenium complexes.²

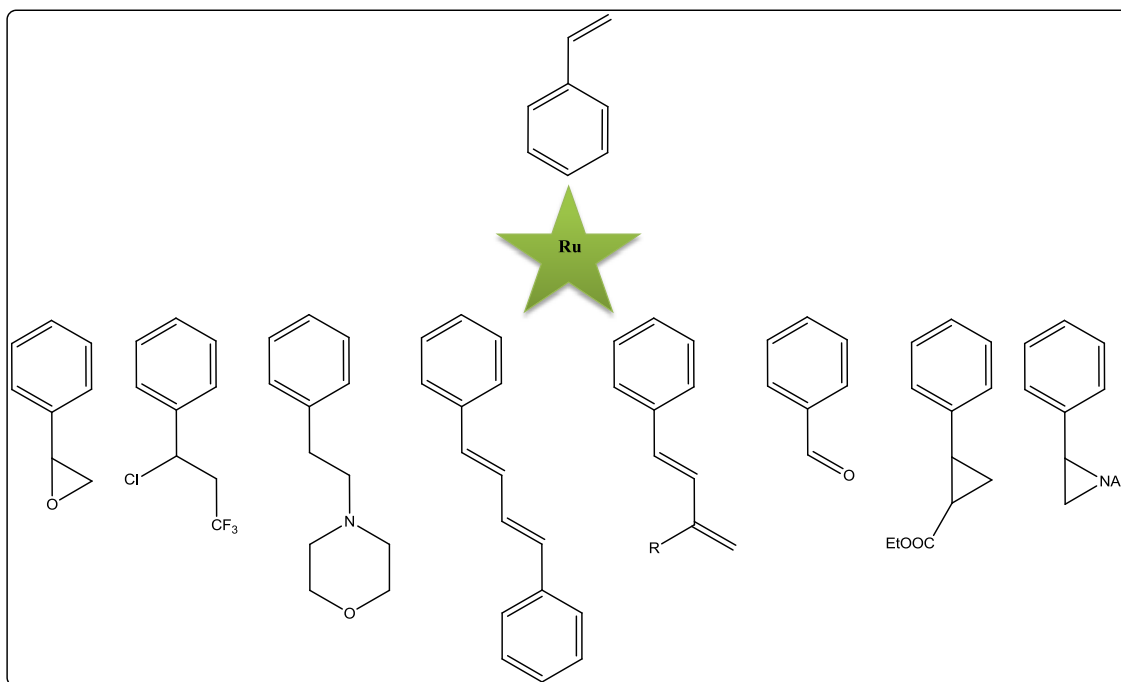


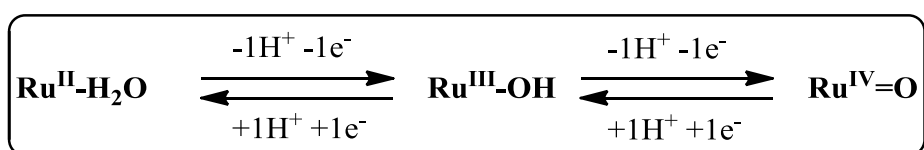
Figure 1 Styrene modification reactions catalyzed by different Ru species.

Ruthenium complexes with π -conjugate ligands or systems that enable electronic delocalization have shown specific properties in nonlinear optics,³ magnetism,⁴ molecular sensors⁵ or liquid crystals.⁶ Ruthenium sulfoxide complexes have been extensively studied due to their relevant usefulness in chemotherapy.⁷ Ruthenium complexes with heterocyclic N-donor ligands have received much attention owing to their interesting spectroscopic, photophysical and electrochemical properties, which lead to potential uses in diverse areas such as photo sensitizers for photochemical conversion of solar energy,⁸ molecular electronic devices⁹ and photoactive DNA cleavage agents for therapeutic purposes.¹⁰ Complexes with phosphine and diphosphine ligands are employed in CO₂ reduction¹¹ and enantioselective hydrogenations,¹² as well as in addition reactions¹³ and metathesis.¹⁴ The incorporation of oxazoline ligands has led to the preparation of several Ruthenium catalysts active for the epoxidation of alkenes.¹⁵ Other ligands like carbonyl, tertiary phosphines, cyclopentadienyl, arenes and dienes have proven to serve effectively as the activating factors such as in hydrogen abstraction¹⁶ or generation.¹⁷ Above all, polypyridyl Ruthenium complexes with aqua ligands have been extensively employed in oxidation reactions of organic¹⁸ and inorganic¹⁹ substrates, C-H insertion²⁰ and proton-coupled electron transfer.²¹

I.1.2. Polypyridyl based Ruthenium aqua complexes

The story of polypyridyl Ruthenium complexes began between 1940 and 1960, when an extraordinary set of scientific papers was published by the Australian coordination chemist Frances P. Dwyer.²² These contributions represented the beginning of the synthetic chemistry of polypyridyl Ruthenium complexes. In the late 1960s, Thomas J. Meyer and collaborators started a systematic study of these complexes and drew attention to their relevant reactive properties based in their accessibility to long-lived excited states and oxidation states varying from Ru(II) to Ru(VI).²³

A particularly interesting situation within the redox chemistry of these complexes emerges when a water molecule is directly bounded to the metal centre, because redox properties of these Ru-aqua complexes are affected by proton exchange. As shown in Scheme 1, the successive oxidations from Ru(II) to Ru(IV) are accompanied by a sequential proton losing favoured by the enhanced acidity of the bonded aqua ligand.



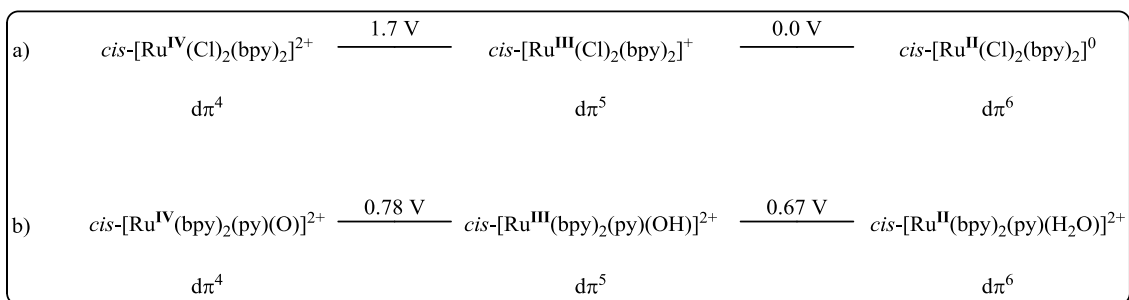
Scheme 1. Proton Coupled Electron Transfer of Ruthenium polypyridyl aqua complexes.

A typical characteristic of these aqua complexes is the pH dependence of its redox potentials. Thus, Ru(III/II) and Ru(IV/III) redox processes are shifted to lower potentials when a drop in the medium acidity takes place, attributable to the fact that higher oxidation states tend to be more acidic. The Nernst equation correlates pH with redox potential in such a way that, for a monoprotic and monoelectronic transfer, the redox coupling diminishes in 59 mV by every pH unit increased, as shown in Scheme 2. The redox equilibria combine with the acid-base equilibria of all species involved and the dependence of the half wave redox potential, $E_{1/2}$, with respect to the complete pH range is represented in the so-called *Pourbaix* diagrams.

$$E_{1/2} = E_{1/2}^0 - 0.059(m/n) \cdot \text{pH}$$

Scheme 2. Nerst Equation where: $E_{1/2}$ = half wave redox potential at a specific pH; $E_{1/2}^0$ = half wave redox potential at standard conditions; m = transferred protons; n = transferred electrons

The most significant trends of these Ruthenium aqua complexes can be observed in Scheme 3, which shows the Latimer diagrams for two different polypyridylic Ruthenium complexes one with two chlorido anions coordinated (a) and the other containing a water molecule (b). In this scheme, the electronic configurations were point out due to their importance in redox processes where electrons are gained and lost from $d\pi$ levels. Changes in the electron content do not occur in the σ -bonding framework, which is the reason for the observed coordinative stability in the three consecutive oxidation states and explains the relevance of these complexes in the study of electron transfer and redox reactions in general. The example shown in eq (a) is typical for Ru polypyridyl couples with oxidation of Ru(II) to Ru(III) occurring at easily accessible potentials. The 1.7 V increase in potential for the Ru(IV/III) couple is due to the increase in charge and oxidation state compared to the Ru(III/II) couple.²⁴ In the couples shown in eq (b), the anionic Cl^- ligands are replaced by the neutral pyridine (py) and H_2O ligands. The increase in charge and changes in bonding increase the potential for oxidation of $\text{cis-}[\text{Ru}^{\text{II}}(\text{bpy})_2(\text{py})(\text{H}_2\text{O})]^{2+}$ ($\text{Ru}^{\text{II}}\text{-OH}_2$) to $\text{cis-}[\text{Ru}^{\text{III}}(\text{bpy})_2(\text{py})(\text{OH})]^{2+}$ ($\text{Ru}^{\text{III}}\text{-OH}$) by over 0.6 V compared to the analogous couple in $\text{cis-}[\text{Ru}^{\text{II}}(\text{Cl})_2(\text{bpy})_2]$.²⁵ The surprising point in eq (b) is the much smaller difference between the Ru(IV/III) and Ru(III/II) couples, 0.11 V compared to 1.7 V in (a). These data point to a dramatic stabilization of Ru(IV) in the aqua-containing coordination environment, causing the near overlap of Ru(IV/III) and Ru(III/II) potentials. There is an important implication for reactivity in this closeness of the redox potentials: thermodynamically, Ru(IV) is nearly as good a two-electron oxidant as a one-electron oxidant at pH 7.



Scheme 3. Latimer diagram of Ruthenium polypyridyl complexes (a) without and (b) with a coordinated water molecule. $E_{1/2}$ measured vs. NHE in aqueous solution (pH = 7). $\mu = 0.1$.

The $d\pi\text{Ru-}2p\pi,\text{O}$ multiple-bond interaction shown in purple in Figure 2 is the key for the Ru(IV) stabilization.²⁶

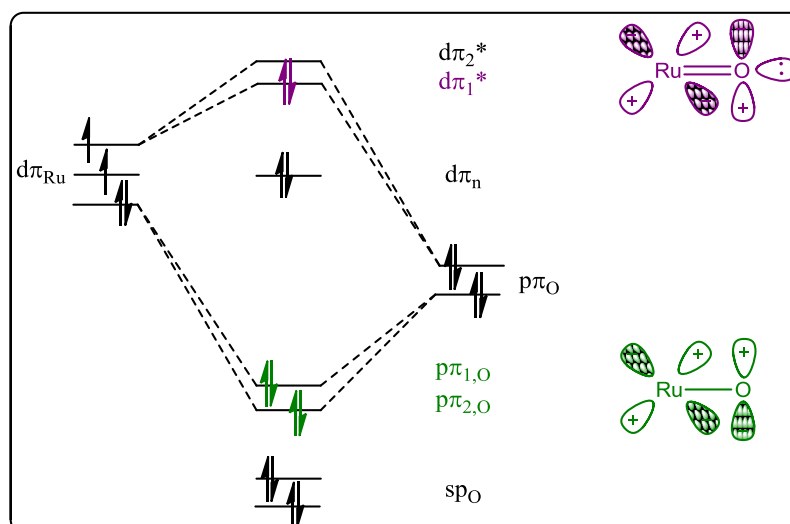


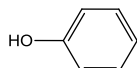
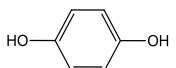
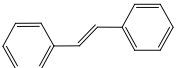
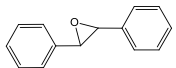
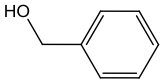
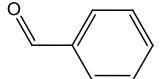
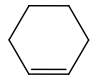
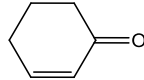
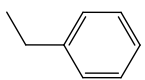
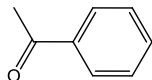


Figure 2. Molecular Orbital energy diagram for a $\text{Ru}^{\text{IV}}=\text{O}$ moiety.

I.1.3. $\text{Ru}^{\text{IV}}=\text{O}$: a catalytically active group

As mentioned above, the oxo groups stabilize high oxidation states and make them accessible at fairly low redox potentials. Furthermore, from a mechanistic point of view, its ability to accept two electrons can avoid radicalary reaction pathways of high energy and reactivity,²⁷ usually generated in monoelectronic transfers. Finally, the robust character of its first coordination sphere makes possible the easy exchange between $\text{Ru}(\text{II})$ and $\text{Ru}(\text{IV})$ without any dramatic change in the catalyst basic structure, being only the oxo group the one that modifies its composition. The chemical versatility of these oxo complexes allows them to act following a wide variety of mechanistic pathways. Thus, Table 1 shows a compilation of oxidative pathways identified for $\text{cis-}[\text{Ru}^{\text{IV}}(\text{bpy})_2(\text{py})(\text{O})]^{2+}$, probably the most paradigmatic and studied complex inside this family.²⁸ The mechanisms cited in this table are the result of a lengthy and exhaustive series of mechanistic studies through UV-visible and Infrared data, isotopic labeling, observation of intermediates, and kinetic isotope effects. The table lists the reductant and oxidized product, the mechanistic pathway, rate constant information, and comments about the mechanism.

Table 1. Mechanistic summary of reactions catalyzed by *cis*-Ru^{IV}(bpy)₂(py)(O)]²⁺

Reduced Form	Oxidized Form	Pathway	k (25°C) ^a M ⁻¹ S ⁻¹	Comment	Ref.
[Os ^{II} (bpy) ₃] ²⁺	[Os ^{III} (bpy) ₃] ³⁺	Outer-sphere e ⁻ transfer	< 1 x 10 ³ ^b	Slowed by initial formation of <i>cis</i> - Ru ^{III} (bpy) ₂ (py)(O) ²⁺	29b
		PCET	9.6 x 10 ⁵ ^b	^k H ₂ O/ ^k D ₂ O = 30	29a
H ₂ O ₂	O ₂	PCET	1.7 ^b	^k H ₂ O/ ^k D ₂ O = 22	29c-d
		Electrophilic ring attack	1.9 x 10 ⁻²	^k H/ ^k D = 5.5 (C ₅ D ₅ OH)	29e
(CH ₃) ₂ SO	(CH ₃) ₂ S ₂ O	O transfer	17	Bound Sulfoxide observed	29f
(CH ₃) ₂ SO	(CH ₃)SO ₂	O transfer	0.14	-	29f
PPh ₃	O=PPh ₃	O transfer	1.8 x 10 ⁵	Bound Ru(II) and O=PPh ₃ observed	29g
		O transfer	0.28 <i>trans</i> 2.5 x 10 ⁻³ , <i>cis</i> .	Bound Ru(II) epoxide observed	29h
		H ⁻ transfer	2.4	^k H/ ^k D = 50	29i
HCO ₂ ⁻	CO ₂	H ⁻ transfer	4.2	^k H/ ^k D = 19	29j
		C-H insertion	0.6	^k H/ ^k D = 18 Bound Ru(II) ketone observed	29k
		C-H insertion	6.6 x 10 ⁻²	Bound Ru(III) ketone observed	29l

^a In CH₃CN except where indicated. ^b H₂O (μ = 0.1). ^c Followed by rapid oxidation to the quinone. ^d Through an intermediate, bound alcohol complex that undergoes further oxidation.

A really interesting point of these high oxidation state oxo complexes is the feasible modulation of its reactivity by tuning the redox potentials, modifying the accompanying ligands. This characteristic, jointly with the growing interest of the fine chemical industry to acquire selective catalysts for oxidation reactions, have promoted a huge number of systematic studies focused on the redox properties of these catalysts

containing ligands of different natures.²⁹ The most relevant electrochemical information extracted from this extensive work is shown in Table 2 where the strong ligand effect over the Ru(IV/III) and Ru(III/II) redox couples can be clearly appreciated.

Table 2. Electrochemical parameters for aqua complexes of Ru^a.

Entry	Complex	E _{1/2} (V) ^b			
		RuIII/II	RuIV/III	RuIV/II	ΔE _{1/2} ^c
1	[Ru(NH ₃)(OH ₂) ²⁺	-0.33	0.35	0.01	0.68
2	[Ru(tpy)(acac)(OH ₂) ⁺	0.19	0.56	0.38	0.37
3	[Ru(tpy)(C ₂ O ₄)(OH ₂) ⁺	0.16	0.45	0.31	0.29
4	[Ru(tpy)(OH ₂) ₃] ²⁺	0.35	0.64	0.50	0.29
5	<i>Trans</i> -[Ru(tpy)(pic)(OH ₂) ⁺	0.21	0.45	0.33	0.24
6	<i>Cis</i> -[Ru(tpy)(pic)(OH ₂) ⁺	0.38	0.56	0.47	0.22
7	<i>Cis</i> -[Ru(6,6'-Me ₂ -bpy) ₂ (OH ₂) ₂] ²⁺ ^d	0.57	0.73	0.65	0.16
8	[Ru(tpy)(tmen)(OH ₂) ²⁺	0.36	0.59	0.48	0.13
9	[Ru(tpy)(phen)(OH ₂) ²⁺	0.50	0.60	0.55	0.10
10	<i>Cis</i> -[Ru(bpy) ₂ (py)(OH ₂) ²⁺	0.43	0.53	0.48	0.11
11	[Ru(tpy)(bpy)(OH ₂) ²⁺	0.49	0.62	0.56	0.13
12	<i>Cis</i> -[Ru(tpy)(4,4'-((CO ₂ Et) ₂ bpy)(OH ₂) ²⁺	0.66	0.80	0.73	0.13
13	<i>Cis</i> -[Ru(tpy)(4,4'-Me ₂ -bpy) ₂ (OH ₂) ²⁺	0.47	0.61	0.54	0.14
14	<i>Cis</i> -[Ru(bpy) ₂ (AsPh ₃)(OH ₂) ²⁺	0.50	0.67	0.59	0.17
15	<i>Cis</i> -[Ru(bpy)(biq)(PEt ₃)(OH ₂) ²⁺	0.45	0.63	0.54	0.18
16	[Ru(tpm)(4,4'-(NO ₂) ₂ -bpy)(OH ₂) ²⁺	0.56	0.75	0.66	0.19
17	<i>Cis</i> -[Ru(bpy) ₂ (PEt ₃)(OH ₂) ²⁺	0.46	0.67	0.57	0.21
18	<i>Cis</i> -[Ru(bpy)(biq)(PPh ₃)(OH ₂) ²⁺	0.48	0.70	0.59	0.22
19	<i>Cis</i> -[Ru(bpy) ₂ (PPh ₃)(OH ₂) ²⁺	0.50	0.76	0.63	0.36
20	<i>Cis</i> -[Ru(bpy) ₂ (P(i-Pr) ₃)(OH ₂) ²⁺	0.45	0.68	0.57	0.23
21	<i>Cis</i> -[Ru(bpy) ₂ (SbPh ₃)(OH ₂) ²⁺	0.52	0.80	0.66	0.28
22	[Ru(tpy)(dppene)(OH ₂) ²⁺ ^e	1.17	1.53	1.35	0.36

^a In H₂O at pH 7.0, T = 22 ± 2 °C, I = 0,1 M vs SSCE. ^b E_{1/2} values for the Ru^{III}-OH/Ru^{II}-OH₂, Ru^{IV}=O/Ru^{III}-OH, and Ru^{IV}=O/Ru^{II}-OH₂ couples. ^c ΔE_{1/2} = E_{1/2}(Ru(IV/III)) - E_{1/2}(Ru(III/II)). ^d pH 4.0. ^e In CH₂Cl₂/H₂O (3:1). Abbreviations: biq = 1,1'-biquinoline; tmen = N,N,N,N-tetramethylethylenediamine; dppene = *cis*-1,2-bis(diphenylphosphino)ethylene; pic: picolinate anion. Acac = acetyl acetonate anion.

The Ru(II) oxidation state is stabilized by dπ-π* back-bonding in the presence of ligands with low-lying acceptor levels, such as PPh₃. On the contrary, Ru(III) oxidation state is stabilized in the presence of electron donating ligands, such as the anionic acac or C₂O₄. In consequence, if we compare the redox potentials of [Ru(tpy)(bpy)(OH₂)²⁺ (entry 11 of Table 2) with [Ru(tpy)(acac)(OH₂)⁺ (entry 2 of Table 2) we observe a decrease in E_{1/2} (III/II); and if we compare the values for *cis*-[Ru(bpy)₂(py)(OH₂)²⁺

(entry 10) with $cis\text{-}[\text{Ru}(\text{bpy})_2(\text{PPh}_3)(\text{OH}_2)]^{2+}$ (entry 19 of Table 2) an increase in $E_{1/2}$ (III/II) is observed.

The Ru(IV/III) couples are in general far less sensitive to ligand variations than are the Ru(III/II) couples. This is illustrated for instance by comparing the complexes in entries 2 and 11 or in entries 3 and 9, where changes in the ligands produce only a slight modification in the potential of the Ru(IV/III) couple whereas the Ru(III/II) couple is strongly influenced. This fact can be understood taking into account the important effect of the oxo group in the $\text{Ru}^{\text{IV}}=\text{O}$ species, where the stabilization promoted by this group is predominant over any other ligand effect. This behaviour is due to the control of the π -bonding exerted by the oxo ligand through a $d\pi_{\text{Ru}}\text{-}p_o$ interaction in the Ru(IV) species (as mentioned above in Figure 2).

Because of the different responses of the Ru(IV/III) and Ru(III/II) couples to ligand variations, the difference between both redox potentials ($\Delta E_{1/2}$) have a significant ligand dependence which mainly follows the ligand dependencies of the Ru(III/II) couple. A number of factors determine the magnitude of $\Delta E_{1/2}$. However, in general, variations in $\Delta E_{1/2}$ can be understood by taking into account that (1) the Ru(III/II) couple is most strongly affected and (2) the net effect represents a balance between stabilization of Ru(II) by back-bonding and of Ru(III) by electron donation.

$\Delta E_{1/2}$ is a quantitative value for the stability of Ru(III) against disproportionation and has an important influence in the reactivity of the corresponding aquo complexes. In general, $\Delta E_{1/2}$ is a positive value; *i.e.* a sequential oxidation of Ru(II) to Ru(III) and from Ru(III) to Ru(IV) takes place. The value of $\Delta E_{1/2}$ can be reduced by modification of the ligands reaching, in special cases, an overlap between $E_{1/2}(\text{III/II})$ and $E_{1/2}(\text{IV/III})$. In this situation the oxidation state III is unstable and a direct 2-electron transfer is favored, avoiding the radicalary reaction pathways of high energy and reactivity usually generated by mono-electronic transfers.³⁰

An example of this kind of Ru complexes is shown in Figure 4, where the Pourbaix diagram of the pyridyl carbenic Ru-OH₂ complex $[\text{Ru}(\text{CNC})(\text{CN})(\text{OH}_2)]^{2+}$ is displayed. The appropriate combination of ligands promotes here the unstability of the Ru(III) species, with direct oxidation/reduction processes between Ru(IV) and Ru(II).^{31a}

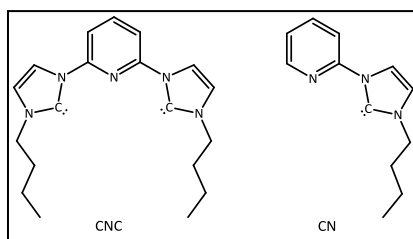


Figure 3 Pyridyl carbenic ligands of $[\text{Ru}(\text{CNC})(\text{CN})(\text{OH}_2)]^{2+}$.

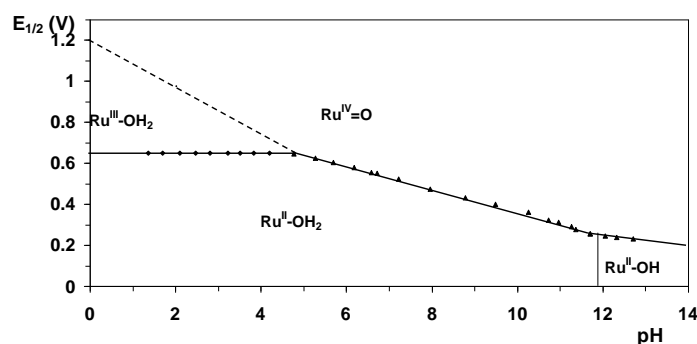


Figure 4. Pourbaix diagram of $[\text{Ru}(\text{CNC})(\text{CN})(\text{OH}_2)]^{2+}$

There are a few more examples of complexes that undergo a direct 2-electron oxidation/reduction. To the best of our knowledge, these complexes are the following ones: $[\text{Ru}(\text{trpy})(\text{azpy})(\text{OH}_2)]^{2+}$,³¹ $[\text{Ru}(\text{trpy})(\text{bpm})(\text{OH}_2)]^{2+}$,³² $[\text{Ru}(\text{trpy})(\text{bpz})(\text{OH}_2)]^{2+}$,³³ $[\text{Ru}(\text{trpy})(\text{Me-CN})(\text{OH}_2)]^{2+}$,³⁴ $[\text{Ru}(\text{S,S-Pr}^i\text{pybox})(\text{py})_2(\text{OH}_2)]^{2+}$ and $[\text{Ru}(\text{S,S-Pr}^i\text{pybox})(\text{bpy})_2(\text{OH}_2)]^{2+}$.³⁵ The two electron nature of these complexes has been established by spectrophotometric redox titration with Ce(IV) or peak current comparisons with $[\text{Fe}(\text{CN})_6]^{4-/3-}$ or $[\text{Ru}(\text{bpy})_3]^{3+/2+}$.

On the whole, the set of properties stated in this section convert the complexes containing the Ru(IV)=O moiety in excellent oxidants, in a catalytic or stoichiometric way, for organic³⁶ and inorganic³⁷ substrates.

I.2. Water Oxidation Catalysis

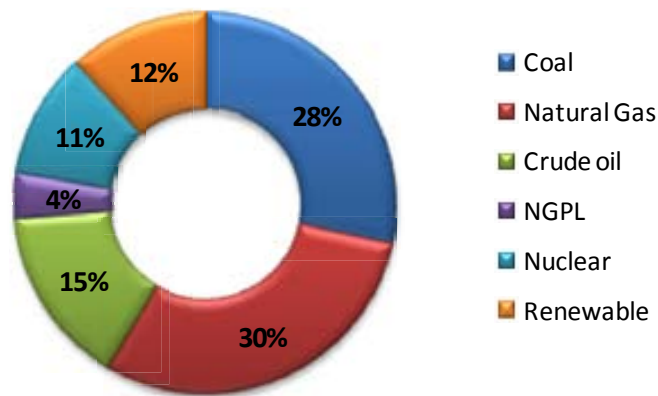
I.2.1. World Energy Outlook

The enormous and day by day increasing consumption of fossil fuels by humanity together with the progressive decrease of their global reserves³⁸ have made clearly patent that a new, cheap and sustainable energy source is urgently needed for the

welfare of our society in the near future. Today *ca.* the 80% of the energy demand is satisfied by fossil based energy (Figure 5a). The employment of fossil fuels produces every year *ca.* 31.6 billion tones of CO₂³⁹, which is clearly related to the global climate change.

Despite the Earth receives a never-failing power flow from the Sun (one hour of sunlight is capable to cover the world energy demand per year), the use of solar energy is only 2 % of all renewable energies used nowadays, as shown in Figure 5b.

a)



b)

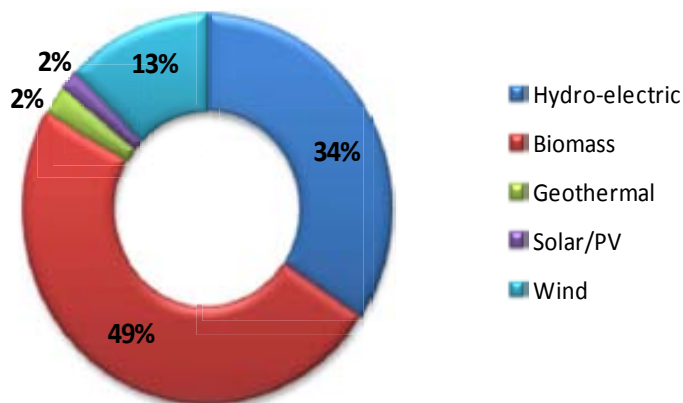
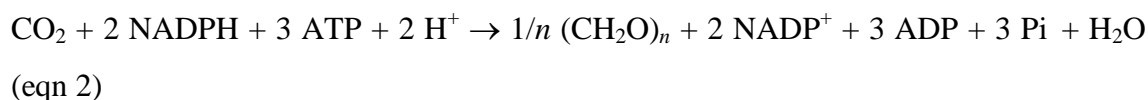
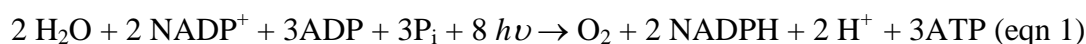


Figure 5 Percentage of (a) energy consumption by fuel source and (b) renewable consumption by type (2011). Source: *Annual Energy Review*, Energy Information Administration. Department of Energy, US. September, **2012**.

I.2.2. Natural and Artificial Photosynthesis

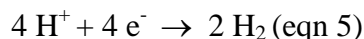
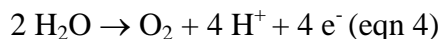
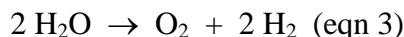
During the last 2400-3000 million years of evolution, Nature has been harvesting sunlight as an energy source through the photosynthetic processes carried out by green plants, algae and cyanobacteria. Throughout the last decade an enormous advance in the knowledge of the molecular machinery involved in photosynthesis has taken place. Two families of electronically coupled protein complexes, named Photosystem I (PSI) and Photosystem II (PSII), are involved in photosynthesis. Basically during this process 4 protons and 4 electrons are removed in PSII from 2 water molecules in a thermodynamically unfavorable reaction ($E^{0'} = 0.82 \text{ V vs. SHE}$ or 0.58 V vs. SSCE at pH 7) thanks to the sunlight energy absorbed by chlorophyll P_{680} (eqn 1). This process generates dioxygen and a gradient of electrons and protons that ends up with 2 equivalents of NADPH and 3 of ATP, which constitute the required reducing equivalents and energy needed for PSI to generate carbohydrates from CO_2 (eqn 2).⁴⁰



The most interesting process occurring during photosynthesis from a chemical viewpoint occurs at the Oxygen Evolving Centre (OEC) of PSII, where the thermodynamically uphill oxidation of water takes place in the dark in a Mn_4CaO_5 cluster.

In order to mimic plants and store solar energy into the bonds of a chemical fuel, the splitting of water into oxygen and hydrogen (eqn 3) is one of the most feasible proposals. However, water does not interact directly with the electromagnetic radiation emitted by the sun. Therefore, a set of redox processes (eqn 4-5) has to be coupled in order to extract protons and electrons from water and end up combining them to form hydrogen. These processes can be assembled, for instance, in a three-component photo-electrochemical cell (PEC) such as the one drawn in Figure 6 that contains: 1) a light harvesting device, 2) a water oxidation catalyst (WOC) and 3) a proton reduction catalyst.^[41] These three components should be assembled into a robust single cell containing a proton-exchange membrane (PEM) that allows diffusion of protons to the cathode and, at the same time, physically separates the anodic and the cathodic

compartments. Moreover, the complete cell should work harmonically, which has been proven to be extremely difficult, and should also be economically viable.



Excellent works have shown the feasibility of hydrogen production *via* proton reduction (eqn 5) using well defined molecular catalysts, particularly those employing first row transition metals.⁴² However, the development of efficient WOCs has been, up till the last six to seven years, continuously hampered by the complex mechanistic and thermodynamic uphill nature of this half-reaction (eqn 4) that involves the removal of 4 H^+ and 4 e^- from two water molecules together with the formation of an $\text{O}=\text{O}$ bond. Despite these inherent difficulties, the field is nowadays effervescent, with numerous research groups involved and an overwhelming number of papers reporting new and improved WOCs appearing every year.

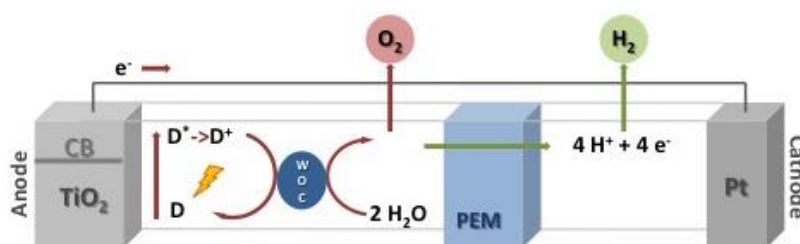


Figure 6 Schematic representation of a light-driven water splitting cell. D: light-harvesting device formed by a dye molecule attached to a semiconductor photoanode, CB: conduction band, WOC: water oxidation catalyst that is oxidized to its active oxidation state by D^+ and from which O_2 is evolved, PEM: proton-exchange membrane, Pt: cathode where H_2 is formed.

Among the different oxidizing equivalents potentially useful to activate a transition-metal catalyst, sacrificial oxidants such as Ce(IV) have been by far the most employed in WO. Despite light-driven systems are the final goal of this research, the use of these chemical oxidants allows a simple and fast way of assessing the catalyst performance. However, their application for constructing real and sustainable cells for the photoproduction of H_2 (PEC, Figure 6) is impractical. Their sacrificial nature (they are irreversibly consumed), non-innocent character (being indiscriminate oxidants) and

energetic inefficiency (usually having huge overpotentials) are main drawbacks that must be considered. The following subsections will point out the most relevant examples reported employing Ru, Ir, Mn, Fe and Co systems, which have been triggered either chemically or electrochemically.

I.2.3. Dinuclear and Polynuclear Ruthenium WOCs

As mentioned in previous sections the Ru-OH₂/Ru=O system is an excellent candidate for playing a prominent role in redox catalysis. Accordingly, Meyer reported in 1982 the first molecular dinuclear Ru complex *cis,cis*-[(bpy)₂(H₂O)Ru(μ-O)Ru(H₂O)(bpy)₂]⁴⁺ (**1**, Figure 7) able to oxidize water to dioxygen.⁴³ The so called “blue dimer” showed low TOF (0.24 min⁻¹) and TON (13.2) when using Ce(IV) as a sacrificial oxidizing equivalent at pH 1.0.^[44] Among the different deactivation pathways proposed for this catalyst, the reductive cleavage of its flexible oxo bridge is one of the most accepted and experimentally proved.⁴⁵ In 2004 Llobet and co-workers reported the *in,in*-{[Ru^{II}(trpy)(H₂O)]₂(μ-bpp)}³⁺ (*in,in*-Ru-bpp) complex **2** (Figure 7).⁴⁶ The flexible μ-oxo bridge of the “blue dimer” was replaced by the anionic and more rigid 3,5-bis-(2-pyridyl)pyrazolate (bpp⁻) bridge, which enhanced the stability of the system. Moreover, two 2,2':6',2''-terpyridine (trpy) ligands were placed occupying each one three meridional positions, thus forcing a close disposition of the O atoms of the two aqua groups occupying the sixth coordination position, and subsequently producing a through space supramolecular interaction.⁴⁷ Addition of excess of Ce(IV) to this complex generates dioxygen efficiently, showing TON and TOF values of 512 and 0.78 min⁻¹, respectively, under optimized conditions.⁴⁸ Our research group undertook a project to anchor catalyst **2** onto solid supports in order to get a deeper insight into the potential deactivation pathways that lead to its decomposition and also to demonstrate the viability of the reaction in the solid state. From an engineering point of view, this could also facilitate the introduction of the catalyst into more complex devices for solar energy harvesting based on the splitting of water. Further information about this section will be found in Chapter III.

Other dinuclear Ru complexes bridged by a rigid ligand and capable to catalize WO have been reported by other groups. A series of 12 different symmetrical complexes were reported by Thummel and co-workers, with those possessing the -OCH₃ pyridine substituent exhibiting the best catalytic performance with TON values above 600 (*e.g.*

catalyst **3**, Figure 7, showed a TON of 689).⁴⁹ Higher TON values, up to 1690, were later on obtained by Sun and co-workers by replacing the terminal pyridylic moieties by negatively charged carboxylate groups at position 6 of the pyridyl scaffold (*trans*-catalyst **4**, Figure 7).⁵⁰ Further modification of the system by forcing a *cis* configuration through replacing the central pyridazine by a phthalazine moiety (catalyst **5**, Figure 7), allowed obtaining one of the best WOCs working under chemically-driven conditions (TON and TOF values of 10400 and 72 min⁻¹ under optimized conditions, respectively).⁵¹

Finally all-inorganic POMs (polyoxometalates) were developed in order to avoid degradation pathways caused by the combination of the surrounding organic ligands and the highly oxidizing reaction conditions used. Catalyst **6** (Figure 7), independently reported by Bonchio and Hill in 2008, is so stable against degradation when chemically triggered with Ce(IV) that its TON is limited by the amount of oxidant employed. It also shows an acceptable TOF value of 7.5 min⁻¹.⁵²

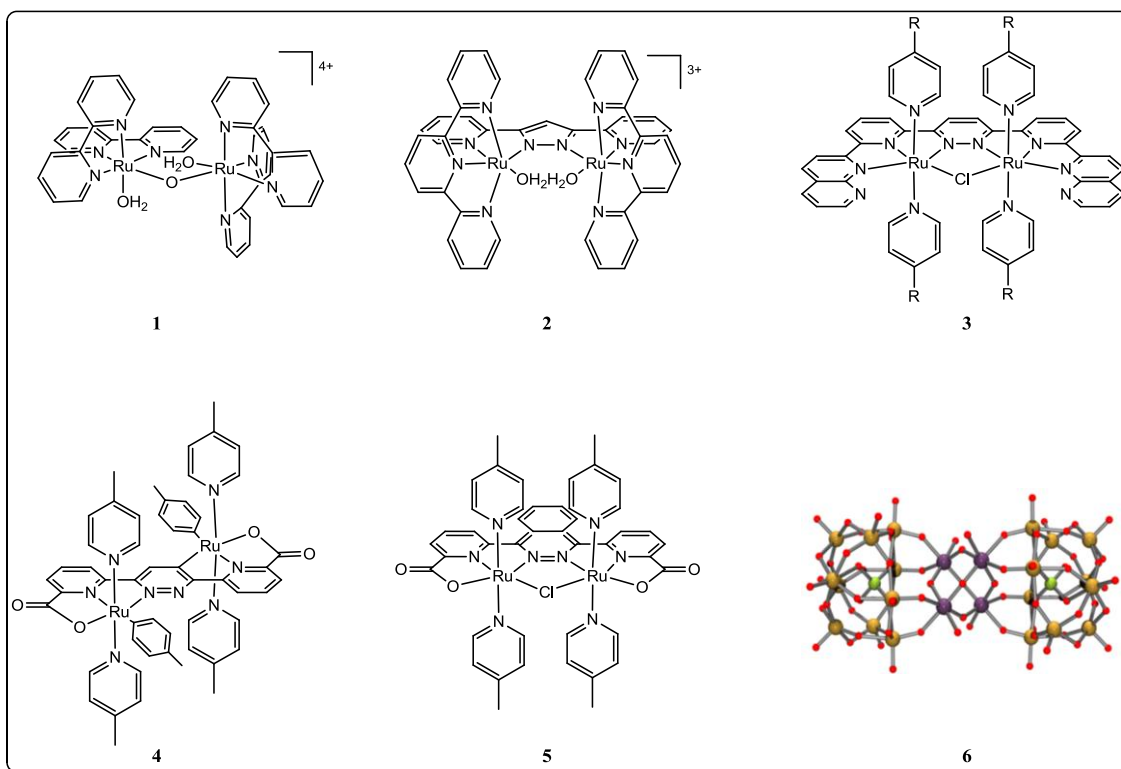


Figure 7 Structures of *cis,cis*-[(bpy)₂(H₂O)Ru(μ-O)Ru(H₂O)(bpy)₂]⁴⁺ (**1**), *in,in*-[[Ru^{II}(trpy)(H₂O)]₂(μ-bpp)]³⁺ (**2**), *trans,trans*-[Ru₂(μ-Cl)(μ-binapypyr)(4-R-py)₄]³⁺ (complex **3** when R = OCH₃, binapypyr = bispyridylpyridazine), *trans,trans*-[Ru₂(μ-1,4-bis(6'-COOH-pyrid-2'-yl)pyridazine)(4-Me-py)₆]²⁺ (**4**) and *cis,cis*-[Ru₂(μ-Cl)(μ-1,4-bis(6'-COOH-pyrid-2'-yl)phthalazine)(4-Me-py)₄]⁺ (**5**) and POV-Ray drawing of the X-Ray structure of catalyst

$[\text{Ru}_4\text{O}_4(\text{OH})_2(\text{H}_2\text{O})_4(\gamma\text{-SiW}_{10}\text{O}_{36})_2]^{10-}$ (**6**). Color code: Ru, violet; O, red; Si, green; W, yellow. All H atoms have been removed for clarity.

I.2.4. Ru-based mononuclear WOCs

Due to the straightforward and versatile synthesis of mononuclear species, which contrasts with the much more demanding preparation of their dinuclear counterparts, dozens of these complexes have been recently tested in WO. Since 2005 Thummel and co-workers have reported several examples of active Ru-N₆ complexes (TON ranging from 20 to 1170) such as $[\text{Ru}(\text{dpp})(4\text{-Me-py})_2]^{2+}$ (**10**) and $[\text{Ru}(\text{trpy})(4\text{-Me-py})_3]^{2+}$ (**11**).⁵³ Meyer and collaborators have conclusively proved the capacity of mononuclear RuN₅-OH₂ species, such as $[\text{Ru}(\text{trpy})(\text{bpm})(\text{OH}_2)]^{2+}$ (**7**) and $[\text{Ru}(\text{trpy})(\text{bpz})(\text{OH}_2)]^{2+}$ (**8**), to oxidize water (Figure 8).^{54a} Especially interesting are complexes $[\text{Ru}(\text{bda})(4\text{-Me-py})_2]$ (**12**) and $[\text{Ru}(\text{pdc})(4\text{-Me-py})_3]$ (**13**) reported by Sun and co-workers as dicarboxylate derivatives of Thummel's **10** and **11** (Figure 8).⁵⁵ These Ru(II)N₄O₂ WOCs achieve spectacular TON and TOF values (2000 and above 2500 min⁻¹ for **13**, and 550 and 13.8 min⁻¹ in the case of **12**, respectively). The stabilization of high oxidation states achieved due to the negatively charged ligands is believed to be responsible of this impressive performance.⁵⁶ Interestingly, mechanistic, structural and theoretical studies of complex **12** have demonstrated the feasibility of expansion to CN 7 of a coordinatively saturated Ru complex by the binding of an extra water molecule and the subsequent O-O bond formation through a WNA (Water Nucleophilic Attack) pathway.⁵⁷ Other active mononuclear Ru-based WOCs have been recently reported by Sakai and Berlinguette (based on the $[\text{Ru}(\text{trpy})(\text{bpy})(\text{OH}_2)]^{2+}$ (**9**) scaffold)⁵⁸ and also by our group, combining the Hbpp or H3p ligands with trpy (*in-14* and *out-15*, Figure 8).⁵⁹

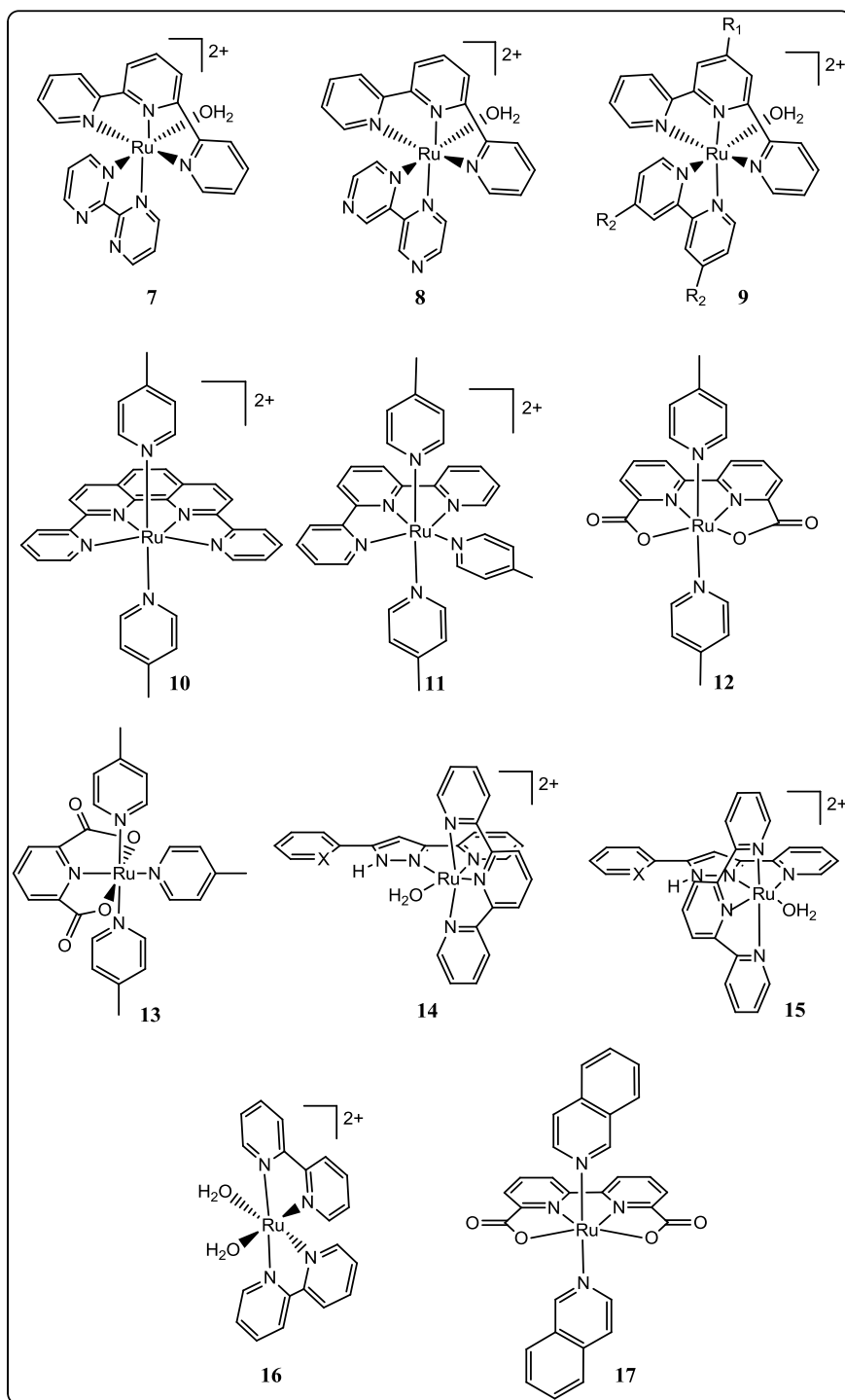


Figure 8 Structure of catalysts $[\text{Ru}(\text{trpy})(\text{bpm})(\text{OH}_2)]^{2+}$ (**7**), $[\text{Ru}(\text{trpy})(\text{bpz})(\text{OH}_2)]^{2+}$ (**8**), $[\text{Ru}(\text{trpy})(\text{bpy})(\text{OH}_2)]^{2+}$ (**9**), $[\text{Ru}(\text{dpp})(4\text{-Me-py})_2]^{2+}$ (**10**), $[\text{Ru}(\text{trpy})(4\text{-Me-py})_3]^{2+}$ (**11**), $[\text{Ru}(\text{bda})(4\text{-Me-py})_2]$ (**12**), $[\text{Ru}(\text{pdc})(4\text{-Me-py})_3]$ (**13**), *in*- $[\text{Ru}(\text{trpy})\text{L}]^{2+}$ (**14**) and *out*- $[\text{Ru}(\text{trpy})\text{L}]^{2+}$ (**15**) (X = N, L = Hbpp; X = CH, L = H3p), *cis*- $[\text{Ru}(\text{bpy})_2(\text{OH}_2)_2]^{2+}$ (**16**) and $[\text{Ru}(\text{bda})(\text{isoq})_2]$ (**17**).

Last but not least, Sun and Llobet described the catalytic activity of the Ru mononuclear complex $[\text{Ru}(\text{bda})(\text{isoq})_2]$ ($\text{H}_2\text{bda} = 2,2'$ -bipyridine-6,6'-dicarboxylic acid; $\text{isoq} =$

isoquinoline; **17**, Figure 8) toward water oxidation in presence of an excess of Ce(IV).⁶⁰ High catalytic activity (TON = 8360) in a very short reaction time (TOF = 303 s⁻¹) was achieved for **17**. Therefore, this represents the best results ever achieved by a chemically triggered molecular catalyst, with a reaction rate close to the Mn₄CaO₅ cluster of photosystem II (TOF 100-400 s⁻¹).

I.2.5. Mechanistic studies on Ru-based WOCs

In order to better understand the mechanistic pathways of either the mononuclear and polynuclear systems shown above, several works have been reported. Herein, only the more relevant results reported for the paradigmatic dinuclear *in, in*-{[Ru^{II}(trpy)(H₂O)]₂(μ-bpp)}³⁺ complex (**2**) and the mononuclear [Ru(bda)(isoq)₂] (**17**), as said the best reported molecular catalyst for WO till now, will be commented.

Kinetic analysis and ¹⁸O labelling studies were employed in order to study the water oxidation mechanism taking place for the complex (**2**).^{49c,61} The {II,II} species is sequentially oxidized by a 1e⁻ process with Ce(IV) up to the {IV,IV} oxidation state (**a** in Figure 9). At this stage, the complex advances to an intermediate that later on progress through an intramolecular (I2M) pathway. The formation of a μ-1,2-peroxo intermediate (**d** in Figure 9) is followed by the formation of a hydroperoxidic intermediate (**f** in Figure 9) that finally evolves oxygen.⁶² This intramolecular mechanistic proposal is further supported by a thorough theoretical analysis of intermediates and transition states based on Density Functional Theory (DFT) and CASPT2 calculations.^{49c} Moreover, ¹⁸O labeling data together with the first order kinetics observed for the formation of the intermediate discards the bimolecular nature of the process.

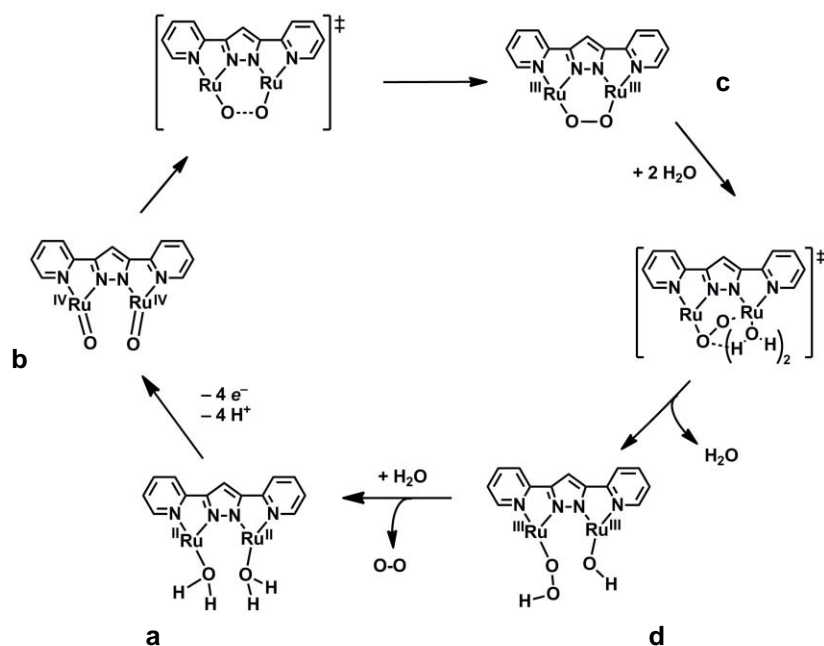


Figure 9 Reaction pathways for the generation of O_2 from $\text{O}=\text{Ru}^{\text{IV}}-\text{Ru}^{\text{IV}}=\text{O}$ in **2**. Trpy ligands omitted for the sake of clarity.

The study of the WO reaction mechanism for the mononuclear and highly efficient **17** has been developed. The catalytic cycle displayed on Figure 10 resulted from several experimental techniques and theoretical calculations.

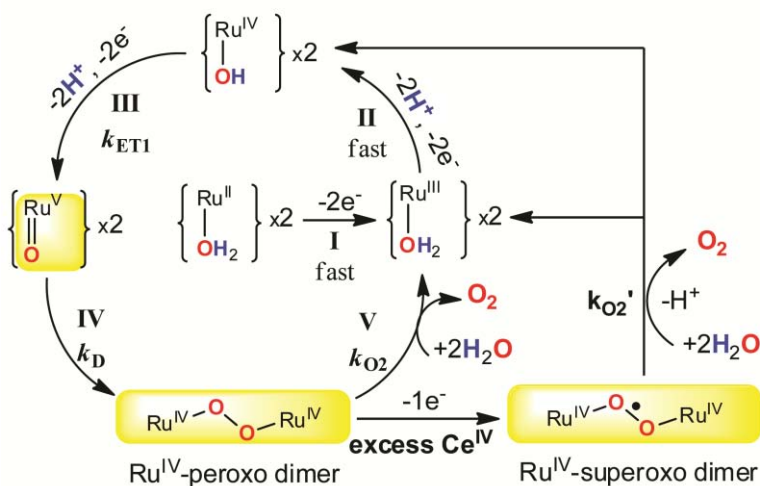


Figure 10 Catalytic reaction mechanism for the WO activity of **17** under stoichiometric and excess amounts of $\text{Ce}(\text{IV})$.

It is believed that are: 1) the stacking of the isoquinolines, that facilitate the formation of the O-O bonds in the radical dimerization of $\text{RuV}=\text{O}$ active species, and 2) the generation of a superoxo species $[\text{Ru}(\text{IV})-\text{O}-\text{O}-\text{Ru}(\text{IV})]^{3+}$ via dimerization, that easily

liberates oxygen *via* a reduction-coupled process, the most remarkable features that converts **17** in a extremely fast and efficient catalyst for water oxidation.

I.2.6. Other Metals as WOCs

Despite Ru WOCs have been largely the most studied up till now, other WOCs based on Iridium, Cobalt and Iron are also extremely interesting. The most relevant examples will be discussed in the present section.

I.2.6.1. Iridium

Water oxidation catalyzed by Iridium complexes can be summarized in three important examples reported by Bernhard, Crabtree-Brudvig and Albrecht. Bernhard and co-workers described in 2008 a family of cyclometalated Ir(III) complexes (**18a-e**, Figure 11) that were capable to catalytically oxidize water to O₂ in presence of Ce(IV) at pH 0.7.⁶² TON up to 2760 and high robustness was achieved for this catalysts. However, traces of CO₂ were also observed, suggesting possible oxidation of the surrounding organic ligands. Crabtree, Brudvig and co-workers reported a wide range of active Ir(III) pentamethylcyclopentadienyl (Cp*) WOCs containing diverse cyclometalated or N,N-bidentate ligands.⁶³ Using Ce(IV) at pH 0.87 the best results were obtained with complex [IrCl(Cp*)(bipy)]Cl (**19**, Figure 11), which showed a high initial TOF (14.4 min⁻¹) and continued activity for several hours (after 8 hours, TON was 320 and TOF 0.7 min⁻¹). In the same work, complexes [Ir(Cp*)(H₂O)₃]SO₄ (**20**) and [(Ir(Cp*))₂(μ-OH)₃]OH (**21**) were also tested, showing the highest TOF (20 min⁻¹ for **19** and 25 min⁻¹ for **20**) among all Ir catalysts tested. The stability and final active nature of **20** and **22** have been also investigated when these species were electrochemically triggered. These studies establish that, upon electrochemical activation of **20**, anodic deposition and amorphous iridium oxide formation takes place. These new material is remarkably active for water oxidation at low overpotentials (*ca.* 200 mV at 0.5 mA cm⁻²) and shows continuous operation for periods of days without loss of activity. The case of **22** is radically different and, upon electrochemical activation, no sign of deposition is found either by CV or EQCN (electrochemical quartz crystal nanobalance). Therefore, despite the data provided does not exclude the potential formation of soluble or suspended products such as iridium oxide nanoparticles, all indications point to the homogeneous nature of this species. Finally in 2010 Albrecht and co workers reported the Ir

complexes containing abnormally bounded N-heterocyclic carbenes **23** and **24** with the best performance in WOC (TON *ca* 10000) of all reported Ir systems.^[64] The use of molecular catalysts based on Iridium is still a hot topic due to the recent publications which indicate the fast formation of iridium oxide nanoparticles (IrOx) upon the dissolution of the molecular systems in CeIV solutions⁶⁵ and those which demonstrate decomposition pathways involving the C-H activation of the Me bonded to the Cp* ligand.⁶⁶

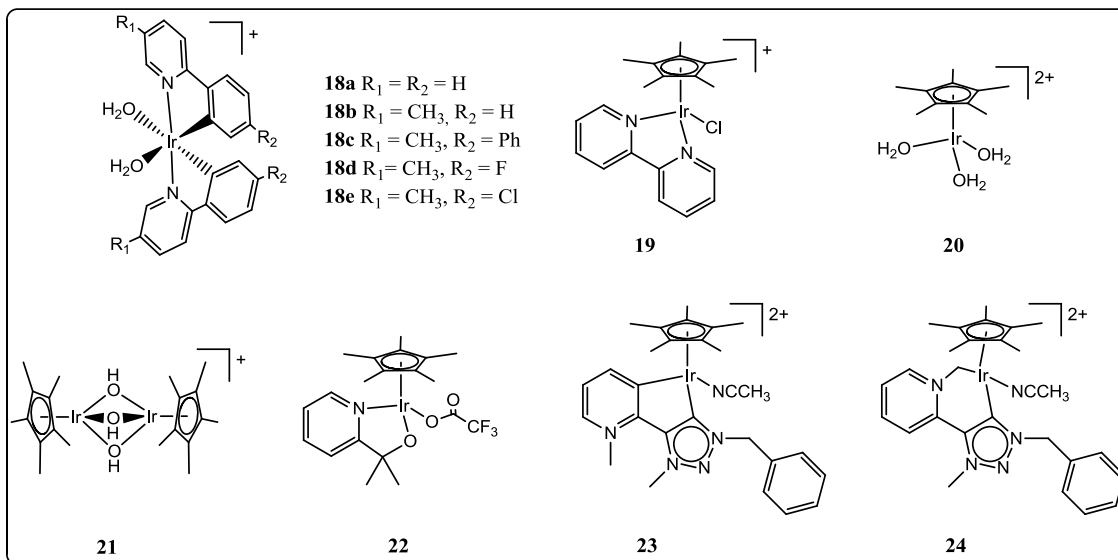


Figure 11 Structure of the most relevant Ir systems reported as WOCs: [Ir(5-R₁,4'-R₂,2-phenylpyridine)₂(OH)₂]⁺ (**18a-e**), [IrCl(Cp*)(bpy)]⁺ (**19**), [Ir(Cp*)(H₂O)₃]²⁺ (**20**), [(Ir(Cp*))₂(μ-OH)₃]⁺ (**21**), [Ir(Cp*)(pyr-CMe₂O)OH₂] (**22**), [Ir(Cp*)(AC_{CN})(MeCN)]²⁺ (**23**) and [Ir(Cp*)(AC_{CC})(MeCN)]²⁺ (**24**).

1.2.6.2. Cobalt

The “all-inorganic” [Co₄(H₂O)₂(PW₉O₃₄)₂]¹⁰⁻ polyoxometalate anion **25** (Figure 12) reported by Hill and co-workers^[67] was the first Co molecular WOC reported. A TON of 1000 in less than 3 minutes (TOF of 333 min⁻¹) could be achieved by employing large excess of [Ru(bpy)₃]³⁺ (sacrificial oxidant). However, Finke and Stracke gave evidence that, at least when electrochemically triggered at pH 8, the real active species in this case is actually CoOx.^[68] Later, Berlinguette and co workers reported the WO activity of **26** (Figure 12) when electrochemically triggered at a pH range of 7.6-10.3. The initial Co^{II}-OH₂ specie undergoes through PCET to Co^{III} and subsequently to Co^{IV}-OH³⁺.⁶⁹

I.2.6.3. Iron

Bernhard and co-workers reported in 2010 a set of Fe(III) complexes containing a family of oxidatively rugged tetraamido macrocyclic ligands. The best results were obtained with complex **27** (Figure 12) chemically oxidized with Ce(IV), which produces fast release of O₂ for 20 seconds (TOF above 78 min⁻¹) and then continues evolving at a much slower rate, with overall TON values above 16.⁷⁰ More recently, Costas, Lloret and co-workers widened the number of octahedral Fe(II) complexes containing easily oxidizable tetradentate ligands. Best results are reported with complex **28** (Figure 12), both employing Ce(IV) (TON of 360 and TOF of 14 min⁻¹) or NaIO₄ (TON > 1050 and TOF 3.7 min⁻¹) as sacrificial oxidants.^[71]

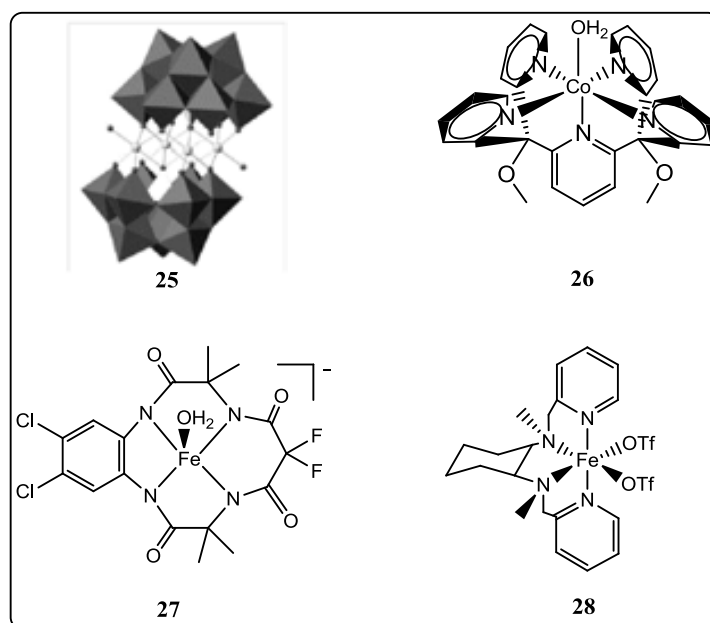


Figure 12 Structures of the most relevant Cobalt and Iron WOCs: [Co₄(H₂O)₂(PW₉O₃₄)₂]¹⁰⁻ anion (**25**), [Co^{II}(Py₅)(OH₂)](ClO₄)₂ (**26**), [Fe(tam)OH₂] (**27**) and [Fe(mcp)(OTf)₂] (**28**).

I.3. Epoxidation Catalysis

The epoxidation of olefins is a reaction of high relevance in both industry and academia. Epoxides are very important intermediates in the chemical industry, particularly for the synthesis of various polymers (polyglycols, polyamides, polyurethanes, etc.),⁷² but they are also being used in the synthesis of fine chemicals, such as pharmaceuticals, food additives, or flavor and fragrance compounds.⁷³ The biggest market is for propylene

oxide, which is currently produced on a scale of 8 million tons per year with an expected annual increase of 5%.⁷⁴ The development of catalytic systems based on transition metals catalysts has been for long time a topic of investigation. One important factor in the transition metal-catalyzed epoxidation of alkenes is the terminal oxidant to generate the metal active specie. Most used oxidants are alkyl hydroperoxides, hypochlorite, iodosylbenzene, peracetic acid, hydrogen peroxide and molecular oxygen. The compatibility with the metal, the total active oxygen content and the waste product generated after oxidize the metal are the important aspects to be considered when electing a potential oxidant for the catalytic system. A wide range of transition metals have been used as potential epoxidation catalysts. Examples of Rhenium,⁷⁵ Vanadium,⁷⁶ Tungsten,⁷⁷ Molybdenum,⁷⁸ Iron,⁷⁹ Manganese⁸⁰ and Titanium⁸¹ can be easily found in the literature. Furthermore, Ru^{IV}=O complexes have also proven to act as efficient catalysts for this organic transformation.

I.3.1. Alkenes epoxidation catalyzed by Ru-based complexes

The epoxidation of alkenes catalyzed by Ruthenium complexes have been reported by means of different ligands and sacrificial oxidants. One of the main challenges of these catalytic systems is to avoid the undesired and competing cleavage of the alkene double bond.⁸² Therefore, for instance, the epoxidation of 1,2-octene (96% yield) and styrene (100% yield) by two Ruthenium porphyrin complexes (Figure 13, **29** and **30**), employing 2,6-dichloropyridine N-oxide as oxidant has been reported.⁸³ The oxidation of trans-stilbene has also been attempted with promising results by Nishiyama and coworkers⁸⁴ and also tested by using H₂O₂ as terminal oxidant⁸⁵ instead of the initially reported [bis(acetoxy)iodo]benzene by using **31**, **32** and **33** (Figure 13). In addition, during the past 30 years asymmetric catalysis has become a powerful tool in order to synthesize enantiomerically pure epoxides from olefines. Ru complexes such as Ru-porphyrin,⁸⁶ Ru-bisamide,⁸⁷ Ru/Schiff base,⁸⁸ [Ru(salen)],⁸⁹ Ru-sulfoxide⁹⁰ and Ru-bis(oxazoline)^{88a-91} have been employed for asymmetric epoxidation catalysis.

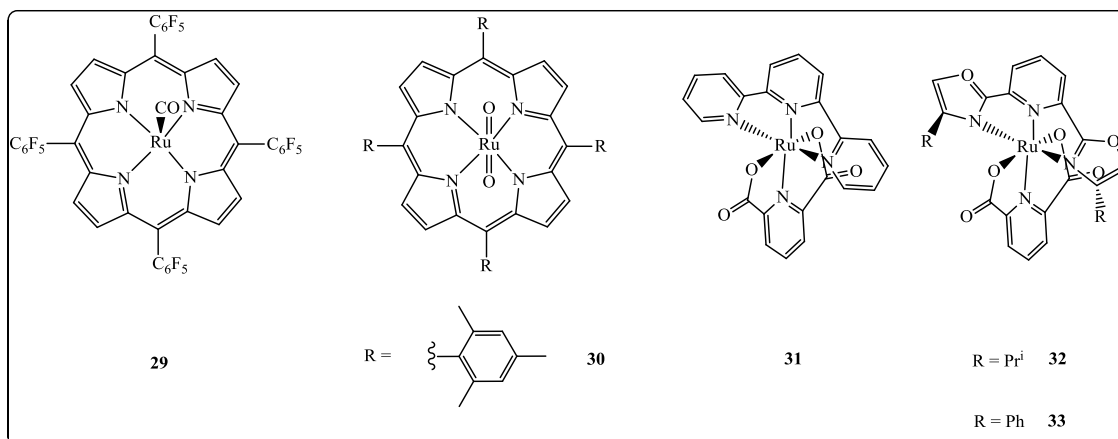
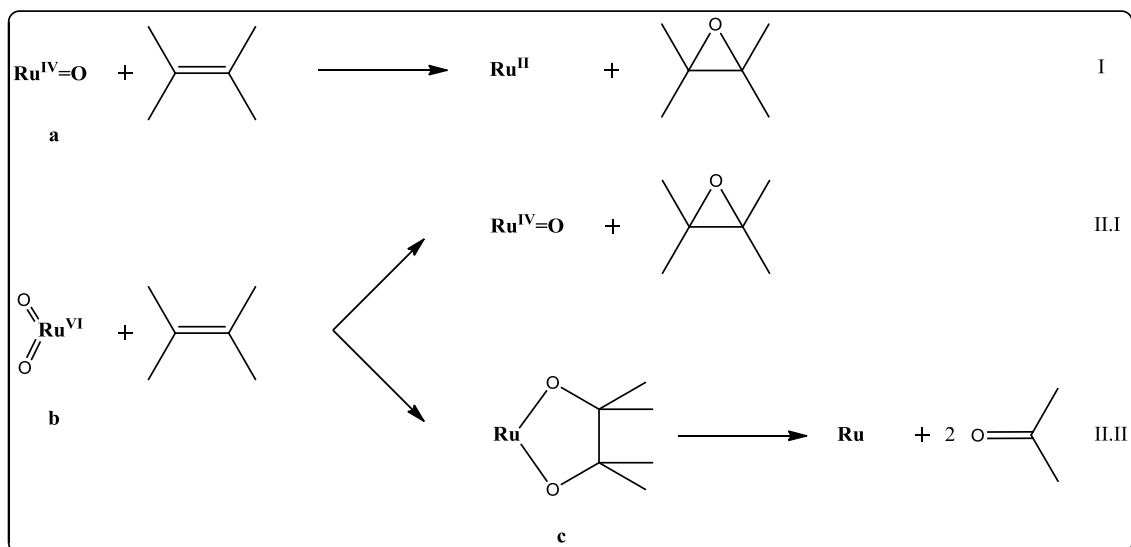


Figure 13. Structures of the most relevant Ruthenium epoxidation catalysts.

I.3.2. Mechanism for the epoxidation of alkenes via Ru(IV)=O

The epoxidation of alkenes occurs *via* an oxygen transfer processes. It is assumed that in the case of Ruthenium species, this mechanism concerns high-valent oxometal complexes which are generated in situ by the corresponding sacrificial oxidant. The nature of these oxometal species is up today a topic of controversy. Due to the experimental evidences that an oxidative cleavage process is a competing side reaction, Drago and coworkers proposed that monoxoruthenium (IV) species (Scheme 4, **a**) are responsible for epoxidation (Eq I) whereas *cis*-dioxoruthenium (VI) (Scheme 4, **b**) the species for competing epoxidation (Eq II.I) and oxidative cleavage⁹² (Eq II.II). This hypothesis is corroborated by the non-observance of oxidative cleavage in porphyrinic Ruthenium complexes, where the bis-oxo groups are forced to be *trans* oriented, thus avoiding the [3+2] cycloaddition (Scheme 4, **c**) needed for the cleavage of the double bond.⁹³



Scheme 4. Epoxidation of alkenes catalyzed by monooxoruthenium(IV) (I) and *cis*-dioxoruthenium (II.I) and competitive oxidative cleavage of the alkene *via* a [3+2] cycloaddition adduct (II.II).

Different mechanisms, both concerted and non-concerted, have been proposed as possible pathways for oxygen atom transfer. In Figure 14 these pathways are presented. An oxygen atom can be transferred directly through a concerted oxene insertion (pathway I); through the formation of a 4 membered ring where both Ru and O atoms are respectively bonded to the $\text{C}\alpha$ and $\text{C}\beta$ of the olefin (pathway II); through a single electron transfer with the formation of a radical cation (pathway III); or through the formation of a benzylic radical intermediate (pathway IV). The investigation of the stereoselectivity provides important information in order to evaluate the mechanism of epoxidation of aromatic alkenes. For instance, if the oxidation of *cis*-alkenes *via* a non-concerted pathway (Figure 14, pathways II-IV) involves the formation of a carboradical, the resulting acyclic intermediate rapidly isomerizes into the more stable *trans*-species *via* C-C bond rotation. In sharp contrast, Meyer reported a high degree of stereoretention for the oxidation of *cis*-stilbene by $[\text{Ru}^{\text{IV}}(\text{bpy})_2(\text{py})\text{O}]^{2+}$, thus suggesting an oxene insertion mechanism (Figure 14, pathway I) for this substrate.⁹⁴

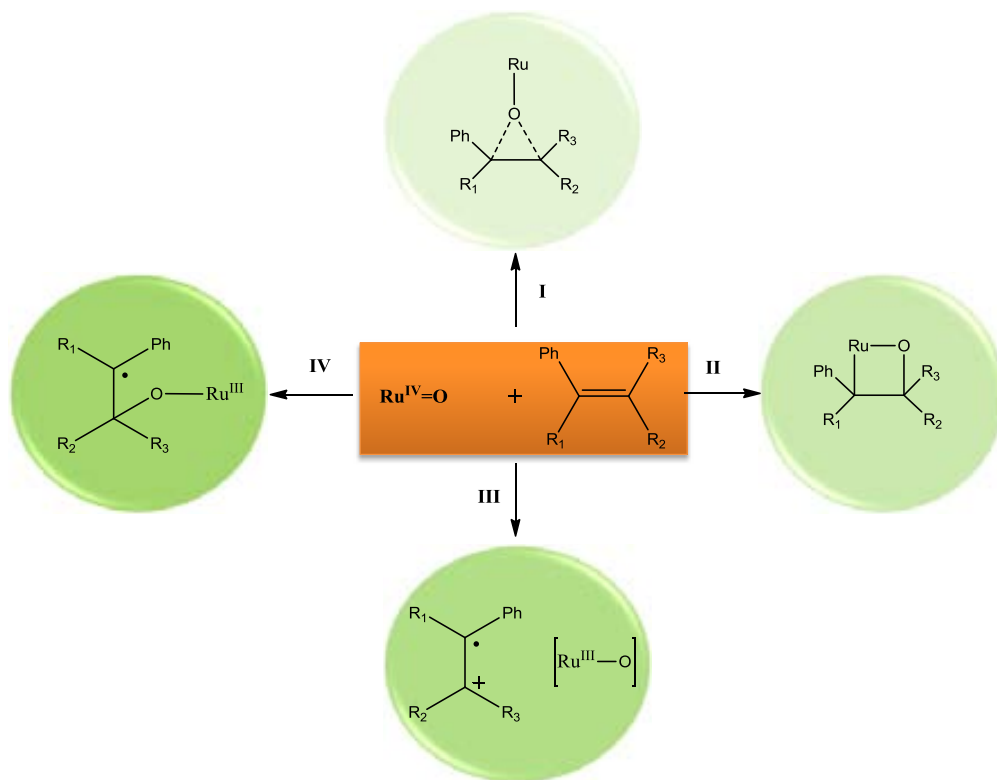


Figure 14 Proposed mechanistic pathways for oxygen atom transfer process.

The mechanisms which are directing the epoxidation of *cis*-stilbene and *cis*- β -methylstyrene when catalyzed by a series of monoxoruthenium(IV) complexes have been thoroughly studied by Che and co workers.⁹⁵ An excellent stereoreneration of the *cis* configuration was observed for *cis*-stilbene, thus pointing out that pathway I (Figure 14) directs this modification. In sharp contrast, mixture of *cis* and *trans* isomers was detected for *cis*- β -methylstyrene, indicating that a non-concerted mechanism was the most probable. Different experiments were performed in order to exactly know which non-concerted (pathways II-IV) was the adequate for the catalytic epoxidation of substrates such as styrene or *cis*- β -methylstyrene. Inverse secondary kinetic effect (KIE) was observed only for the β -*d*₂-styrene and not for the α -deuteriostyrene suggesting that not both α and β olefinic carbon atoms undergo into rehybridization, thus rejecting the mandatory formation of a 4-membered ring of pathway II (Figure 14, II). Both product distribution analysis and kinetic experiments were in concordance with the formation of a benzylic radical intermediate in the rate-determining step (Figure 14, IV). In consequence, this mechanism was proposed for the epoxidation of aromatic alkenes with Ru(IV)=O complexes (Figure 15). The carbocation intermediate formed would undergo ring closure to produce the corresponding epoxide (Figure 15, I). Prior to this closure, the sigma C-C bond could rotate, leading to the formation of the isomerized

epoxide (Figure 15, II). The formed radical species could also lead to the formation of byproducts, such as aldehydes, etc. (Figure 15, III).

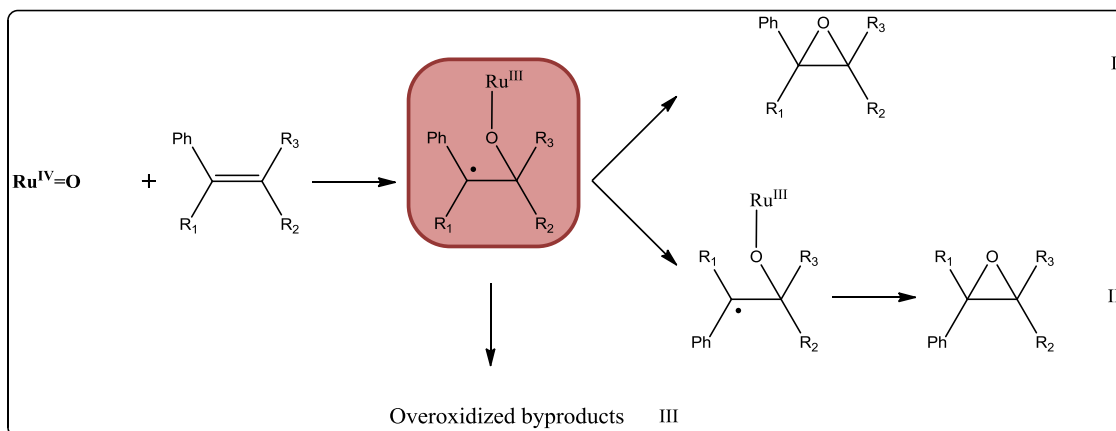


Figure 15 Proposed mechanism for *cis*- β -methylstyrene and analogue substrates. (I) Ring closure of the benzylic radical intermediate to generate the *cis*-epoxide, (II) rotation of the C-C bond prior to ring closure to form the *trans*-epoxide and (III) formation of overoxidized byproducts.

I.4. References

- ¹ Bruneau, C. *Ruthenium catalysts and fine chemistry*; Springer-Verlag: Berlin, **2004**.
- ² *Homogeneous Catalysis. Understanding the Art*; van Leeuwen, P. W. N. M. Kluwer Academic Publishers; Amsterdam, **2004**.
- ³ (a) Whittall, I. R. M., A. M.; Humphrey, M. G.; Samoc, M *Advances in Organomet. Chem.* **1999**, *43*, 349. (b) Whittall, I. R. M., A. M.; Humphrey, M. G.; Samoc, M *Advances in Organomet. Chem.* **1998**, *42*, 291. (c) Verbiest, T. H., S.; Kauranen, M.; Clays, K.; Persoons, A *J. Mater. Chem.* **1997**, *7*, 2175.
- ⁴ (a) Larionova, J. M., B.; Sanchiz, J. n.; Kahn, O. *Inorg. Chem.* **1998**, *37*, 679. (b) Hmyene, M. Y., A.; Escorne, M.; Percheron-Guegan, A.; Garnier, F *Adv. Mater.* **1994**, *6*, 564.
- ⁵ Constable, E. C. *Angew. Chem., Int. Ed.* **1991**, *30*, 407.
- ⁶ Dembek, A. A. B., R. R.; Feiring, A *J. Am. Chem. Soc.* **1993**, *115*, 2087
- ⁷ Ioannis Bratsosa, S. J., Teresa Gianferrara, and Enzo Alessio *Chimia* **2007**, *61*, 692.
- ⁸ (a) Adeloye, A. O.; Ajibade, P. A. *Int. J. Mol. Sci.* **2010**, *11*, 3158. (b) Prasanna de Silva, A. F., D.B.; Moody, T.S.; Weir, S.M. *Pure Appl. Chem.* **2001**, *73*, 503. (c) Robertson, N. M., C.A. *Chem. Soc. Rev.* **2003**, *32*, 96.
- ⁹ Newkome, G. R.; Cho, T. J.; Moorefield, C. N.; Mohapatra, P. P.; Godinez, L. A. *Chem. Eur. J.* **2004**, *10*, 1493-1500.
- ¹⁰ (a) Jiang, C. W.; Chao, H.; Hong, X. L.; Li, H.; Mei, W. J.; Ji, L. N. *Inorg. Chem. Commun.* **2003**, *6*, 773-775. (b) Ossipov, D.; Gohil, S.; Chattopadhyaya, J. *J. Am. Chem. Soc.* **2002**, *124*, 13416-13433. (c) Chao, H.; Mei, W. H.; Huang, Q. W.; Ji, L. N. *J. Inorg. Biochem.* **2002**, *92*, 165-170.
- ¹¹ (a) Planas, N.; Ono, T.; Vaquer, L.; Miro, P.; Benet-Buchholz, J.; Gagliardi, L.; Cramer, C. J.; Llobet, A. *Phys. Chem. Chem. Phys.* **2011**, *13*, 19480. (b) Federsel, C.; Jackstell, R.; Beller, M. *Angew. Chem., Int. Ed.* **2010**, *49*, 6254. (c) Jessop, P. G. *Handbook Homogeneous Hydrogenation*, H. de Vries, K. Elsevier (eds.), Wiley-VCH, Weinheim, **2007**, *1*, 489. (d) Jessop, P. G.; Joó, F.; Tai, C. C.; *Coord. Chem. Rev.* **2004**, *248*, 2425. (e) Leitner, W. *J. Am. Chem. Soc.* **1997**, *119*, 4432. (f) Leitner, F. G. a. W. *J. Chem. Soc., Chem. Commun.* **1993**, 1465. (g) Angermund, K.; Baumann, W.; Dinjus, E.; Fornika, R.; Gørls, H.; Kessler, M.; Kruger, C.; Leitner, W.; Lutz, F. *Chem. Eur. J.* **1997**, *3*, 755. (h) Tanaka, R.; Yamashita, M.; Nazaki, K. *J. Am. Chem. Soc.* **2009**, *131*, 14168. (i) Ng, S. M.; Yin, C.; Yeung, C. H.; Chan, T. C.; Lau, C. P. *Eur. J. Inorg. Chem.* **2004**, *9*, 1788. (j) Himeda, Y.; Onozawa-Komatsuzaki, N.; Sugihara, H.; Kasuga, K. *Organometallics* **2007**, *26*, 702. (k) Jessop, P. G.; Hsiao, Y.; Ikariya, T.; Noyori,

R. *J. Am. Chem. Soc.* **1996**, *118*, 344. (l) Munshi, P.; Denise Main, A.; Linehan, J. C.; Tai, C.-C.; Jessop, P. G. *J. Am. Chem. Soc.* **2002**, *124*, 7963.

¹² (a) Mashima, K.; Kusano, K.-h.; Sato, N.; Matsumura, Y.-i.; Nozaki, K.; Kumobayashi, H.; Sayo, N.; Hori, Y.; Ishizaki, T. *J. Org. Chem.* **1994**, *59*, 3064. (b) Ohta, T.; Miyake, T.; Seido, N.; Kumobayashi, H.; Takaya, H. *J. Org. Chem.* **1995**, *60*, 357. (c) Wabnitz, T. C.; Rizzo, S.; Goette, C.; Buschauer, A.; Benincori, T.; Reiser, O. *Tetrahedron Lett.* **2006**, *47*, 3733. (d) Starodubtseva, E. V.; Vinogradov, M. G.; Pavlov, V. A.; Gorshkova, L.S.; Ferapontov, V. A. *Russ. Chem. Bull.* **2004**, *53*, 2172. (e) Starodubtseva, E. V.; Turova, O. V.; Vinogradov, M. G.; Gorshkova, L. S.; Ferapontov, V. A. *Russ. Chem. Bull.* **2005**, *54*, 2374. (f) Doherty, S.; Knight, J. G.; Bell, A. L.; Harrington, R. W.; Clegg, W. *Organometallics* **2007**, *26*, 2465. (g) Bronze-Uhle, E. S.; Ines, d. S. M.; Donate, P. M.; Frederico, D. *J. Mol. Catal. A: Chem.* **2006**, *259*, 103. (h) Daley, C. J. A.; Wiles, J. A.; Bergens, S. H. *Inorg. Chim. Acta* **2006**, *359*, 2760. (i) Arai, N.; Azuma, K.; Nii, N.; Ohkuma, T. *Angew. Chem., Int. Ed.* **2008**, *47*, 7457.

¹³ (a) Fernández-Zúmel, M. A.; Kiefer, G.; Thommes, K.; Scopelliti, R.; Severin, K. *Eur. J. Inorg. Chem.* **2010**, 3596-3601. (b) Nair, R. P.; Kim, T. H.; Frost, B. J. *Organometallics* **2009**, *28*, 4681-4688. (c) Dabb, S. L.; Messerle, B. A.; Wagler, J. *Organometallics* **2008**, *27*, 4657-4665.

¹⁴ (a) Antonucci, A.; Bassetti, M.; Bruneau, C.; Dixneuf, P. H.; Pasquini, C. *Organometallics* **2010**. (b) van der Eide, E. F.; Piers, W. E. *Nature Chem* **2010**, *2*, 571-576. (c) Nolan, S. P.; Clavier, H. *Chem. Soc. Rev.* **2010**, *39*, 3305. (d) Ben-Asuly, A.; Aharoni, A.; Diesendruck, C. E.; Vidavsky, Y.; Goldberg, I.; Straub, B. F.; Lemcoff, N. G. *Organometallics* **2009**, *28*, 4652-4655. (e) Ager, D. *Handbook of chiral chemicals*; 2nd ed.; Taylor & Francis: Boca Raton, **2006**.

¹⁵ (a) Serrano, I.; López, M. I.; Ferrer, I. N.; Poater, A.; Parella, T.; Fontrodona, X.; Solà, M.; Llobet, A.; Rodríguez, M. Romero, I. *Inorg. Chem.* **2011**, *50*, 6044. (b) Bhor, S.; Tse, M. K.; Klawonn, M.; Doebler, C.; Maegerlein, W.; Beller, M. *Adv. Synth. Catal.* **2004**, *346*, 263.

¹⁶ (a) Wada, T.; Tsuge, K.; Tanaka, K. *Chem. Lett.* **2000**, 910-911. (b) Bernhard, P.; Anson, F. C. *Inorg. Chem.* **1988**, *27*, 4574-4577.

¹⁷ (a) Siebert, B. Hl, M. *J. Am. Chem. Soc.* **2010**, *132*, 8056-8070. (b) Fukuzumi, S.; Kobayashi, T.; Suenobu, T. *J. Am. Chem. Soc.* **2010**, *132*, 1496-1497. (c) Morris, D. J.; Clarkson, G. J.; Wills, M. *Organometallics* **2009**, *28*, 4133-4140

¹⁸ (a) Singh, P.; Das, D.; Singh, M.; Singh, A. K. *Inorg. Chem. Com.* **2010**, *13*, 223-226. (b) Tada, M.; Muratsugu, S.; Kinoshita, M.; Sasaki, T.; Iwasawa, Y. *J. Am. Chem. Soc.* **2010**, *132*, 713-724. (c) Chatterjee, D.; Nayak, K. A.; Ember, E.; van Eldik, R. *Dalton Trans.* **2010**, *39*, 1695. (d) Murali, M.; Mayilmurugan, R.; Palaniandavar, M. *Eur. J. Inorg. Chem.* **2009**, 3238-3249. (e) Chatterjee, D. *Catal Surv Asia* **2009**, *13*, 132-142. (f) Nunes, G.; Alexiou, A.; Toma, H. *J. Catal.* **2008**, *260*, 188-192. (g) Jiang, G.; Chen, J.; Thu, H.; Huang, J.; Zhu, N.; Che, C. *Angew. Chem. Int. Ed.* **2008**, *47*, 6638-6642. (h)

Huynh, M. H. V.; Meyer, T. *J. Chem. Rev.* **2007**, *107*, 5004-5064. (i) Punniyamurthy, T.; Velusamy, S.; Iqbal, *J. Chem. Rev.* **2005**, *105*, 2329-2364. (j) Jitsukawa, K.; Oka, Y.; Yamaguchi, S.; Masuda, H. *Inorg. Chem.* **2004**, *43*, 8119-8129. (k) Catalano, V. J.; Heck, R. A.; Immoos, C. E.; Öhman, A.; Hill, M. G. *Inorg. Chem.* **1998**, *37*, 2150-2157. (l) Marmion, M. E.; Takeuchi, K. *J. Am. Chem. Soc.* **1988**, *110*, 1472-1480. (m) Thompson, M. S.; De Giovanni, W. F.; Moyer, B. A.; Meyer, T. *J. Org. Chem.* **1984**, *49*, 4972-4977.

¹⁹ (a) Meyer, Thomas J. Plenum: New York, **1988**; 33-47. (b) Holm, R. H. *Chem. Rev.* **1987**, *87*, 1401-1449. (c) Gulliver, D. *Coord. Chem. Rev.* **1982**, *46*, 1-127.

²⁰ (a) Doyle, M. P.; Duffy, R.; Ratnikov, M.; Zhou, L. *Chem. Rev.* **2010**, *110*, 704-724. (b) Chatterjee, D.; Mitra, A.; Shepherd, R. E. *Inorg. Chim. Acta* **2004**, *357*, 980-990.

²¹ (a) Miyazaki, S.; Kojima, T.; Mayer, J. M.; Fukuzumi, S. *J. Am. Chem. Soc.* **2009**, *131*, 11615-11624. (b) Manner, V. W.; Mayer, J. M. *J. Am. Chem. Soc.* **2009**, *131*, 9874-9875. (c) Miyazaki, S.; Kojima, T.; Sakamoto, T.; Matsumoto, T.; Ohkubo, K.; Fukuzumi, S. *Inorg. Chem.* **2008**, *47*, 333-343. (d) Concepcion, J. J.; Brennaman, M. K.; Deyton, J. R.; Lebedeva, N. V.; Forbes, M. D. E.; Papanikolas, J. M.; Meyer, T. *J. Am. Chem. Soc.* **2007**, *129*, 6968-6969. (e) Kojima, T.; Hayashi, K.; Matsuda, Y. *Inorg. Chem.* **2004**, *43*, 6793-6804.

²² Dwyer, F. P. J.; Mellor, D. P. *Chelating agents and metal chelates*; New York: Academic Press: **1964**.

²³ (a) Durham, B.; Caspar, J.V.; Nagle, J.K.; Meyer, T.J., *J. Am. Chem. Soc.* **1982**, *104*, 4803-4810. (b) Meyer, T.J. *Acc. Chem. Res.* **1989**, *22*, 163-170. (c) Prugh, J.R.; Bruce, M.R.M.; Sullivan, B.P.; Meyer, T.J. *Inorg. Chem.* **1991**, *30*, 86-91. (d) Gersten, S.W.; Samuels, G.J.; Meyer, T.J. *J. Am. Chem. Soc.* **1982**, *104*, 4029-4030. (e) Murphy, W.R.; Takeuchi, K.J.; Meyer, T.J. *J. Am. Chem. Soc.* **1982**, *104*, 5817-5819.

²⁴ Eggleston, D.S.; Goldsby, K.A.; Hodgson, D.J.; Meyer, T.J. *Inorg. Chem.* **1985**, *24*, 4573-4580.

²⁵ (a) Moyer, B.A.; Meyer, T.J. *Inorg. Chem.* **1981**, *20*, 436-444. (b) Moyer, B.A.; Meyer, T.J. *J. Am. Chem. Soc.* **1978**, *100*, 3601-3603. (c) Binstead, R.A.; Moyer, B.A.; Samuels, G.J.; Meyer, T.J. *J. Am. Chem. Soc.* **1981**, *103*, 2897-2899.

²⁶ Che, C.M.; Yam, V.W.W. *Adv. Inorg. Chem.* **1992**, *39*, 233.

²⁷ (a) Masllorens, E.; Rodríguez, M.; Romero, I.; Roglans, A.; Parella, T.; Benet-Buchholz, J.; Poyatos, M.; Llobet, A. *J. Am. Chem. Soc.* **2006**, *128*, 5306-5307. (b) Meyer, T. *J. Electrochem. Soc.* **1984**, *131*, 221C. (c) Keene, F. R. *Coord. Chem. Rev.* **1999**, *187*, 121.

²⁸ (a) Binstead, R.A.; McGuire, M.E.; Dvletoglou, A.; Seok, W.K.; Roecker, L.E.; Meyer, T.J. *J. Am. Chem. Soc.* **1992**, *114*, 173-186. (b) Lebeau, E.L.; Binstead, R.A.; Meyer, T.J. *J. Am. Chem. Soc.* **2001**, *123*, 10535-10544. (c) Gilbert, J.A.; Gersten, S.W.; Meyer, T.J.; *J. Am. Chem. Soc.* **1982**, *104*, 6872-

6873. (d) Gilbert, J.; Roecker, L.; Meyer, T.J. *Inorg. Chem.* **1987**, 26, 1126-1132. (e) Seok, W.K.; Dobson, J.C.; Meyer, T.J. *Inorg. Chem.* **1988**, 27, 3-5. (f) Roecker, L.; Dobson, J.C.; Vining, W.J.; Meyer, T.J. *Inorg. Chem.* **1987**, 26, 779-781. (g) Moyer, B.A.; Sipe, B.K.; Meyer, T.J. *Inorg. Chem.* **1981**, 20, 1475-1480. (h) Stultz, L.K.; Binstead, R.A.; Reynolds, M.S.; Meyer, T.J. *J. Am. Chem. Soc.* **1995**, 117, 2520-2532. (i) Roecker, L.; Meyer, T.J. *J. Am. Chem. Soc.* **1987**, 109, 746-754. (j) Roecker, L.; Meyer, T.J. *J. Am. Chem. Soc.* **1986**, 108, 4066-4073. (k) Stultz, L. K.; Huynh, M. H. V.; Binstead, R. A.; Curry, M.; Meyer, T. J.; Bryant, J. R.; Mayer, J. M. Unpublished results. (l) Curry, M.; Huynh, M.H.V.; Stultz, L.K.; Binstead, R.A.; Meyer, T.J. *J. Am. Chem. Soc.* **1995**, 117, 5984-5996.

²⁹ (a) Roecker, L.; Kutner, W.; Gilbert, J.A.; Simmons, M.; Murray, R.W.; Meyer, T.J. *Inorg. Chem.* **1985**, 24, 3784. (b) Takeuchi, K.J.; Thompson, M.S.; Pipes, D.W.; Meyer, T.J. *Inorg. Chem.* **1984**, 23, 1845. (c) Dovletoglou, A.; Adeyemi, S.A.; Meyer, T.J. *Inorg. Chem.* **1996**, 35, 4120. (d) Suen, H.F.; Wilson, S.W.; Pomerantz, M.; Walsh, J.K. *Inorg. Chem.* **1989**, 28, 786.

³⁰ (a) Masllorens, E.; Rodriguez, M.; Romero, I.; Roglans, A.; Parella, T.; Benet-Buchholz, J.; Poyatos, M.; Llobet, A. *Journal of the American Chemical Society* **2006**, 128, 5306-5307. (b) Richard Keene, F. *Coordination Chemistry Reviews* **1999**, 187, 121-149. (c) Meyer, T. J. *J. Electrochem. Soc.* **1984**, 131, 221C-228C.

³¹ Pramanik, N. C.; Bhattacharya, S. *Transition Metal Chemistry* **1997**, 22, 524-526.

³² Concepcion, J. J.; Jurss, J. W.; Templeton, J. L.; Meyer, T. J. *J. Am. Chem. Soc.* **2008**, 130, 16462-16463.

³³ Gerli, A.; Reedijk, J.; Lakin, M. T.; Spek, A. L. *Inorg. Chem.* **1995**, 34, 1836-1843.

³⁴ Dakkach, M.; Fontrodona, X.; Parella, T.; Atlamsani, A.; Romero, I.; Rodríguez, M. *Advanced Synthesis & Catalysis* **2011**, 353, 231-238.

³⁵ Hua, X.; Shang, M.; Lappin, A. G. *Inorg. Chem.* **1997**, 36, 3735-3740.

³⁶ (a) Marmion, M.L.; Tadeuchi, K.J.; *J. Am. Chem. Soc.* **1988**, 110, 1472; **1986**, 108, 510. (b) Thompson, M.S.; De Giovanni, W.F.; Moyer, B.A.; Meyer, T.J. *J. Org. Chem.* **1984**, 25, 4972. (c) Catalano, V.J.; Heck, R.A.; Immoos, C.E.; Hill, M.G. *Inorg. Chem.* **1998**, 37, 2150. (d) Che, C-M; Ho, C.; Lau, T-C. *J. Chem. Soc. Dalton Trans.* **1991**, 24, 1901. (e) Che, C-M.; Cheng, K-W.; Chan, M.C.W.; Lau, T-C.; Mak, C-K. *J. Org. Chem.* **2000**, 65, 7996. (f) Stultz, L.K.; Huynh, H.V.; Binstead, R.A.; Curry, M.; Meyer, T.J. *J. Am. Chem. Soc.* **2000**, 122, 5984.

³⁷ (a) Nugent, W.A.; Mayer, J.M. *Metall-Ligand Multiple Bonds*; Wiley: New York, **1988**. (b) Meyer, T.J. *In Metal Oxo Complexes and Oxygen Activation*; Martell, A.E., Ed.; Plenum: New York, **1988**; p 33-47. (c) Holm, R.H.; *Chem. Rev.* **1987**, 87, 1401. Gulliver, D.J.; Levason, W. *Coord. Chem. Rev.* **1982**, 46, 1.

(d) Sheldon, R. A.; Kochi, J.K. *Metal-Catalyzed Oxidations of Organic Compounds*; Academic: New York, **1981**.

³⁸ N. Armaroli, V. Balzani, *Angew. Chem. Int. Ed.* **2007**, *46*, 52–66.

³⁹ International Energy Agency.

⁴⁰ P. H. Raven, R. F. Evert, S. E. Eichhorn, *Biology of Plants*, 7th ed., W.H. Freeman and Company Publishers, New York, **2005**, pp. 124–127.

⁴¹ (a) L. Francàs, X. Sala, J. Benet-Buchholz, L. Escriche, A. Llobet, *ChemSusChem* **2009**, *2*, 321-329; (b) C. Herrero, A. Quaranta, W. Leibl, A. W. Rutherford, A. Aukauloo, *Energy Environ. Sci.* **2011**, *4*, 2353-2365; (c) D. Gust, T. A. Moore, A. L. Moore, *Acc. Chem. Res.* **2009**, *42*, 1890-1898; (d) C. Herrero, B. Lassalle-Kaiser, W. Leibl, A. W. Rutherford, A. Aukauloo, *Coord. Chem. Rev.* **2008**, *252*, 456-468.

⁴² (a) M. Wang, L. Sun, *ChemSusChem* **2010**, *3*, 551-554; (b) H. I. Karunadasa, C. J. Chang, J. R. Long, *Nature* **2011**, *464*, 1329-1333; (c) V. Fourmond, S. Canaguier, B. Golly, M. J. Field, M. Fontecave, V. Artero, *Energy Environ. Sci.* **2011**, *4*, 2417-2427; (d) U. J. Kilgore, J. A. S. Roberts, D. H. Pool, A. M. Appel, M. P. Stewart, M. R. DuBois, W. G. Dougherty, W. S. Kassel, R. M. Bullock, D. L. DuBois, *J. Am. Chem. Soc.* **2011**, *133*, 5861-5872.

⁴³ S. W. Gestern, G. J. Samuels, T. J. Meyer, *J. Am. Chem. Soc.* **1982**, *104*, 4029-4030.

⁴⁴ (a) K. Nagoshi, S. Yamashita, M. Yagi, M. Kaneko, *J. Mol. Catal. A: Chem.* **1999**, *144*, 71-76; (b) J. P. Collin, J. P. Sauvage, *Inorg. Chem.* **1986**, *25*, 135-141.

⁴⁵ E. L. Lebeau, S. A. Adeyemi, T. J. Meyer, *Inorg. Chem.* **1998**, *37*, 6476-6484.

⁴⁶ C. Sens, I. Romero, M. Rodríguez, A. Llobet, T. Parella, J. Benet-Buchholz, *J. Am. Chem. Soc.* **2004**, *126*, 7798-7799.

⁴⁷ N. Planas, J. G. Christian, E. Mas-Marzà, X. Sala, X. Fontrodona, F. Maseras, A. Llobet, *Chem. Eur. J.* **2010**, *16*, 7965–7968.

⁴⁸ (a) X. Sala, I. Romero, M. Rodríguez, L. Escriche, A. Llobet, *Angew. Chem. Int. Ed.* **2009**, *48*, 2842–2852; (b) I. Romero, M. Rodríguez, C. Sens, J. Mola, M. R. Kollipara, L. Francàs, E. Mas-Marzà, L. Escriche, A. Llobet, *Inorg. Chem.* **2008**, *47*, 1824-1834; (c) F. Bozoglian, S. Romain, M. Z. Ertem, T. K. Todorova, C. Sens, J. Mola, M. Rodríguez, I. Romero, J. Benet-Buchholz, X. Fontrodona, C. J. Cramer, L. Gagliardi, A. Llobet, *J. Am. Chem. Soc.* **2009**, *131*, 15176-15187.

⁴⁹ Z. Deng, H. W. Tseng, R. Zong, D. Wang, R. Thummel, *Inorg. Chem.* **2008**, *47*, 1835-1848.

- ⁵⁰ Y. Xu, T. Åkermark, V. Gyollai, D. Zou, L. Eriksson, L. Duan, R. Zhang, B. Åkermark, L. Sun, *Inorg. Chem.* **2009**, *48*, 2717-2719.
- ⁵¹ Y. Xu, A. Fischer, L. Duan, L. Tong, E. Gabrielsson, B. Åkermark, L. Sun, *Angew. Chem. Int. Ed.* **2010**, *49*, 8934-8937.
- ⁵² (a) Y. V. Geletii, B. Botar, P. Kögerler, D. A. Hillesheim, D. G. Musaev, C. L. Hill, *Angew. Chem., Int. Ed.* **2008**, *47*, 3896-3899; (b) A. Sartorel, M. Carraro, G. Scorrano, R. D. Zorzi, S. Geremia, N. D. McDaniel, S. Bernhard, M. Bonchio, *J. Am. Chem. Soc.* **2008**, *130*, 5006-5007.
- ⁵³ H. W. Tseng, R. Zong, J. T. Muckerman, R. Thummel, *Inorg. Chem.* **2008**, *47*, 11763-11773.
- ⁵⁴ (a) J. J. Concepcion, J. W. Jurss, J. L. Templeton, T. J. Meyer, *J. Am. Chem. Soc.* **2008**, *130*, 16462-16463; (b) J. J. Concepcion, M.-K. Tsai, J. T. Muckerman, T. J. Meyer, *J. Am. Chem. Soc.* **2010**, *132*, 1545-1557; (c) J. J. Concepcion, J. W. Jurss, M. R. Norris, Z. Chen, J. L. Templeton, T. J. Meyer, *Inorg. Chem.* **2010**, *49*, 1277-1279.
- ⁵⁵ L. Duan, Y. Xu, M. Gorlov, L. Tong, S. Andersson, L. Sun, *Chem. Eur. J.* **2010**, *16*, 4659-4668.
- ⁵⁶ L. Duan, Y. Xu, L. Tong, L. Sun, *ChemSusChem* **2011**, *4*, 238-244.
- ⁵⁷ (a) L. Duan, A. Fischer, Y. Xu, L. Sun, *J. Am. Chem. Soc.* **2009**, *131*, 10397-10399; (b) J. Nyhlén, L. Duan, B. Åkermark, L. Sun, T. Privalov, *Angew. Chem., Int. Ed.* **2010**, *49*, 1773-1777; (c) L. Tong, L. Duan, Y. Xu, T. Privalov, L. Sun, *Angew. Chem. Int. Ed.*, **2011**, *50*, 445-449.
- ⁵⁸ (a) S. Masaoka, K. Sakai, *Chem. Lett.* **2009**, *2*, 182-183. (b) D. J. Wasylenko, C. Ganesamoorthy, B. D. Koivisto, M. A. Henderson, C. P. Berlinguette, *Inorg. Chem.* **2010**, *49*, 2202-2209.
- ⁵⁹ S. Roeser, P. Farràs, F. Bozoglian, M. Martínez-Belmonte, J. Benet-Buchholz, A. Llobet, *ChemSusChem* **2011**, *4*, 197-207.
- ⁶⁰ Duan, L.; Bozoglian, F.; Mandal, S.; Stewart, B.; Privalov, T.; Llobet, A.; Sun, L. *Nat. Chem.* **2012**, *4*, 418.
- ⁶¹ S. Romain, F. Bozoglian, X. Sala, A. Llobet, *J. Am. Chem. Soc.* **2009**, *131*, 2768-2769.
- ⁶² N. D. McDaniel, F. J. Coughlin, L. L. Tinker, S. Bernhard, *J. Am. Chem. Soc.* **2008**, *130*, 210-217.
- ⁶³ a) J. F. Hull, D. Balcells, J. D. Blakemore, C. D. Incarvito, O. Eisenstein, G. W. Brudvig, R. H. Crabtree, *J. Am. Chem. Soc.* **2009**, *131*, 8730-8731; b) J. D. Blakemore, N. D. Schley, D. Balcells, J. F. Hull, G. W. Olack, C. D. Incarvito, O. Eisenstein, G. W. Brudvig, R. Crabtree, *J. Am. Chem. Soc.* **2010**, *132*, 16017-16029.

- ⁶⁴ M. Albrecht, *Chem. Commun.* **2008**, 3601-3610.
- ⁶⁵ D. B. Grotjahn, D. B. Brown, J. K. Martin, D. C. Marelius, M.-C. Abadjian, H. N. Tran, G. Kalyuzhny, K. S. Vecchio, Z. G. Specht, S. A. Cortes-Llamas, V. Miranda-Soto, C. van Niekerk, C. E. Moore, A. L. Rheingold, *J. Am. Chem. Soc.* **2011**, *133*, 19024-19027.
- ⁶⁶ A. Savini, P. Belanzoni, G. Bellachioma, C. Zuccaccia, D. Zuccaccia, A. Macchioni, *Green Chem.* **2011**, *13*, 3360-3374.
- ⁶⁷ Q. Yin, J. M. Tan, C. Besson, Y. V. Geletii, D. G. Musaev, A. E. Kuznetsov, Z. Luo, K. I. Hardcastle, C. L. Hill, *Science* **2010**, *328*, 342-345.
- ⁶⁸ J. J. Stracke, R. G. Finke, *J. Am. Chem. Soc.* **2011**, *133*, 14872-14875.
- ⁶⁹ D. J. Wasylenko, C. Ganesamoorthy, J. Borau-Garcia, C. P. Berlinguette, *Chem. Commun.* **2011**, *47*, 4249-4251.
- ⁷⁰ W. C. Ellis, N. D. McDaniel, S. Bernhard, T. J. Collins, *J. Am. Chem. Soc.* **2010**, *132*, 10990-10991.
- ⁷¹ J. Lloret Fillol, Z. Codolà, I. Garcia-Bosch, L. Gómez, J. J. Pla, M. Costas, *Nat. Chem.* **2011**, *3*, 807-813.
- ⁷² Cavani, F.; Teles, J.H. *ChemSusChem*, **2009**, *2*, 508.
- ⁷³ *Catalysts for fine chemical synthesis regio- and stereo-controlled oxidations and reductions*, ed. S. M. Roberts and J. Whittall, John Wiley Sons, Ltd., England, **2007**, vol. 5.
- ⁷⁴ Nijhuis, T.A.; Makkee, M.; Moulijn, J.A.; Weckhuysen, B.M.; *Ind. Eng. Chem. Res.*, **2006**, *45*, 3447.
- ⁷⁵ Herrmann, W., Fischer, R. W., and Marz, D. W. *Angew. Chem., Int. Ed.* **1991**, *30*.
- ⁷⁶ (a) Mizuno, N., Nakagawa, Y., and Yamaguchi, K. *J. Mol. Catal. A: Chem.* **2006**, *251*. (b) Nakagawa, Y. a. M., N. *Inorg. Chem.* **2007**, *46*.
- ⁷⁷ (a) Sato, K., Aoki, M., Ogawa, M., Hashimoto, T., and Noyori, R. *J. Org. Chem.* **1996**, *61*. (b) Sato, K., Aoki, M., Ogawa, M., Hashimoto, T., Paynella, D., and Noyori, R. *Bull. Chem. Soc. Jpn.* **1997**, *70*. (c) Kamata, K., Yonehara, K., Sumida, Y., Yamaguchi, K., Hikichi, S., and Mizuno, N. *Science* **2003**, *300*. (d) Kamata, K., Kotani, M., Yamaguchi, K., Hikichi, S., and Mizuno, M. *Chem. Eur. J.* **2007**, *13*.
- ⁷⁸ (a) Wahl, G., Kleinhenz, D., Schorm, A., Sundermeyer, J., Stowasser, R., Rummey, C., Bringmann, G., Fickert, C., and Kiefer, W. *Chem. Eur. J.* **1999**, *5*. (b) Gharah, N.; Drew, M.; Bhattacharyya, R. *Transit. Metal Chem.* **2009**, *34*, 549.

⁷⁹ (a) Anilkumar, G.; Bitterlich, B.; Gelalcha, F. G.; Tse, M. K.; Beller, M. *Chem. Commun* **2007**, 89. (b) Traylor, T. G., Tsuchiya, S., Byun, Y.-S., and Kim, C. *J. Am. Chem. Soc.* **1993**, *115*. (c) White, M. C.; Doyle, A. G.; Jacobsen, E. N. *J. Am. Chem. Soc.* **2001**, *123*, 7194. (d) Anilkumar, G., Bitterlich, B., Gelalcha, F. G., Tse, M. K., and Beller, M. *Chem. Commun.* **2007**. (e) Bitterlich, B., Anilkumar, G., Gelalcha, F. G., Spilker, B., Grotevendt, A., Jackstell, R., Tse, M. K., and Beller, M. *Chem. Asian J.* **2007**, *2*. (f) Bitterlich, B., Schroder, K., Tse, M. K., and Beller, M. *Eur. J. Org. Chem.* **2008**. (g) Schröder, K., Tong, X., Bitterlich, B., Tse, M. K., Gelalcha, F. G., Brückner, A., and Beller, M. *Tetrahedron Lett.*, *48*. (h) Schröder, K., Enthaler, S., Bitterlich, B., Schulz, T., Spannenberg, A., Tse, M.K., Junge, K., and Beller, M. *Chem. Eur. J.* **2009**, *15*.

⁸⁰ (a) Battioni, P.; Renaud, J. P.; Bartoli, J. F.; Reina-Artiles, M.; Fort, M.; Mansuy, D. *J. Am. Chem. Soc.* **1988**, *110*, 8462. (b) Zhang, W., Loebach, J. L., Wilson, S. R., and Jacobsen, E. N. *J. Am. Chem. Soc.* **1990**, *112*. (c) Irie, R., Noda, K., Ito, Y., Matsumoto, N., and Katsuki, T. *Tetrahedron Lett.* **1990**, *31*. (d) Jacobsen, E. N.; Wu, M. H. *Comprehensive Asymmetric Catalysis*; Springer, Heidelberg, 1999. (e) Berkessel, A., Frauenkron, M., Schwenkreis, T., Steinmetz, A., Baum, G., and Fenske, D. *J. Mol. Catal. A: Chem.* **1996**, *113*. (f) Irie, R., Hosoya, N., and Katsuki, T. *Synlett.* **1994**. (g) Pietikainen, P. *J. Mol. Catal. A: Chem.* **2001**, *165*. (h) Kureshy, R. I., Khan, N. H., Abdi, S. H. R., Patel, S. T., and Jasra, R. V. *Tetrahedron: Asymmetr.* **2001**, *12*. (i) Kureshy, R. I., Kahn, N. H., Abdi, S. H. R., Singh, S., Ahmed, I., Shukla, R. S. and Jasra, R. V. *J. Catal.* **2003**, *219*. (j) Garcia-Bosch, I.; Company, A.; Fontrodona, X.; Ribas, X.; Costas, M. *Org. Lett.* **2008**, *10*, 2095. (k) Garcia-Bosch, I., Ribas, X., and Costas, M. *Adv. Synth. Catal.* **2009**, *351*. (l) Brinksma, J., Hage, R., Kerschner, J., and Feringa, B. L. *Chem. Commun.* **2000**. (m) Rich, J.; Rodríguez, M.; Romero, I.; Fontrodona, X.; van Leeuwen, P. W. N. M.; Freixa, Z.; Sala, X.; Poater, A.; Solà, M. *Eur. J. Inorg. Chem.* **2012**, (early view-published online DOI:10.1002/ejic.201201154)

⁸¹ (a) Katsuki, T. a. S., K. B. *J. Am. Chem. Soc.* **1980**, *102*. (b) Matsumoto, K., Sawada, Y., Saito, B., akai, K., and Katsuki, T. *Angew. Chem., Int. Ed.* **2005**, *44*. (c) Sawada, Y., Matsumoto, K., Kondo, S., Watanabe, H., Ozawa, T., Suzuki, K., Saito, B., and Katsuki, T. *Angew. Chem., Int. Ed.* **2006**, *45*. (d) Matsumoto, K., Sawada, Y., and Katsuki, T. *Synlett.* **2006**.

⁸² Murahashi, S.-I.; Komiya, N. *Ruthenium in Organic Synthesis*; Wiley-VCH, Weinheim, **2004**.

⁸³ (a) Groves, J. T., Bonchio, M., Carofiglio, T., and Shalyaev, K. *J. Am. Chem. Soc.* **1996**, *118*. (b) Higuchi, T., Othake, H., and Hirobe, M. *Tetrahedron Lett.* **1989**, *30*.

⁸⁴ Nishiyama, H.; Shimada, T.; Itoh, H.; Sugiyama, H.; Motoyama, Y. *Chem. Commun.* **1997**, 1863.

⁸⁵ Tse, M. K.; Klawonn, M.; Bhor, S.; Dobler, C.; Anilkumar, G.; Hugl, H.; Magerlein, W.; Beller, M. *Org Lett* **2005**, *7*, 987.

-
- ⁸⁶ (a) Murahashi, S.-I.; Editor *Ruthenium in Organic Synthesis*; Wiley-VCH Verlag GmbH & Co. KGaA, **2004**. (b) Fierman, M; Nelson, A.; Khan, S.I.; Barfield, M.; O'Leary, D.J. *Org. Lett.* **2000**, *2*, 2077-2080. (c) Lai, T.S.; Zhang, R.; Cheung, K.K.; Che, C.M.; Kwong, H.L. *Chem. Commun.* (Cambridge) **1998**, 1583-1584.
- ⁸⁷ (a) End, N.; Pfaltz, A. *Chem. Commun.* (Cambridge) **1998**, 589-590. (b) End, N.; Macko, L.; Zehnder, M; Pfaltz, A. *Chem Eur. J.* **1998**, *4*, 818-824.
- ⁸⁸ Kureshy, R.I.; Khan, N.H.; Abdi, S.H.R. *J Mol Catal A: Chem.* **1995**, *96*, 117-122.
- ⁸⁹ Nakata, K.; Takeda, T.; Mihara, J.; Hamada, T.; Irie, R.; Katsuki, T. *Chem. Eur. J.* **2001**, *7*, 3776-3782.
- ⁹⁰ Pezet, F.; Ait-Haddou, H.; Daran, J.C.; Sakai, I.; Balavoine, G.G.A. *Chem. Commun.* (Cambridge) **2002**, 510-511.
- ⁹¹ Nishiyama, H.; Shimada, T.; Itoh, H.; Sugiyama, H.; Motoyama, Y. *Chem Commun.* (Cambridge) **1997**, 1863-1864.
- ⁹² (a) Bailey, C. L.; Drago, R. S. *J. Chem. Soc., Chem. Commun.* **1987**, 179. (b) Drago, R. S. *Coordination Chemistry Reviews* **1992**, *117*, 185.
- ⁹³ (a) Groves, J. T.; Quinn, R. *J. Am. Chem. Soc.* **1985**, *107*, 5790. (b) Groves, J. T.; Quinn, R. *Inorg. Chem.* **1984**, *23*, 3844.
- ⁹⁴ Stultz, L. K.; Binstead, R. A.; Reynolds, M. S.; Meyer, T. J. *J. Am. Chem. Soc.* **1995**, *117*, 2520.
- ⁹⁵ Fung, W.-H.; Yu, W.-Y.; Che, C.-M. *J. Org. Chem.* **1998**, *63*, 7715.

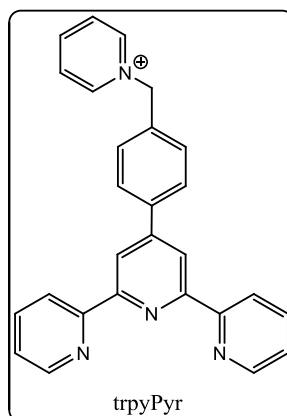
CHAPTER II

Objectives



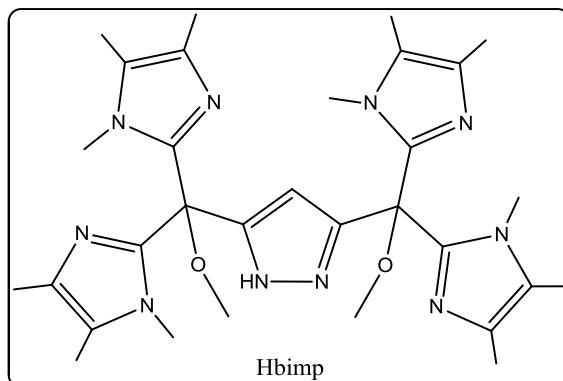
According to all the conclusions extracted from the General Introduction, the main objectives of this thesis are exposed in the present Chapter.

I. One of the more exciting challenges for the scientists nowadays involved in the artificial photosynthesis field is the set up of a real light-driven water splitting cell for the photo-production of hydrogen. In order to achieve this difficult goal, investigate new water oxidation catalyst-electrode hybrid systems able to evolve oxygen in the solid state is a key point. Therefore, the first goal of this PhD is the synthesis, thorough structural, spectroscopic and electrochemical characterization and catalytic evaluation of a new family of complexes with general formula $\{[\text{Ru}^{\text{II}}(\text{trpyPyr})]_2(\mu\text{-bpp})(\mu\text{-X})\}^{4+}$ ($\text{X} = \text{Cl}^-, \text{CH}_3\text{COO}^-$). These species, based on the well-known “Ru-Hbpp” family but containing an extra positively charged pyridylic ring on the trpy ligand, are intended to be anchored onto solid conductive and non-conductive electrodes such as Silica, FTO-TiO₂ and Nafion. Therefore, the study of their stability and catalytic performance is also proposed.

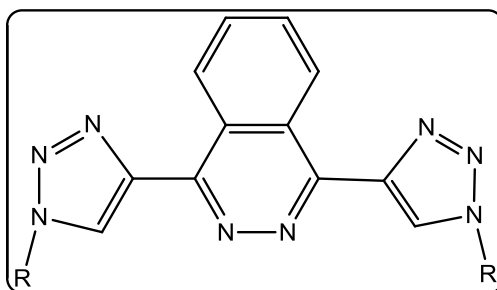


II. The catalytic epoxidation of alkenes in a really efficient and stereoselective manner is still one of the aims of the scientific community; thereby the preparation of a diruthenium complex capable to effectively perform this process is the second target of this thesis. The bis-facial bridging ligand Hbimp is proposed in order to ensure a highly encumbered disposition of the active sites, thus presumably enhancing the stereoselectivity of the epoxidation by supramolecular interactions of both metal centres with the incoming substrate. The analysis of the product distribution and

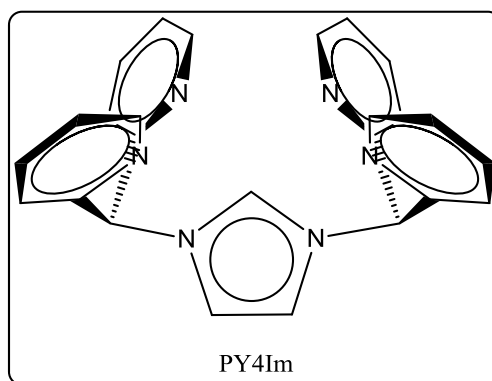
selectivity of the catalytic epoxidation for a wide range of substrates are also goals of this second project.



III. The feasible preparation of N-heterocyclic carbenes (NHCs), which has extraordinarily grow up during the last years together with the interesting properties of this compounds when used as ligands in very diverse catalytic systems, pushed us to the development of ligands of this kind to be applied in Ru catalyzed water oxidation. Thus, the main goal of this chapter is to synthesize and characterize a new set of hybrid N/C-donor ligands and the evaluation of their effect on the electrochemical properties and catalytic activity of the corresponding mono- and dinuclear ruthenium complexes.



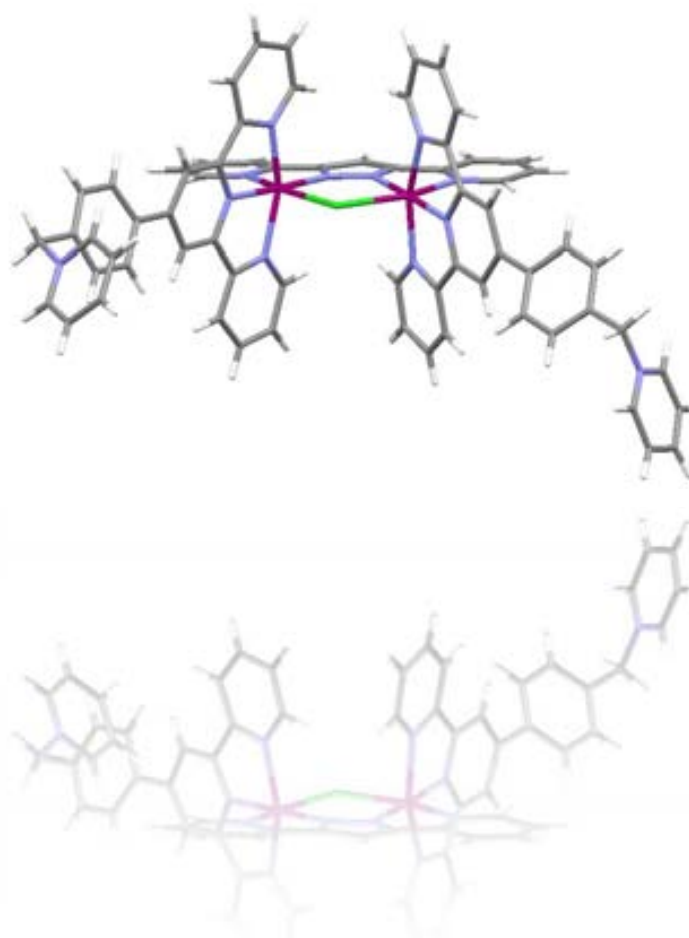
IV. In spite of intensive research by many groups in this field, no ruthenium aqua-complexes have been reported containing pentadentat-NHC ligands. Thus, the target of this final project is the synthesis and characterization of a new family of this kind of complexes, being the pentadentate ligand PY4Im the ligand of choice. The spectroscopic and redox characterization of the prepared Ru(II) complex and its corresponding high oxidation states is also a goal of the current project. Comparison of these features and the observed water oxidation and epoxidation capacity with related pentapyridylic systems is also planned in order to better understand the effect of the NHC in the prepared compound.



CHAPTER III

"Ru-Hbpp" Complexes Containing the TrpyPyr Scaffold:

Heterogenization and Water Oxidation Catalysis



In this chapter we present the immobilization of two new “*Ru-Hbpp*” complexes on the surface of Silica, FTO-TiO₂ films and Nafion polymer. The catalytic performance of these new hybrid materials towards the oxidation of water will be discussed and compared with their homogeneous counterparts and other related systems previously reported.

TABLE OF CONTENTS

CHAPTER III. "Ru-Hbpp" Complexes Containing the TrpyPyr Scaffold: Heterogenization and Water Oxidation Catalysis

- III.1. Introduction
- III.2. Results & Discussion
 - III.2.1. Ligand synthesis
 - III.2.2. Synthesis of complexes
 - III.2.3. Characterization of **4**(PF₆), **5**(PF₆)₄, **7**(PF₆)₄ and **8**⁵⁺
 - III.2.3.1. NMR spectroscopy
 - III.2.3.2. X-ray Crystal Structures
 - III.2.3.3. Electrochemistry
 - III.2.3.4. UV-vis
 - III.2.4. Synthesis and characterization of supported systems
 - III.2.4.1. Silica-**7**⁴⁺
 - III.2.4.2. FTO-TiO₂-**5**⁴⁺
 - III.2.4.3. Nafion®
 - III.2.5. Water Oxidation Catalysis
 - III.2.5.1. Chemically triggered materials
 - III.2.5.2 Electrochemically triggered materials
- III.3. Conclusions
- III.4. Experimental Section
- III.5. References
- III.6. Supporting Information

III.1. Introduction

The use of stable redox-active catalysts such as Ruthenium mono- or dinuclear complexes is an interesting strategy in order to succeed in water oxidation catalysis. Our group has developed several complexes of this type (mainly the so-called Ru-Hbpp family, see Chart 1) presenting a relatively good performance with regards to this challenging reaction. Furthermore, most of them have been mechanistically investigated.¹ In terms of catalyst stability, one of the common deactivation pathways operating in the above mentioned systems is the catalyst-catalyst intermolecular oxidative degradation, which generates non-active species and/or CO₂ as ligand degradation product.^{1c,2} The immobilization of these catalysts onto conductive solid supports has been one of the used strategies to overcome their degradation. In addition, the use of conductive materials allows their electrochemical activation, thus avoiding the employment of the non-environmentally friendly Ce(IV) as sacrificial oxidant.² In 2007, Meyer and co-workers developed the anchoring of an active dinuclear water oxidation catalysts (WOC) onto FTO-TiO₂ and ITO-TiO₂ surfaces, that improving the catalytic efficiency with regards to its homogeneous counterpart.³ The first approach of our research group towards the preparation of heterogeneous WOCs was, in 2008, the electropolymerization of a pyrrole-modified Ru-Hbpp system onto vitreous carbon sponges (VCS) and fluorinated tin oxide electrodes (Chart 1, **B**).² Despite the observed robustness increase, the final oxidation of the polypyrrole backbone employed ended up with leaching and deactivation of the catalyst. However, this system catalyzes the oxidation of water to dioxygen through electroactivation at 1.17 V *vs.* SSCE and confirmed the feasibility of the solid-state approach.

Next was the further modification of the Ru-Hbpp catalyst through the introduction of a carboxylate functional group into the bridging ligand. That allowed its anchoring onto a more rugged, all inorganic solid support such as nanoparticulate TiO₂ (Chart 1, **C**).⁴ The chemical (Ce(IV)) mediated activation of this system ended up with the concomitant generation of O₂ and CO₂, the later due to the intermolecular ligand oxidation beginning at the benzylic position of the modified Hbpp ligand. Therefore, in order to avoid the presence of activated and easily oxidizable methylenic groups, the introduction of a phosphonate functional group directly bound to the terpyridine ligand was envisaged.⁵ The phosphonate-modified Ru-Hbpp catalyst (Chart 1, **D**) was anchored onto FTO-TiO₂ electrodes. However, the anchoring process changed the electrochemical properties of

the complex to the extent that it was no longer active as WOC. In addition to this, it is proposed that the generation of a hydrophobic cavity and the subsequent block of the active sites of the metal centre is the reason for this electrochemical change and the subsequent lack of activity.

Despite a considerable part of these results was published and/or developed in parallel to the work reported in this chapter, they have been extremely useful to plan the experiments here presented and also for the rationalization of the results obtained.

Taking into account all the aforementioned results presented above we envisaged a new strategy based on the electrostatic interaction between different solid supports/electrodes and positively charged Ru-Hbpp catalytic species. All inorganic rugged supports such as SiO₂ or TiO₂ and the polymeric and anionic Nafion[®], were selected for this project. Therefore, the use of the **L3** ligand (Chart 1), bearing positively charged external pyridylic sites should allow (once with the corresponding dinuclear species on hand) the electrostatic interaction with the above-mentioned surfaces. Therefore, herein we present the synthesis, characterization and catalytic activity of a new catalyst of the Ru-Hbpp family containing extra positively charged pyridylic ring on the terpy ligands (Chart 1). Furthermore, we report its anchoring onto TiO₂, SiO₂ and Nafion[®] surfaces, the characterization of this new hybrid materials and their catalytic evaluation with regards to the oxidation of water to dioxygen.

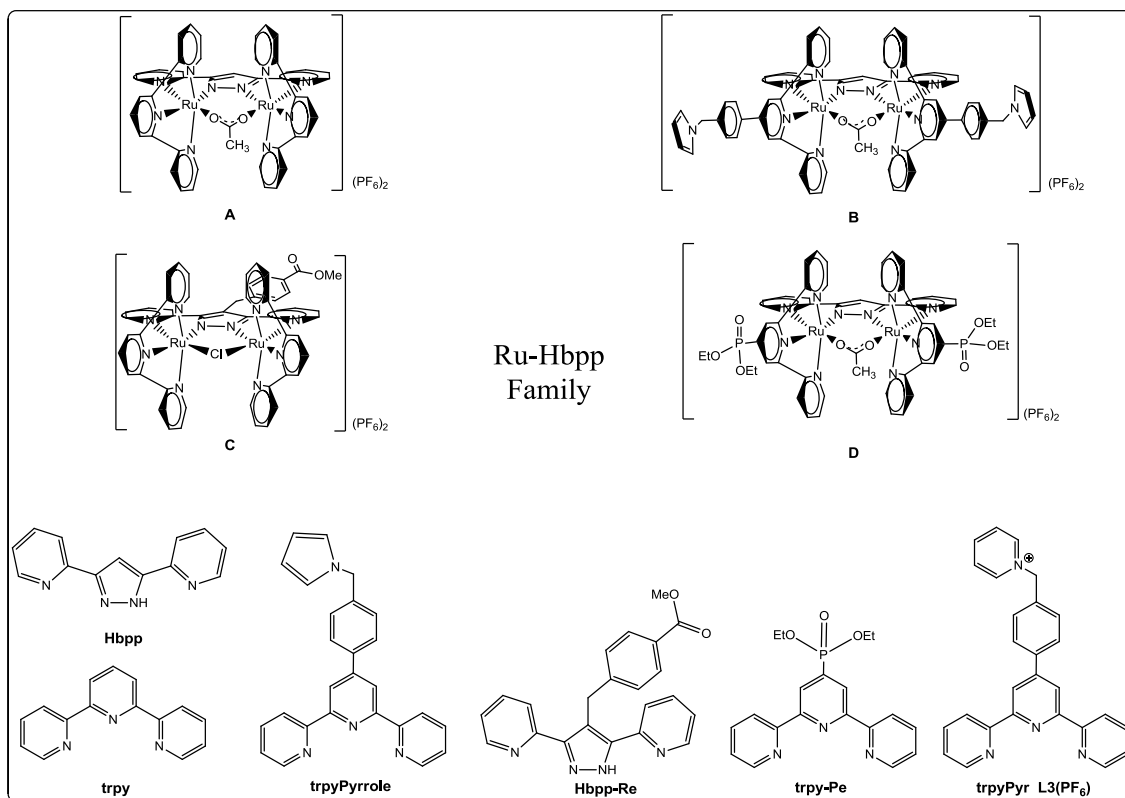
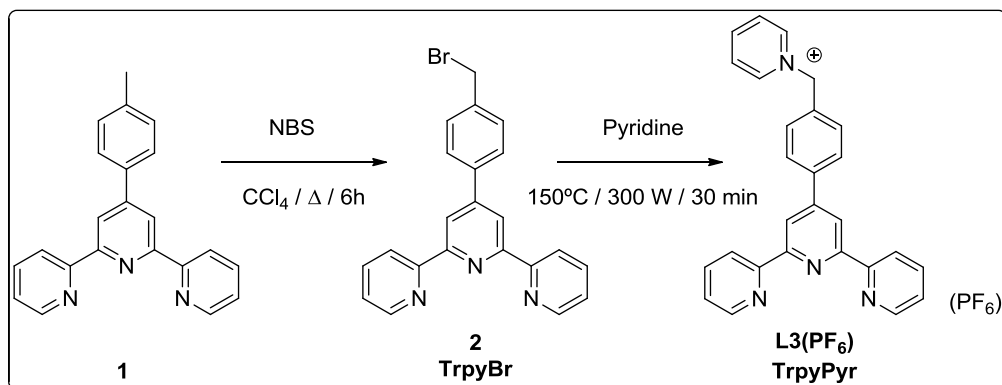


Chart 1. Drawing of previously reported Ru-Hbpp complexes (**A**, **B** and **C**), original Hbpp and trpy ligands and their modified counterparts including the trpyPyr ligand used in this work.

III.2. Results & Discussion

III.2.1. Ligand Synthesis

The synthesis of the trpyPyr ligand **L3(PF₆)** was carried out following the steps depicted in Scheme 1.



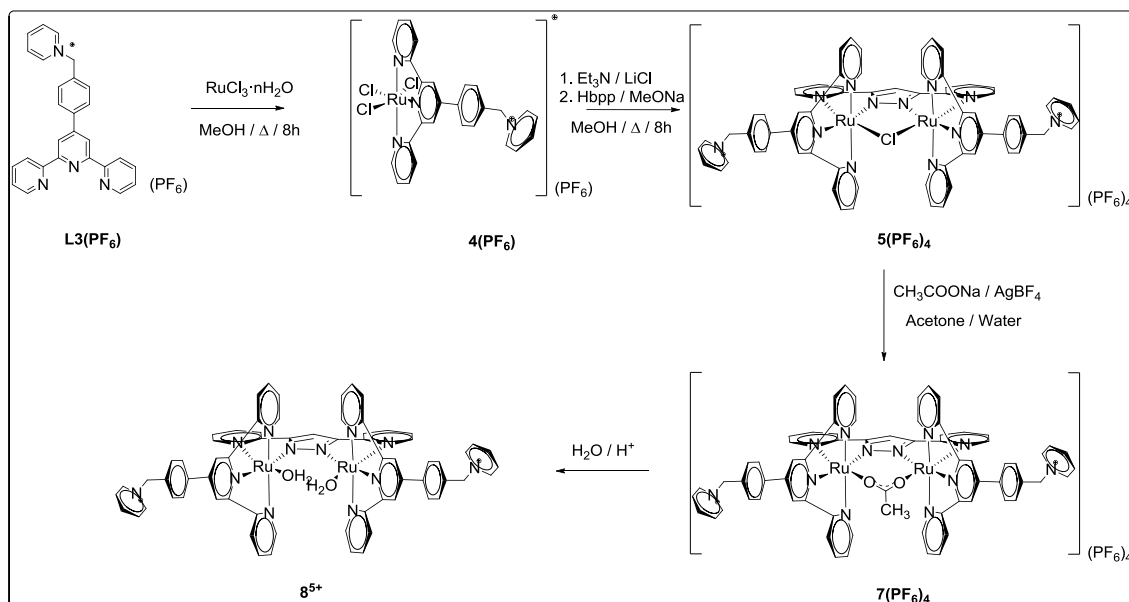
Scheme 1. Synthetic route for ligand **L3(PF₆)**.

TrpyBr **2** was obtained following an already published methodology,⁶ by the radical reaction of 4'-(4-Methylphenyl)-2,2':6',2''-terpyridine (**1**) with *N*-Bromosuccinimide (NBS) initiated by dibenzoyl peroxide. The bromomethyl derivative **2** was then subjected to a nucleophilic attack with pyridine which generates the cationic **L3** ligand. Although there was an already reported methodology for the synthesis of **L3**⁺,⁷ this procedure was improved by using a microwave reactor. After optimizing power, temperature and time parameters, shorter reaction times (from 48 h to 30 min) and better yields (from 70 % to 80 %) were obtained. After solvent evaporation and redissolution in water, the pure ligand was obtained by precipitation with NH₄PF_{6(aq)}. The purity of **2** and **L3(PF₆)** was checked by usual techniques: 1D and 2D NMR spectra of **L3(PF₆)** are shown in Figure S1 of the Supporting Information.

III.2.2. Synthesis of complexes

Synthesis of complexes **4(PF₆)**, **5(PF₆)₄**, **7(PF₆)₄** and **8⁵⁺** was carried out by following the usual procedures of our research group for this kind of complexes (Scheme 2).⁸ Reaction of RuCl₃·nH₂O with **L3(PF₆)** in refluxing methanol for four hours afforded a large amount of brown precipitate that increase after freezing. The brown solid material

was washed with cold MeOH to remove starting terpyridine **L3(PF₆)** ligand. **4(PF₆)** was then used for the next step without further purification; in fact Mass Spectrometry and Cyclic Voltammetry indicated the unique presence of our desired product (see Figures S5 and S8 in the Supporting Information).

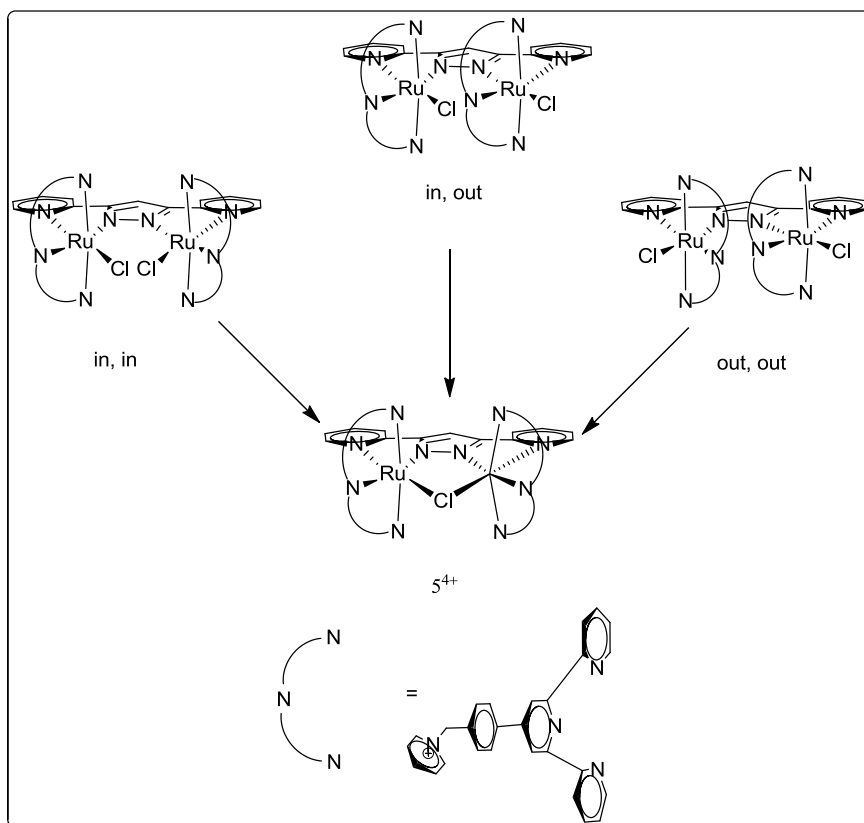


Scheme 2. Synthetic route for complexes **4(PF₆)**, **5(PF₆)₄**, **7(PF₆)₄** and **8⁵⁺**.

The synthesis of **5⁴⁺** was initially attempted following the usual conditions employed for the preparation of this kind of diruthenium chlorido-bridged complexes.^{1c} It is already known that $[\text{Ru}^{\text{II}}(\text{trpy})_2](\text{PF}_6)_2$ (usually called bis-terpyridine complex) use to be a secondary byproduct of this reaction. Therefore, for instance, this complex is also observed during the synthesis of the analogous $[\text{Ru}^{\text{II}}_2(\mu\text{-Cl})(\text{bpp})(\text{trpy})_2](\text{PF}_6)_2$ compound where, in order to get ride of it, an initial filtration of the reaction crude is mandatory. In our case, however, this filtration wasn't enough for removing all the $[\text{Ru}^{\text{II}}(\mathbf{3})_2](\text{PF}_6)_4$ (**6⁴⁺**) formed. Therefore, modification of the reaction conditions was necessary to obtain pure **5⁴⁺**. After several attempts modifying temperature and reaction times, a definitive process that minimize the formation of $[\text{Ru}^{\text{II}}(\mathbf{3})_2](\text{PF}_6)_4$ was established. Thus, the synthesis of **5⁴⁺** begins dissolving the ruthenium precursor **4⁺**, lithium chloride and triethylamine in methanol. On one hand, the lithium chloride salt ensures an excess of chlorido anions that avoids the coordination of more than one Hbpp ligand per ruthenium nuclei and keeps this anion occupying the sixth coordination position of the metal center. On the other hand, triethylamine is employed to reduce the ruthenium oxidation estate from Ru^{III} to Ru^{II} , which is the final oxidation state of our

complex. This reduction is easily monitored by the clear color switching, from brown to purple, of the initial Ru^{III} precursor. Subsequently, a methanolic solution of the Hbpp ligand and sodium methoxide is added to the reaction mixture. The base allows the deprotonation of the pyrazolic ring of the Hbpp ligand, which promote the chelating behavior of the ligand.

The synthesis of dinuclear species such as **5**⁴⁺ usually ends up with mixture of isomeric *in,out*, *in,in*, and *out,in* complexes, as shown in Scheme 3. The terms *in* and *out* indicate whether the Cl ligand is oriented toward or away, respectively, from the center of the Hbpp ligand. The irradiation of the reaction mixture with a Tungsten lamp shifts the equilibriums to obtain the desired Cl-bridged product **5**⁴⁺.



Scheme 3. Isomerization processes of *in,in*, *in,out* and *out,out* species towards **5**⁴⁺ forced by the irradiation of a tungsten lamp.

The reaction of **5**(PF₆)₄ with silver nitrate and sodium acetate results in the generation of **7**(PF₆)₄, which corresponds to the acetato-bridged derivate of our system. Therefore, the combination of silver and acetate sources promotes the decoordination of the Cl bridged (silver chloride is formed as a grey-white precipitate) and subsequent

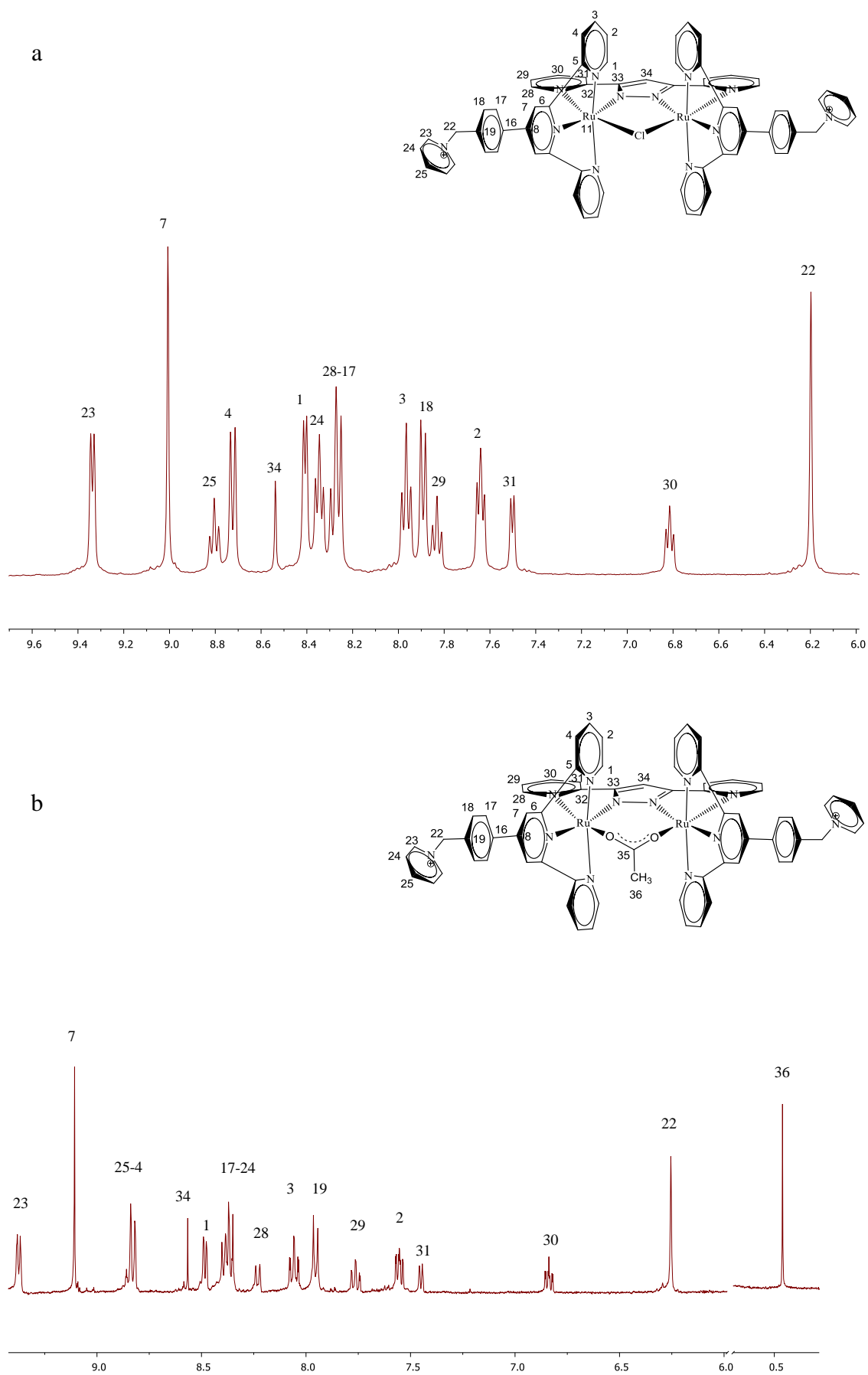
coordination of the acetato moiety. The dissolution of **7(PF₆)₄** in aqueous solution pH=1 (triflic acid 0.1 M) results in the generation of the bis-aqua complex **8⁵⁺**.

III.2.3. Characterization of **4(PF₆)**, **5(PF₆)₄**, **7(PF₆)₄** and **8⁵⁺**

The new compounds **4(PF₆)**, **5(PF₆)₄** and **7(PF₆)₄** have been fully characterized by the usual structural, spectroscopic and electrochemical techniques. In the present section the most important features of their characterization, in terms of NMR, X-Ray, Electrochemistry and UV-vis, will be discussed.

III.2.3.1. NMR spectroscopy

Nuclear Magnetic Resonance (NMR) experiments have been carried out for the diamagnetic **5(PF₆)₄** and **7(PF₆)₄** compounds (Figure 1 and Figures S2-S3 in the Supporting Information). Both 1D (¹H and ¹³C {¹H}) and 2D (COSY, HSQC and HMBC) experiments have proven to be the best tools in order to structurally characterize them in solution. The full assignment of the observed resonances can be made based on their integrals, symmetry and multiplicity. When assigning the ¹H-NMR of these molecules, their symmetry becomes a very useful tool. **5(PF₆)₄** displays C_{2v} symmetry in solution, with one symmetry plane containing the bpp⁻ ligand, the two Ru atoms, both central terpyridine nitrogen atoms and the bridging chlorido moiety. A second plane (perpendicularly bisecting the former) passes through the chlorido bridge and the central pyrazolic carbon and bisects the N-N bond of the same pyrazolic ring, thus interconverting the two terpyridine ligands. In the case of **7(PF₆)₄**, the same symmetry operations can be considered. The downfield shift of the singlet corresponding to H22 is in accordance with the high electron withdrawing effect of the closer pyridinium moiety and with others reported earlier in the literature.⁹



In the case of complex 7^{4+} , the up shift of the methylenic singlet with regards to 5^{4+} (from 6.2 to 6.3 ppm) and the presence of the acetate singlet peak at 0.45 ppm (Figure 1b) are experimental evidences of the successful exchange of the chlorido bridge by the acetato moiety.

III.2.3.2. X-ray Crystal Structures

Suitable crystals for X-Ray diffraction analysis have been obtained for $4(\text{PF}_6)$ and $5(\text{PF}_6)_4$. Figures 2 and 3 display an Ortep plot for the cationic moiety of these two complexes together with their corresponding atom labeling scheme. Acquisition and crystallographic data is reported as Supporting Information (Tables S1-S2).

Monocrystals of 4^+ were obtained by preparing a saturated solution of $4(\text{PF}_6)$ in nitric acid. Upon allowing the solution to stand at room temperature in an open vessel for one week, small brown crystals appeared. The resolution of the structure of 4^+ (Figure 2a) is especially interesting due to the typical difficulties on getting good crystals for these kind of $[\text{Ru}^{\text{III}}(\text{tpyX})\text{Cl}_3]$ precursors. A selection of the more relevant bond distances and angles is reported in Table 1.

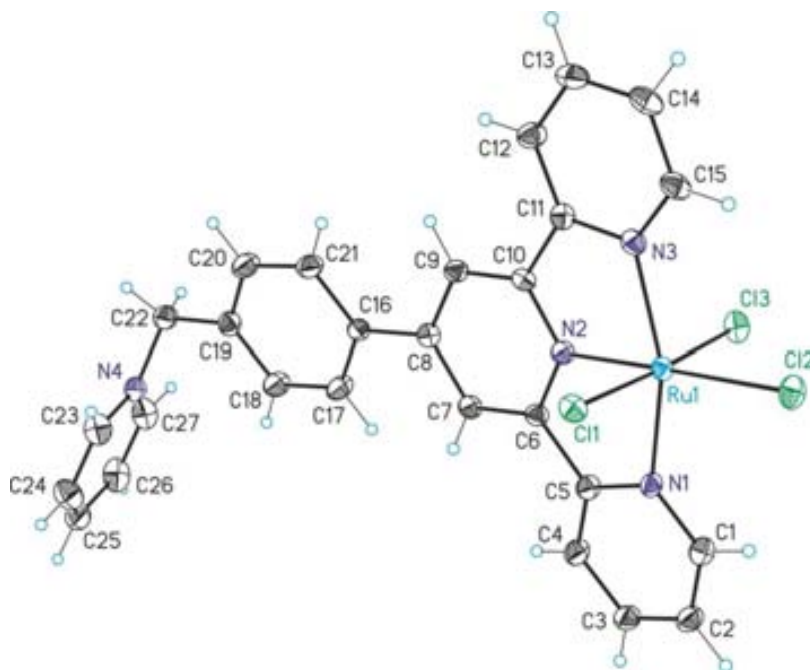
Table 1. Selected interatomic distances (Å) and angles (°) for complex 4^+ .

BOND DISTANCES			
Ru(1)-N(3)	2.073(2)	Ru(1)-N(1)	2.080(2)
Ru(1)-N(2)	1.961(2)	Ru(1)-Cl(3)	2.3429(6)
Ru(1)-Cl(2)	2.3787(6)	Ru(1)-Cl(1)	2.3435(6)
ANGLES			
N(3)-Ru(1)-N(1)	159.61(8)	N(3)-Ru(1)-N(2)	79.51(8)
N(1)-Ru(1)-N(2)	80.10(8)	N(3)-Ru(1)-Cl(3)	91.02(6)
N(1)-Ru(1)-Cl(3)	88.86(6)	N(2)-Ru(1)-Cl(3)	91.02(6)
N(3)-Ru(1)-Cl(2)	101.51(6)	N(1)-Ru(1)-Cl(2)	98.87(6)
N(2)-Ru(1)-Cl(2)	178.94(6)	Cl(3)-Ru(1)-Cl(2)	92.22(2)
N(3)-Ru(1)-Cl(1)	86.90(6)	N(1)-Ru(1)-Cl(1)	92.12(6)
N(2)-Ru(1)-Cl(1)	88.84(6)	Cl(3)-Ru(1)-Cl(1)	176.52(2)
Cl(2)-Ru(1)-Cl(1)	90.93(2)		

As expected, the ruthenium center is meridionally coordinated by the modified trpyPyr ligand $\text{L}3^+$ and three chlorido ions occupy the three remaining coordination sites. It can

be observed how the ruthenium ion adopts a distorted octahedral geometry with bond distances and angles comparable to analogous complexes reported earlier in the literature.¹⁰ The constrain imposed by the geometry of the trpy $\mathbf{L3}^+$ ligand is clearly detected in the N1-Ru-N3 angle, reduced from the ideal 180° to the observed 159° . $\mathbf{4}^+$ crystallizes with one nitrate anion and one nitric acid molecule linked by a hydrogen bond. Both molecules are situated next to the pyridinium positive charge. In contrast to the parent $[\text{RuCl}_3(\text{trpy})]$ complex, no hydrogen bond interactions and a less ordered packing are observed. Figure 2b represents the unit cell of the structure with a total of eight $\mathbf{4}^+$ cations. A head to tail orientation between the two central molecules of the unit cell is also observed.

a



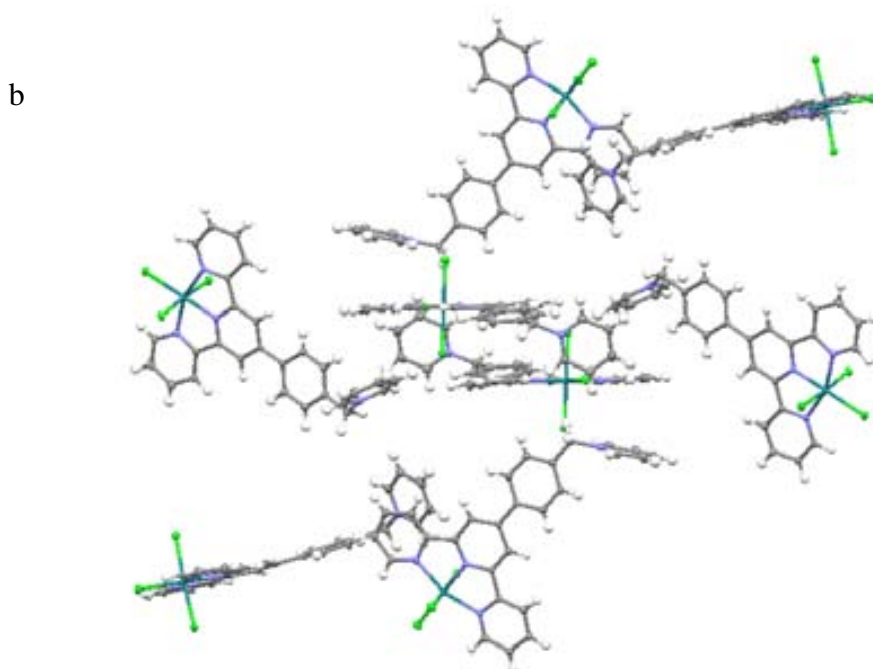


Figure 2. (a) Ortep plot (ellipsoid at 50 % probability) of the X-ray crystal structure of the cationic moiety of 4^+ with its corresponding labeling scheme. (b) Stereoscopic view of the unit cell for 4^+ (counteranions omitted for clarity).

The Ortep plot (ellipsoid at 50 % probability) of the X-ray crystal structure of the cationic moiety of 5^{4+} with the corresponding heteroatom-labeling scheme is reported in Figure 3a (see the full labeling Scheme in Figure S13 of the Supporting Information). Because of the packing effect imposed by the pyridinium moiety in the modified trpy $L3^+$ ligand, $5(PF_6)_4$ crystallizes in an extremely large cell with four independent complex molecules, sixteen PF_6 anions and several acetone and toluene molecules in the asymmetric unit (Figure 3b). In total 8 positions for acetone and 13 positions for toluene could be localized which were partially highly disordered. In order to avoid the highly disordered solvent molecules the program SQUEEZE was applied leading to a refined model with a R1 value of 7.43 % in which all the solvent molecules were removed.¹¹ Despite the different orientation of the pyridinium moieties in each molecule regarding the others, observed in Figure 3b, the four independent molecules have slightly different metric parameters, thus only the so called “A” complex will be described here. Each ruthenium metal adopts pseudo-octahedral coordination geometry with two positions occupied by the bpp ligand, three by the meridional functionalized terpyridine $L3^+$ ligand and the latest by a Cl-bridged ligand. Bond distances and angles have no significant differences with regards to related complexes previously described in the

literature.⁸ The different orientation of the pyridinium moieties in each molecule regarding the others, can be observed in Figure 3b.

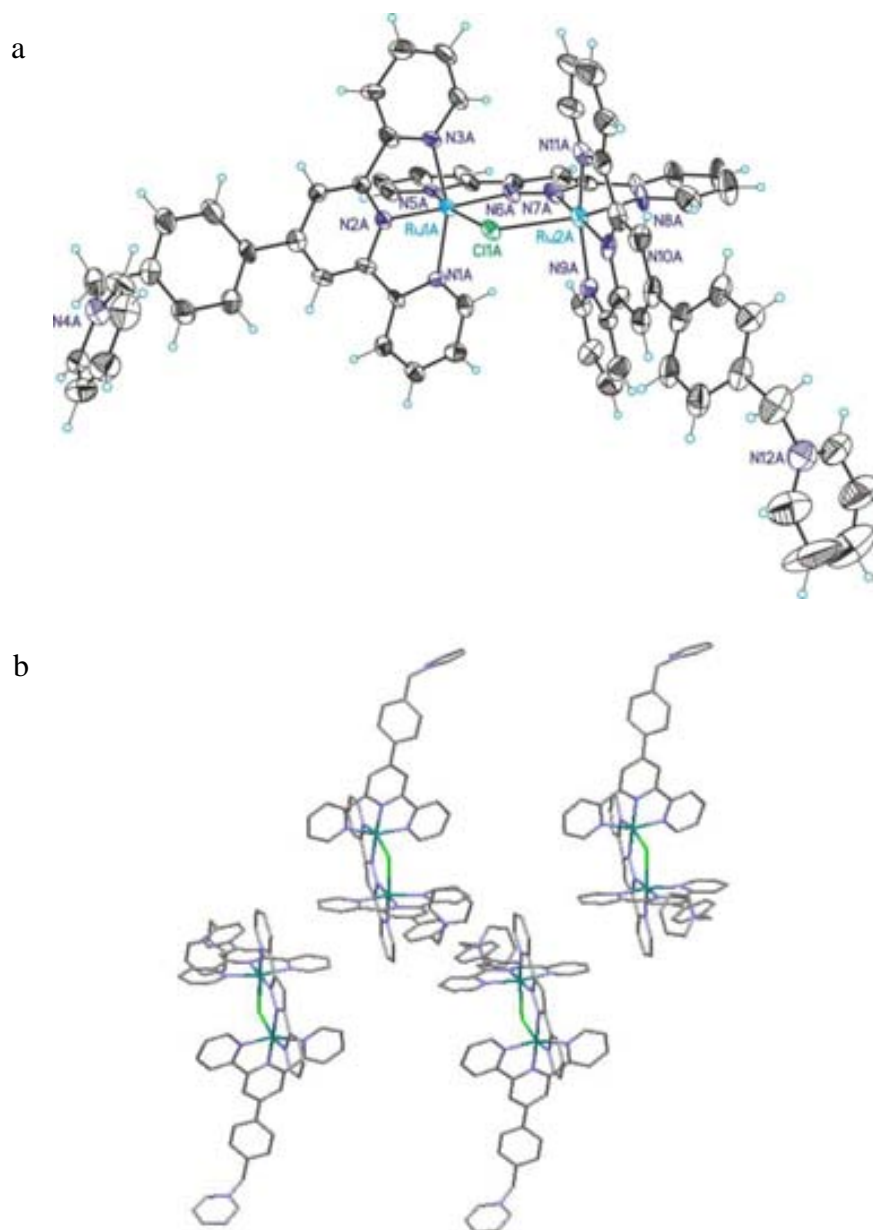


Figure 3. (a) Ortep plot (ellipsoid at 50 % probability) of the X-ray crystal structure of the cationic moiety of 5^{4+} with its corresponding labeling scheme for heteroatoms. (b) Stereoscopic view of the asymmetric unit for 5^{4+} (counteranions omitted for clarity).

III.2.3.3. Electrochemistry

The redox properties of the complexes described in the present work were investigated by means of CV and DPV and are reported in Table 2 and Figures 4-6. Unfortunately

the complexes were not soluble in CH₂Cl₂, so all experiments were performed in acetonitrile (**4**⁺), acetone (**5**⁴⁺ and **7**⁴⁺) and pH=1 water (**8**⁵⁺).

Table 2. Redox potentials in V (vs. SSCE) at a scan rate of 100 mV/s for **4**⁺, **5**⁴⁺, **7**⁴⁺, **8**⁵⁺ and their respective trpy homologues for comparison purposes.

	III/II			
Ru^{III}Cl₃(trpy)^a	0.01			
4⁺^a	0.05			
	III,II/II,II	III,III/III,II	IV,III/III,III	IV,IV/IV,III
[Ru^{II}₂(μ-Cl)(bpp)(trpy)₂]²⁺^c	0.71	1.12	-	-
5⁴⁺^b	0.79	1.20	-	-
[Ru^{II}₂(μ-AcO)(bpp)(trpy)₂]²⁺^c	0.73	1.05	-	-
7⁴⁺^b	0.76	1.09	-	-
[Ru^{II}₂(H₂O)₂(bpp)(trpy)₂]³⁺^d	0.54	0.61	0.81	1.10
8⁵⁺^d	0.59	0.59	0.90	1.00

^a Acetonitrile using 0.1 M of TABH as electrolyte. ^b Acetone using 0.1 M of TABH as electrolyte. ^c CH₂Cl₂ using 0.1 M of TABH as electrolyte. ^d Aqueous solution at pH=1 (0.1 M triflic acid)

The CV of **4**⁺ (Figure S5) exhibits a unique reversible wave at E_{1/2} = 0.05 V, (ΔE = 71 mV) corresponding to the following process:



Comparison with the related complex, [Ru^{III}Cl₃(trpy)] (Figure S4) (E_{1/2} = 0.01 V, ΔE = 69 mV) revealed an up shift of the E_{1/2}. This expected behavior was assigned to the electron-withdrawing effect of the extra pyridinium group.

The CV of **5**⁴⁺ in acetone exhibits two reversible waves and is displayed in Figure 4. These two processes are assigned to the following electrochemical reactions (the **L3**⁺ and bpp ligands are not shown for the sake of clarity):



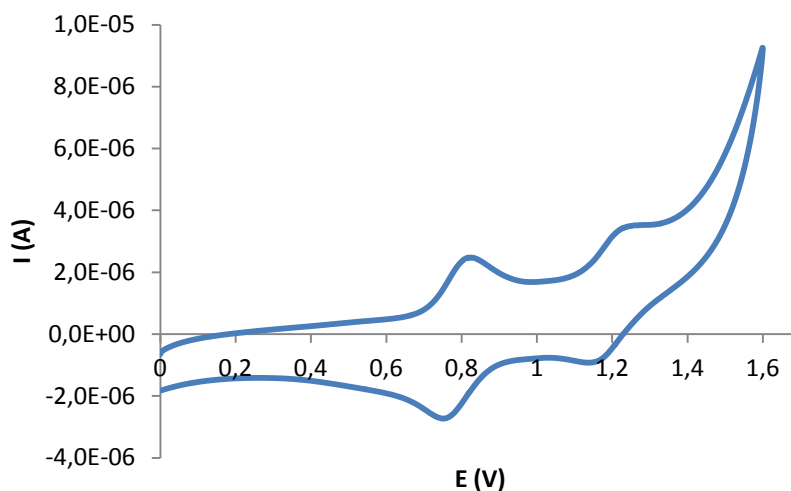


Figure 4. Cyclic voltammogram for the chlorido-bridged complex 5^{4+} in 0.1 M $n\text{-Bu}_4\text{NPF}_6$ in acetone at 100 mV/s scan rate. Glassy carbon electrode is used as working electrode and the potential is measured vs. SSCE.

The CV in acetone of 7^{4+} is displayed in Figure 5. Two reversible waves are observed at 0.76 and 1.09 V corresponding to the RuIII-RuII/RuII-RuII and RuIII-RuIII/RuIII-RuII processes. Both 5^{4+} and 7^{4+} contain two extra terminal pyridylic rings with a positive charge, which is expected to influence the redox potentials of the Ru metal ions.¹² Accordingly, a clear up shift of the $E_{1/2}$ is observed when comparing their redox potentials with the ones previously reported for the related complexes $[\text{Ru}^{\text{II}}_2(\mu\text{-Cl})(\text{bpp})(\text{trpy})_2]^{2+}$ and $[\text{Ru}^{\text{II}}_2(\mu\text{-AcO})(\text{bpp})(\text{trpy})_2]^{2+}$ (see Table 2).

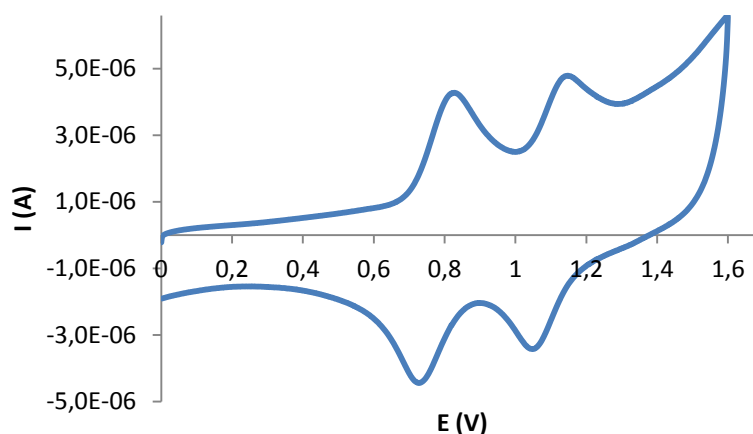


Figure 5. Cyclic voltammogram for the acetato-bridged complex 7^{4+} in 0.1 M $n\text{-Bu}_4\text{NPF}_6$ in acetone at 100 mV/s scan rate. Glassy carbon electrode is used as working electrode and the potential is measured vs. SSCE.

The electrochemistry of $\mathbf{8}^{5+}$ has been investigated after its “in-situ” generation in a pH 1 aqueous solution (0.1 M triflic acid) using $\mathbf{7}^{4+}$ as a precursor (see Scheme 2).

From the CV (Figure S6) and DPV (Figure 6) of $\mathbf{8}^{5+}$ a total of three waves are observed. These have been tentatively assigned, taking into account previous results on related complexes,⁸ to a total of four redox processes (the first wave contains two electrochemical processes).



As can be observed in Table 2, in this case no significant changes are observed when comparing the potentials of $\mathbf{8}^{5+}$ with regard to those of the related Hbpp complex $[\text{Ru}^{\text{II}}_2(\text{H}_2\text{O})_2(\text{bpp})(\text{trpy})_2]^{3+}$. When the potential is increased further up to 1.3 V a large anodic current is observed in the DPV that is associated with a further one electron oxidation of the complex concomitant with the electrocatalytic oxidation of water to dioxygen in agreement with equations (8) and (9).



The oxidation process related to the equation 8 is not observed in the DPV (Figure 6) given the concomitant and fast electrocatalytic current corresponding to the oxidation of water.

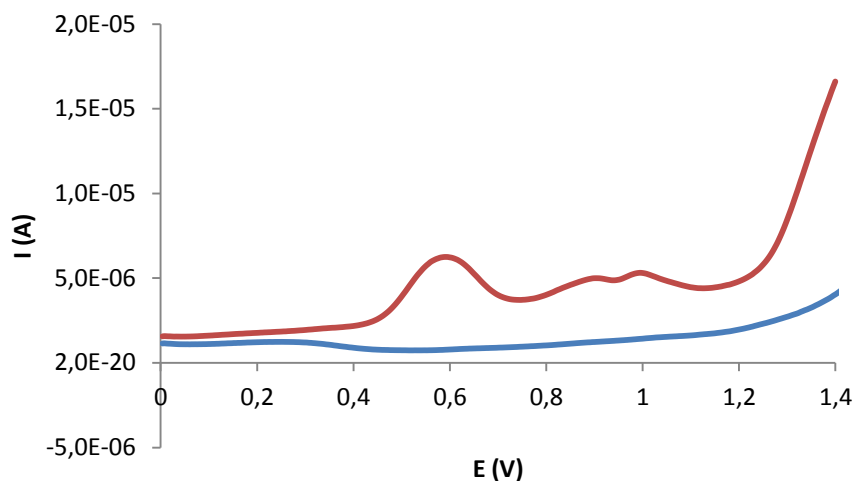


Figure 6. Differential Pulse Voltammetry for 8^{5+} (red line) and for the corresponding blank (blue line) at pH = 1.0 in 0.1 M triflic acid aqueous solution. Glassy carbon electrode is used as working electrode and the potential is measured vs. SSCE.

III.2.3.4. UV-vis

The UV-vis spectrums of 5^{4+} , 7^{4+} and 8^{5+} have been recorded and are displayed in Figure 7. As general trend two regions can be observed: one between 350 nm and 550 nm, where unsymmetrical broad typical metal-to-ligand charge transfer (MLCT) bands appear, and a second one above 550 nm in which d-d transitions are observed. Above 350 nm 7^{4+} displays three bands at 366, 497 and 525 nm that can be tentatively assigned to $d\pi(\text{Ru}) \rightarrow \pi^*$ N-ligands transitions.¹³

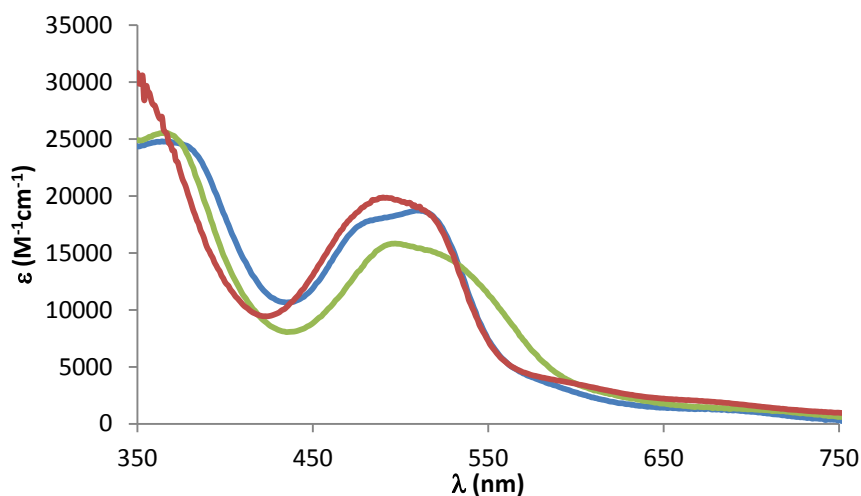
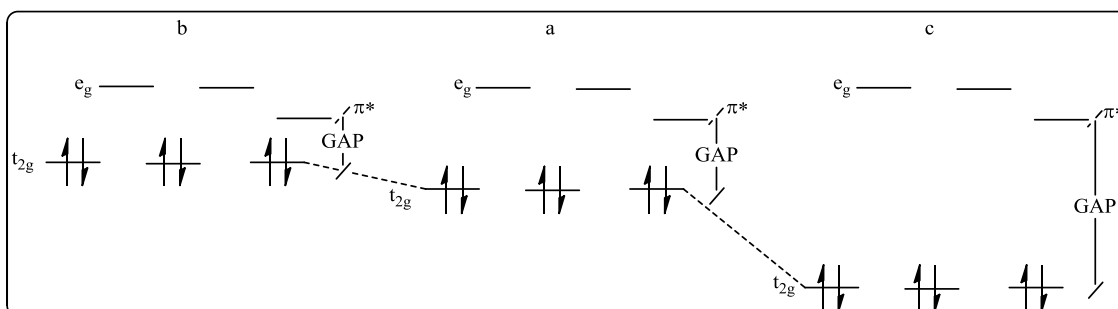


Figure 7. UV-vis spectra for 5^{4+} (blue line) and 7^{4+} (green line) in 26 μM acetone solutions and 8^{5+} (red line) in 96 μM acetone:water (pH=1) (20:80) solution.

For the acetato-bridged complex 7^{4+} the MLCT bands are shifted to longer wavelengths due to the relative destabilization of $d\pi(\text{Ru})$ levels provoked by the acetato ligand. The relative stabilization or destabilization caused by the bridging ligand is displayed in Scheme 4. As it can be observed, the higher the $d\pi(\text{Ru})$ destabilization (Scheme 4b) the shorter the GAP and consequently the longer the wavelength observed.¹⁴



Scheme 4. MO diagram for ideal MLCT (a), affected by a $d\pi$ destabilizing ligand (b) and MLCT affected by a $d\pi$ stabilizing ligand (c).

III.2.4. Synthesis and characterization of supported systems

Once with well characterized molecular systems on hand the next step of this project was the preparation of hybrid materials by combining the molecular species with solid supports such as SiO_2 , TiO_2 and Nafion. In all cases the attachment took place by means of ionic interactions, as described in the following subsections.

III.2.4.1. Silica- 7^{4+}

SiO_2 is an all-inorganic oxide potentially able to strongly interact with complexes 5^{4+} and 7^4 by means of ionic interactions between the pyridinium moieties of the complexes and the negatively charged SiO^- residues of the inorganic support. Moreover, silica does not contain any organic framework and, therefore, no degradation of the solid support in the harsh WO catalytic conditions is expected.

The SiO_2 material was previously activated by treatment in a muffle oven at 500 °C for 5 h. When 10 ml of 0.803 mM acetone solution of 7^{4+} were poured into 3 g of silica, the wine colorful solution became almost instantly colorless. The final colorless nature of the solution clearly indicates the successful anchoring of 7^{4+} . The pink powder is

filtrated on a plate, washed with fresh acetone and water and finally air dried. The absence of UV-vis signal in the washing acetone revealed the stability of the new hybrid material (see Figure S7 in the Supporting Information).

III.2.4.2. FTO-TiO₂-5⁴⁺

As previously mentioned in the introductory section, FTO-TiO₂ films have been widely used by our research group and others due to they are rugged solid supports that not suffer oxidative degradation. However, till now all the reported systems had a covalent bond between the molecular unit and the TiO₂ surface. In our case and as a project in parallel to the silica system, TiO₂ has been tested as a potential anionic support, also able to ionically interact with the positively charged pyridinium group of the 5⁴⁺ complex.

FTO-TiO₂ films have been prepared following the common procedure of our laboratory (see Experimental Section for further details). FTO-TiO₂ films were soaked overnight in a 0.3 mM acetone solution of 5⁴⁺. After that time the films were washed with fresh acetone several times and air-dried. The amount of anchored catalyst was confirmed by means of UV-vis spectroscopy. The use of films previously activated at pH=12 (overnight soaked on a 10 ml pH 12 solution) ended up in higher amounts of catalyst anchored as displayed on Figure 8. It is proposed that, under these conditions, TiO⁻ residues are generated on the surface of the solid support, thus allowing a better support/catalyst ionic interaction.

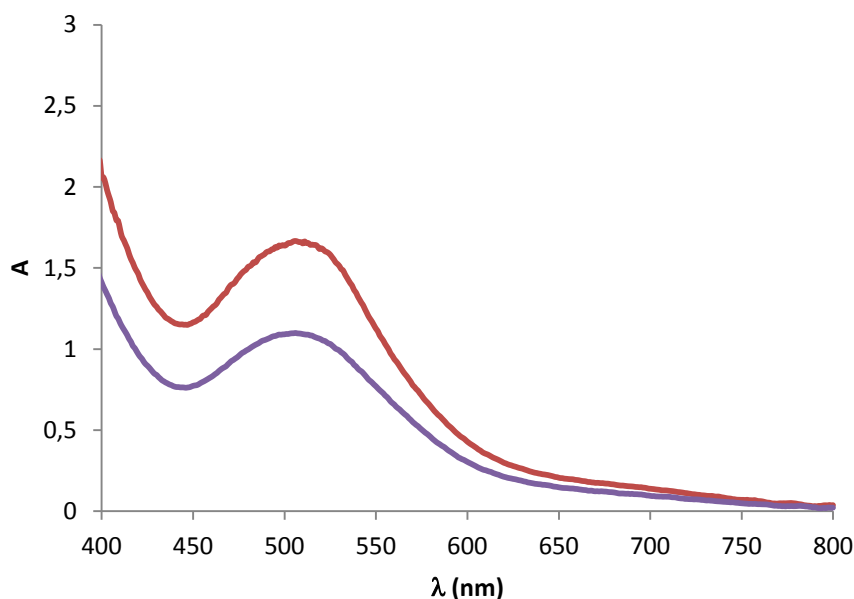


Figure 8. UV-vis spectra of a FTO-TiO₂-5⁴⁺ film with (red line) and without (purple line) previous overnight activation at pH=12.

The number of moles of metal complex per square centimeter (Γ) was calculated as reported in the literature,^{15,3(a)} considering the following equation:

$$\Gamma = A(\lambda) / [10^3 \varepsilon(\lambda)]$$

Where $A(\lambda)$ and $\varepsilon(\lambda)$ are, respectively, the absorbance and molar extinction coefficient at a given wavelength λ .

The electrochemical properties of FTO-TiO₂-5⁴⁺ have been also investigated by means of CV in DCM. The corresponding voltammogram is shown in Figure 9. This new hybrid material presents similar potentials (0.81 V and 1.18 V) to those found for complex 5⁴⁺ (0.79 and 1.20 V), revealing that no changes in the electrochemical (and thus structural) properties of the catalyst have occurred during the anchoring process.

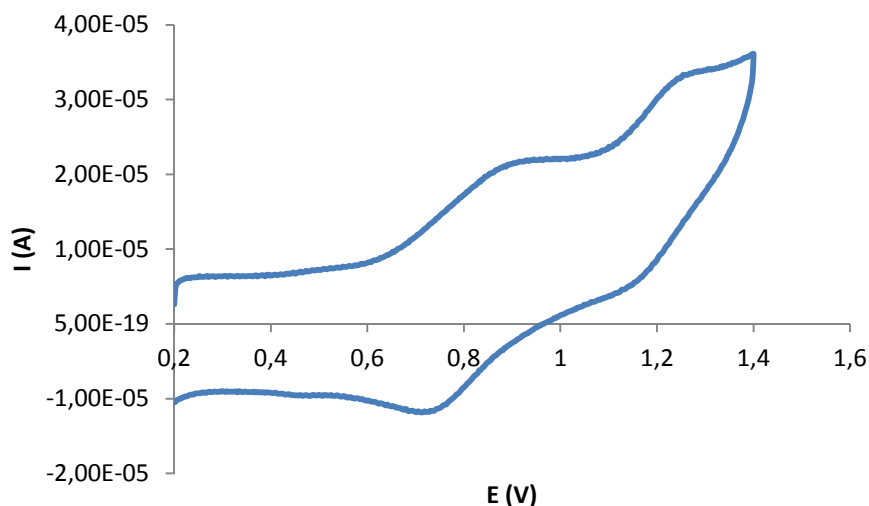
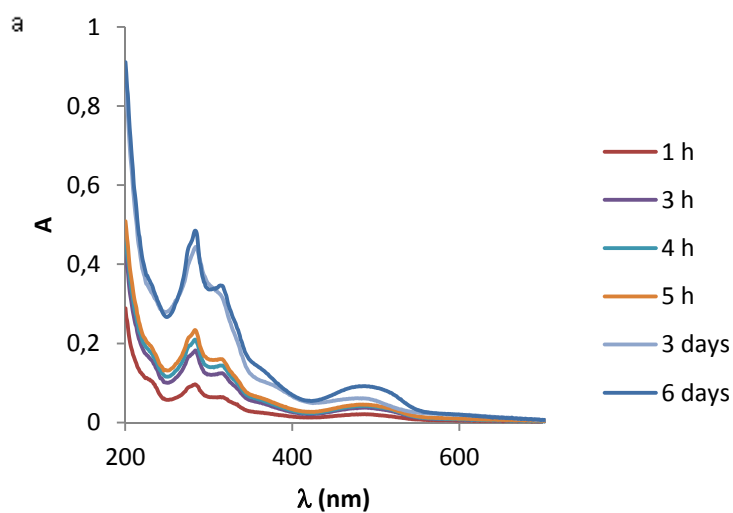


Figure 9. Cyclic voltammogram for FTO-TiO₂-5⁴⁺ in 0.1 M *n*-Bu₄NPF₆ in CH₂Cl₂ at 100 mV/s scan rate. FTO is used as working electrode and the potential is measured vs. SSCE.

The stability of the films under acidic (pH=1), neutral (pH=7) and basic (pH=12) solutions has been tested and monitored by UV-vis. The spectra of those solutions recorded along several hours/days are displayed in Figure 10.



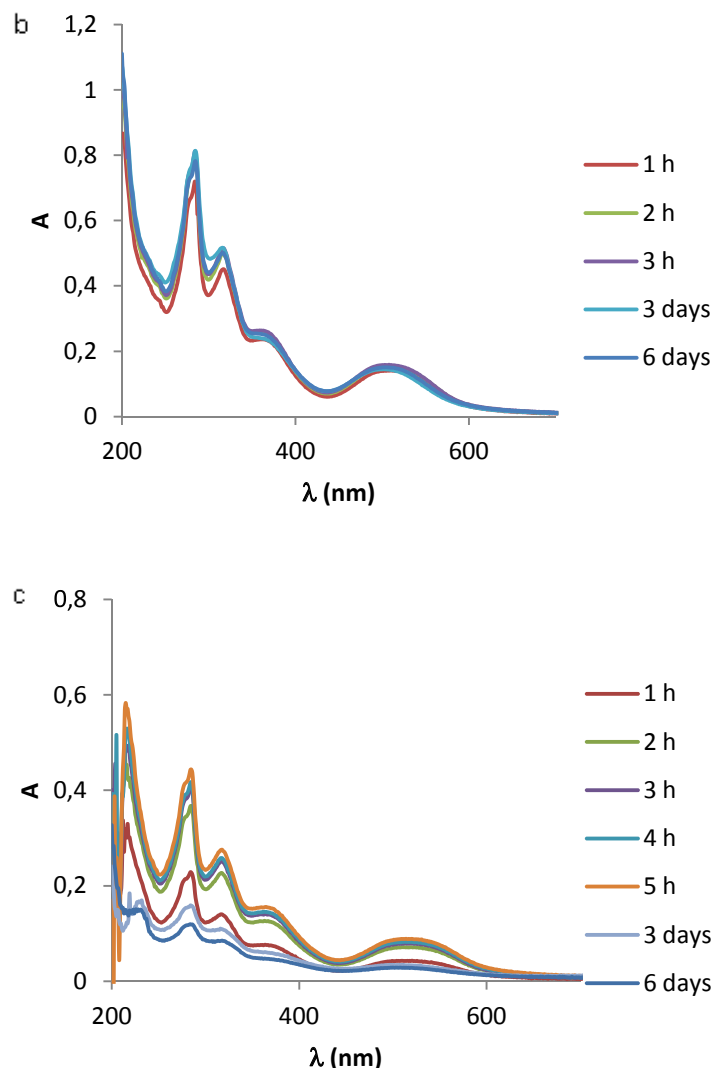


Figure 10. UV-vis monitoring of the stability of the generated FTO-TiO₂-5⁴⁺ films when soaked in pH = 1 (a), pH = 7 (b) and pH = 12 (c) aqueous solutions.

The observed absorbance increase with time of the acidic and neutral solutions containing soaked FTO-TiO₂-5⁴⁺ films points out the instability of the anchoring at these pH values. Surprisingly, a detachment/reattachment process of 5⁴⁺ is observed when the electrode is soaked at pH 12 (Figure 10c). The early absorbance increase reveals an initial leaching that, after three days, is clearly reversed (a decrease in absorbance is then observed). This latter behavior can be due to the activation of the TiO₂ surface (generation of TiO⁻ anions at basic pH) like previously indicated.

III.2.4.3. Nafion[®]

Nafion[®] is a polymer of perfluorinated carbon chains, which end up with sulfonate residues as shown in Figure 11. Once deprotonated, each sulfonate group can interact electrostatically with the positive charges of the pyridinium salts of our catalyst. The absence of any $-CH-$ suitable to be oxidized and the presence of these sulfonate groups converts this material in an excellent candidate for the anchoring of both 5^{4+} and 7^{4+} . For the purposes of this work, nafion was obtained from Sigma Aldrich as a 5% solution in a mixture of water and low-weight alcohols.

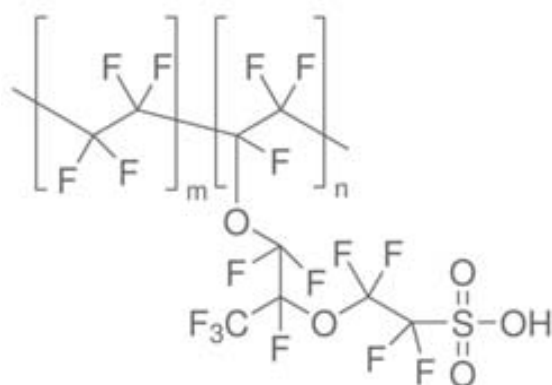
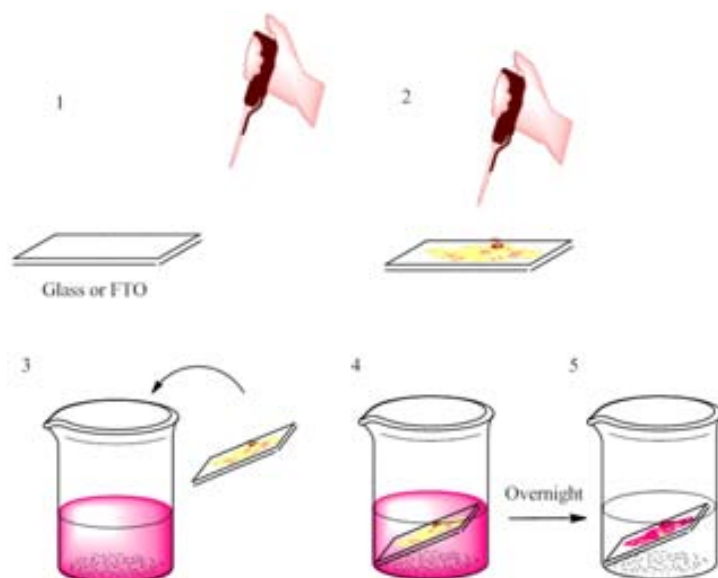


Figure 11. Schematic representation of the Nafion[®] Polymer

FTO-Nafion films have been prepared depositing a known volume of the Nafion[®] solution on a piece of FTO film as shown in Scheme 5. The films are then oven dried at 100 °C for 30 min. After cooling at room temperature the FTO-Nafion supports are soaked overnight into acetone solutions of 5^{4+} or 7^{4+} . The final colorless nature of the solution after that time clearly points out the complete attachment of the catalyst onto the Nafion[®] polymer.



Scheme 5. Procedure for the production of Nafion films over FTO electrodes and the subsequent attachment of 5^{4+} and 7^{4+} to prepare FTO-Nafion- 5^{4+} and FTO-Nafion- 7^{4+} . (1-2) Deposition and drying of the Nafion solution. (3-5) Attachment of the catalyst onto the FTO-Nafion surface.

The new hybrid materials FTO-Nafion- 5^{4+} and FTO-Nafion- 7^{4+} have been electrochemically characterized by means of CV and DPV (See Figures 12-13) and its redox potentials has been compared with their homogeneous counterparts. The CV of FTO-Nafion- 5^{4+} , shown in Figure 12, displays two chemically reversible redox waves at $E_{1/2} = 0.64$ V ($\Delta E_p = 113$ mV) and at $E_{1/2} = 1.05$ V ($\Delta E_p = 113$ mV) that are assigned to the RuIII/RuII \rightarrow RuII/RuII and RuIII/RuIII \rightarrow RuIII/RuII couples. At this point, we were not able to assign a less intense and new band observed at 0.04 V.

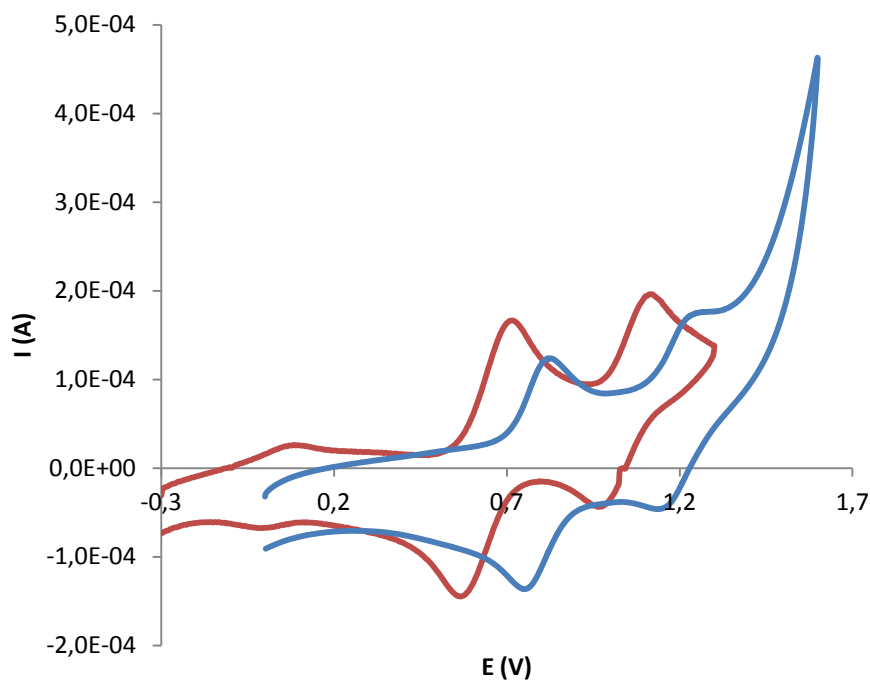
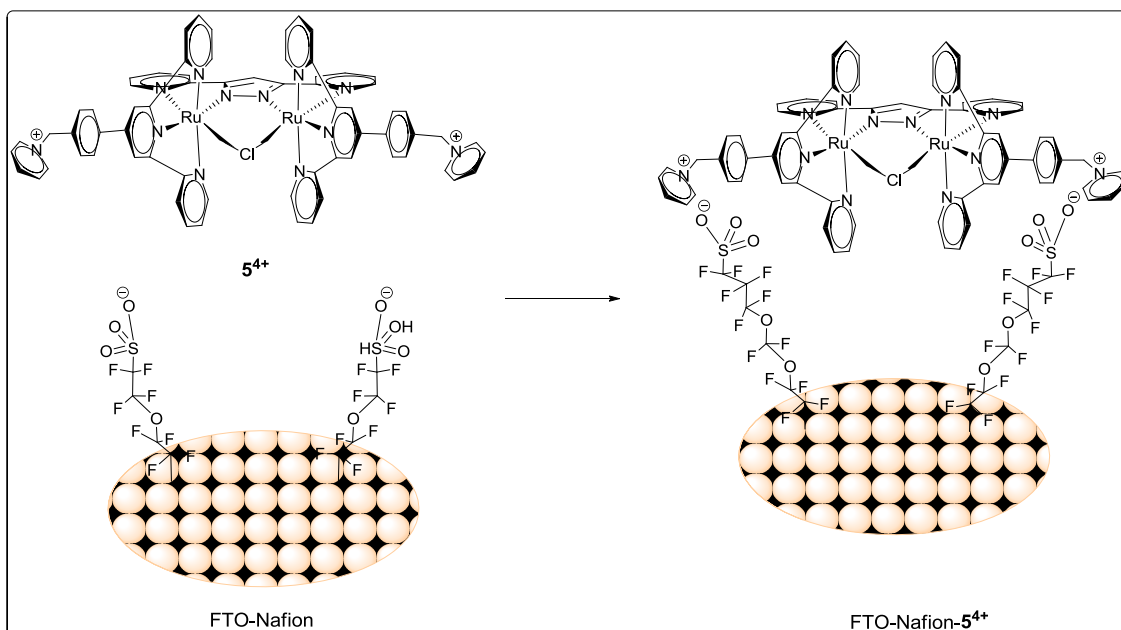


Figure 12. Cyclic voltammogram for the chlorido-bridged complex 5^{4+} (in blue, signal increased 50 times for purposes of comparison) and FTO-Nafion- 5^{4+} (red line) in 0.1 M n -Bu₄NPF₆ in acetone at 100 mV/s scan rate. Glassy carbon electrode for 5^{4+} and FTO for FTO-Nafion- 5^{4+} are used as working electrodes. The potential is measured vs. SSCE.

A downshift of about 100 mV in $E_{1/2}$ is observed when comparing the FTO-Nafion- 5^{4+} with its homogeneous counterpart, 5^{4+} . This behavior can be explained by the less electron withdrawing effect of the pyridinium salts when its positive charge ionically interacts with the Nafion sulfonate residues as drawn in Scheme 6.



Scheme 6. Schematic representation of the proposed interaction between a FTO-Nafion support and catalyst 5^{4+} .

The CV of FTO-Nafion- 7^{4+} shown in Figure 13 displays two chemically reversible redox waves at $E_{1/2} = 0.10$ V ($\Delta E_p = 115$ mV) and at $E_{1/2} = 0.79$ V ($\Delta E_p = 200$ mV) that are assigned to the RuIII/RuII \rightarrow RuII/RuII and RuIII/RuIII \rightarrow RuIII/RuII couples.

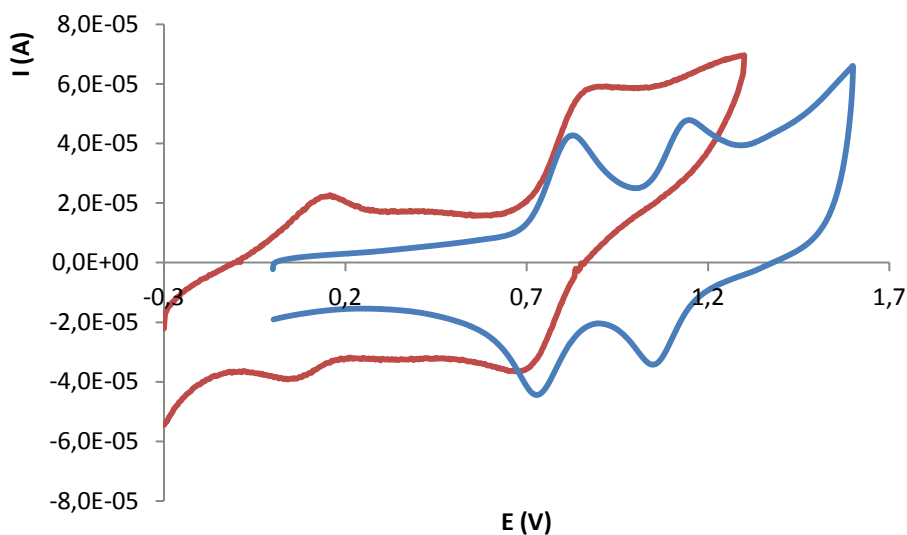
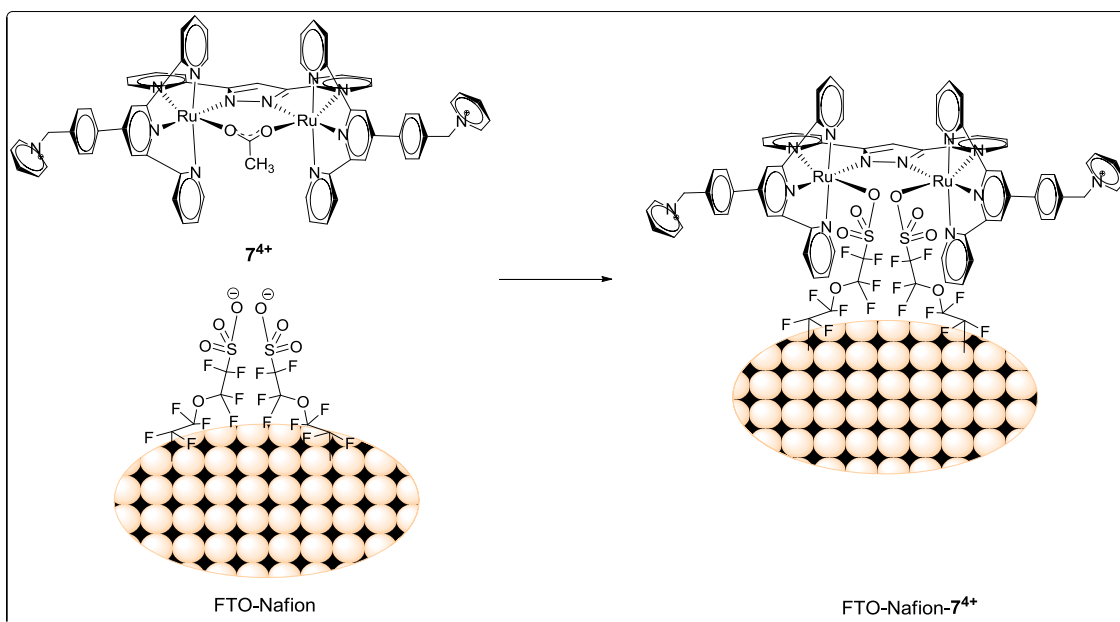


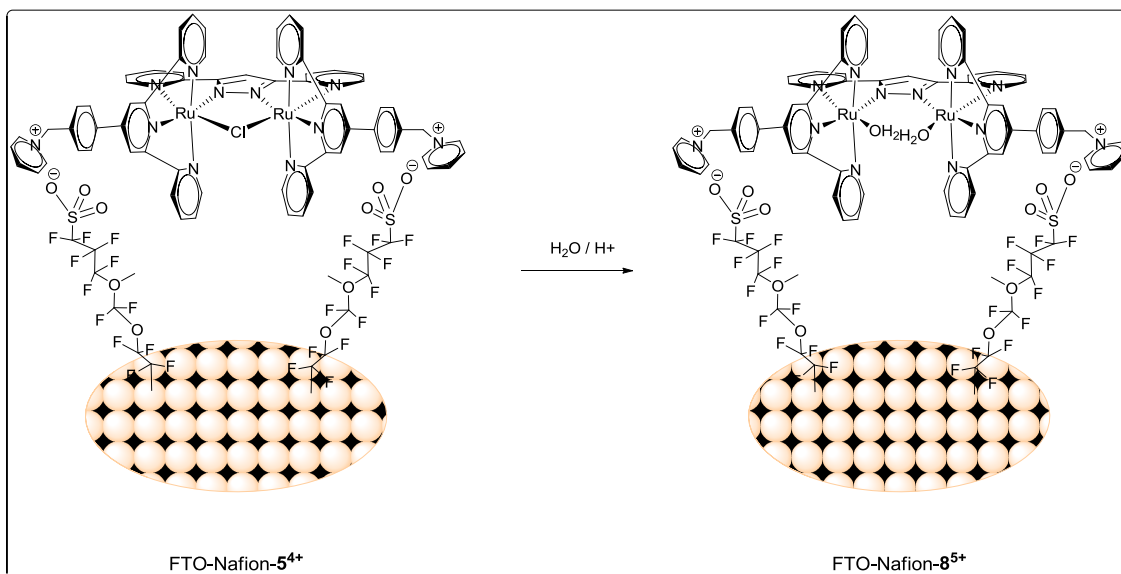
Figure 13. Cyclic voltammogram for the acetato-bridged complex 7^{4+} (blue line, signal increased 10 times for comparison purposes) and FTO-Nafion- 7^{4+} (red line) in 0.1 M n -Bu₄NPF₆ in acetone at 100 mV/s scan rate. Glassy carbon electrode for 7^{4+} and FTO for FTO-Nafion- 7^{4+} are used as working electrodes. The potential is measured vs. SSCE.

The clear and large downshift of both redox waves (660 mV and 300 mV) when compared with the ones observed for its homogeneous counterpart 7^{4+} suggests changes in the first coordination sphere of the ruthenium metal ions during the anchoring process and towards a more electron-donating environment. Taking into account this experimental result, the coordination of at least one sulfonate residue to the Ru metal centre is proposed, as drawn in Scheme 7.



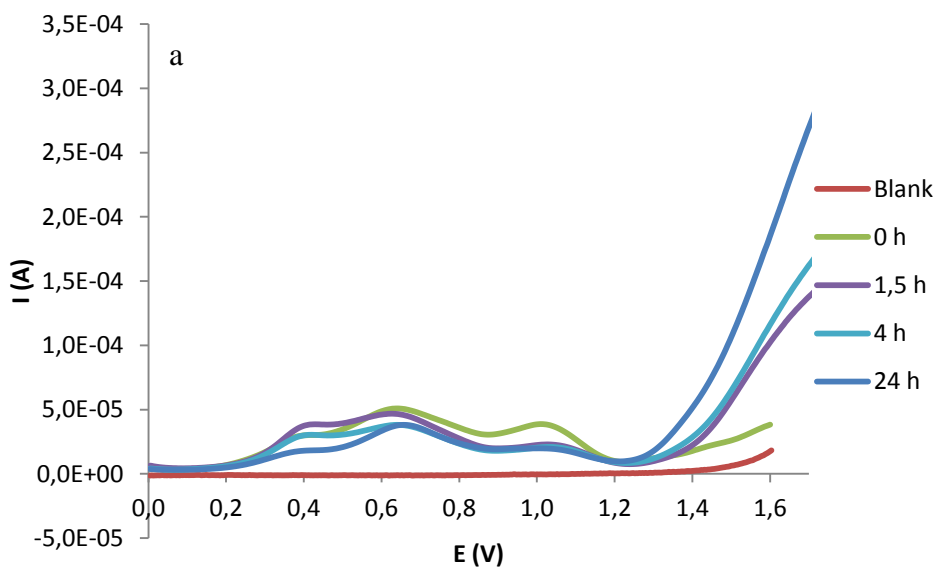
Scheme 7. Schematic representation of the proposed interaction between FTO-Nafion and complex 7^{4+} .

Both films have been investigated in terms of their electrocatalytic capacity to oxidize water to dioxygen at pH = 1.0 in a 0.1 M triflic acid aqueous solution and the results are displayed in Figure 14. The DPV of FTO-Nafion- 5^{4+} (Figure 14a) shows the lower intensity of the redox waves (when compared with the ones observed in organic solvents) and the “activation” of the film characterized by the growing of an electrocatalytic wave at around 1.4 V, assigned to electrochemically triggered water oxidation reaction. These results are in agreement with the exchange of the chlorido-bridged ion for two water molecules as shown in Scheme 8. As here reported, the “in-situ” generation of Ru-OH₂ species from Ru-Cl counterparts in acidic media usually implies a decrease on the intensity of the redox waves and allows observing both, several oxidation states in a narrow potential range and electrocatalytic currents due to WO catalysis. This has been extensively studied for several related systems^{1 c,5,12}



Scheme 8. Schematic representation of the proposed exchange of the chlorido-bridged ion for two water molecules in FTO-Nafion-5⁴⁺.

In contrast, the DPV of FTO-Nafion-7⁴⁺ (Figure 14b) shows neither exchange of the redox waves nor increase of the electrocatalytic current. The latest is in agreement with the above-proposed coordination of at least one sulfonate group to the Ru metal center and the consequent blocking of the catalytic activity.



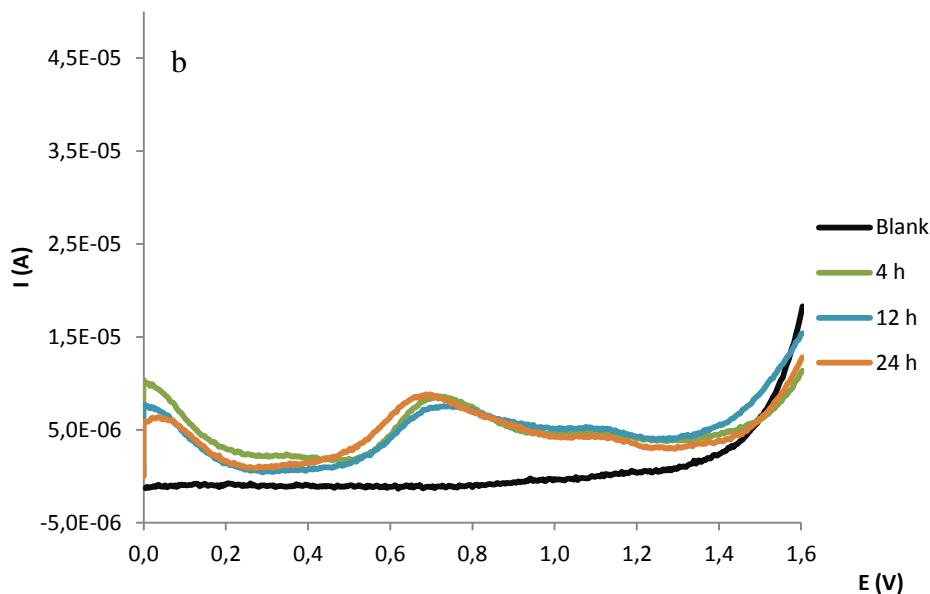
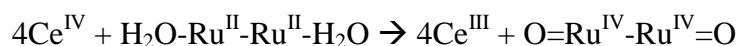


Figure 14. DPV of FTO-Nafion- 5^{4+} (a) and FTO-Nafion- 7^{4+} (b) in aqueous solutions at pH = 1.0 in 0.1 M triflic acid. FTO is used as working electrode and the potential measured vs. SSCE.

III.2.5. Water Oxidation Catalysis

Complex 7^{4+} and the hybrid materials Silica- 7^{4+} , FTO-TiO₂- 5^{4+} and FTO-Nafion- 5^{4+} have been tested as potentials catalysts towards the oxidation of water to dioxygen. Depending on the stability, molar concentration and catalytic efficiency of those new materials, different oxidants and oxygen measurement techniques have been used. The oxidation of the Ru(II) metal ions towards the Ru(IV) active species was carried out by two different methodologies:

- i Chemically** Ce(IV) species act as sacrificial oxidant for the diruthenium aqua complex following the reaction:



When using Ce(IV) as oxidant, manometry (measuring the total gas evolved) and a Clark electrode in solution (O₂ selective) have been the oxygen measurement techniques employed.

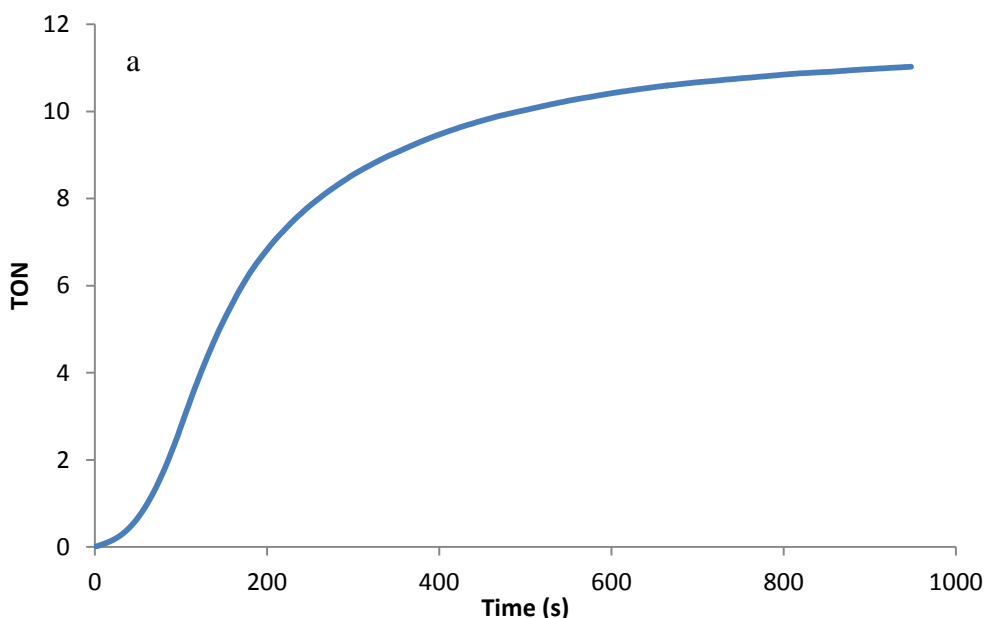
- ii Electrochemically** The application of a controlled potential (CPE, controlled potential electrolysis) allows the oxidation of Ru(II) species towards

Ru(IV) without adding any chemical oxidant. In this case a Clark electrode followed oxygen evolution in the gas phase.

Clark electrodes (in solution and in the gas phase) are O₂ selective sensors. However, manometric measurements allow measuring the total amount of gas formed during the catalytic process. Therefore their combination with Mass Spectrometry is required in order to determine the nature of the evolved gases.

III.2.5.1. Chemically triggered materials

The complex **8**⁵⁺ (Figure 15) and the hybrid materials Silica-**8**⁵⁺ (Figure 16) and FTO-Nafion-**8**⁵⁺ (Figure S14) have been tested as water oxidation catalysts in presence of (NH₄)₂Ce^{IV}(NO₃)₆ as sacrificial oxidant. All have been generated *in situ* from **7**⁴⁺, Silica-**7**⁴⁺ and FTO-Nafion-**5**⁴⁺ respectively when poured into the catalytic conditions (as previously demonstrated in the electrochemistry section). The total gas evolved has been manometrically measured and the O₂:CO₂ ratio analyzed by means of Mass Spectrometry for **8**⁵⁺ and Silica-**8**⁵⁺ meanwhile the O₂ generated in solution was detected by a Clark electrode for the FTO-Nafion-**8**⁵⁺. The overall catalytic results, together with the ones corresponding to related systems for purposes of comparison, are displayed in Table 3.



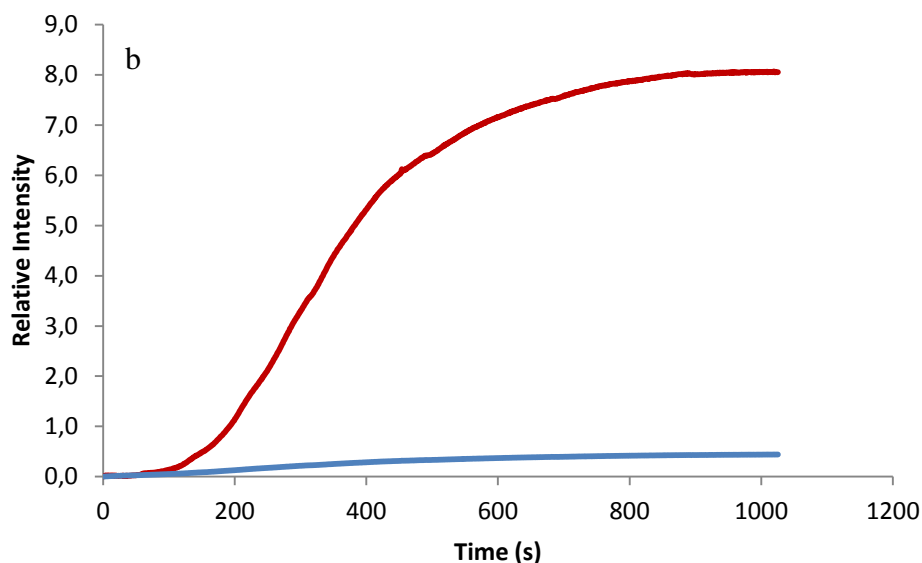


Figure 15. Chemical water oxidation with 7^{4+} (1 mM) at pH =1.0 in 0.1M triflic acid solution in the presence of $(\text{NH}_4)_2\text{Ce}^{\text{IV}}(\text{NO}_3)_6$ (100 mM). (a) Manometric measurement. (b) On-line mass spectroscopy (red line: O_2 blue line: CO_2)

As shown in Figure 15a (and Table 2, entry 3), when the acetato-bridged 7^{4+} is employed as precursor, 12 TONs are achieved. Comparison with the related $[\text{Ru}^{\text{II}}_2(\text{H}_2\text{O})_2(\text{bpp})(\text{trpy})_2]^+$ complex (entry 1, 16 TON⁸) revealed a decrease in the catalytic activity. However, no CO_2 generation was detected when the catalytic process was on line monitored by means of mass spectrometry (Figure 15b).

Silica- 8^{5+} has performed a catalytic activity of 16 TON (Figure 16a) which are almost totally due to the evolution of CO_2 (Figure 16b and table 2, entry 4). A higher rate of gas evolution is also observed due to the fast decomposition of the system.

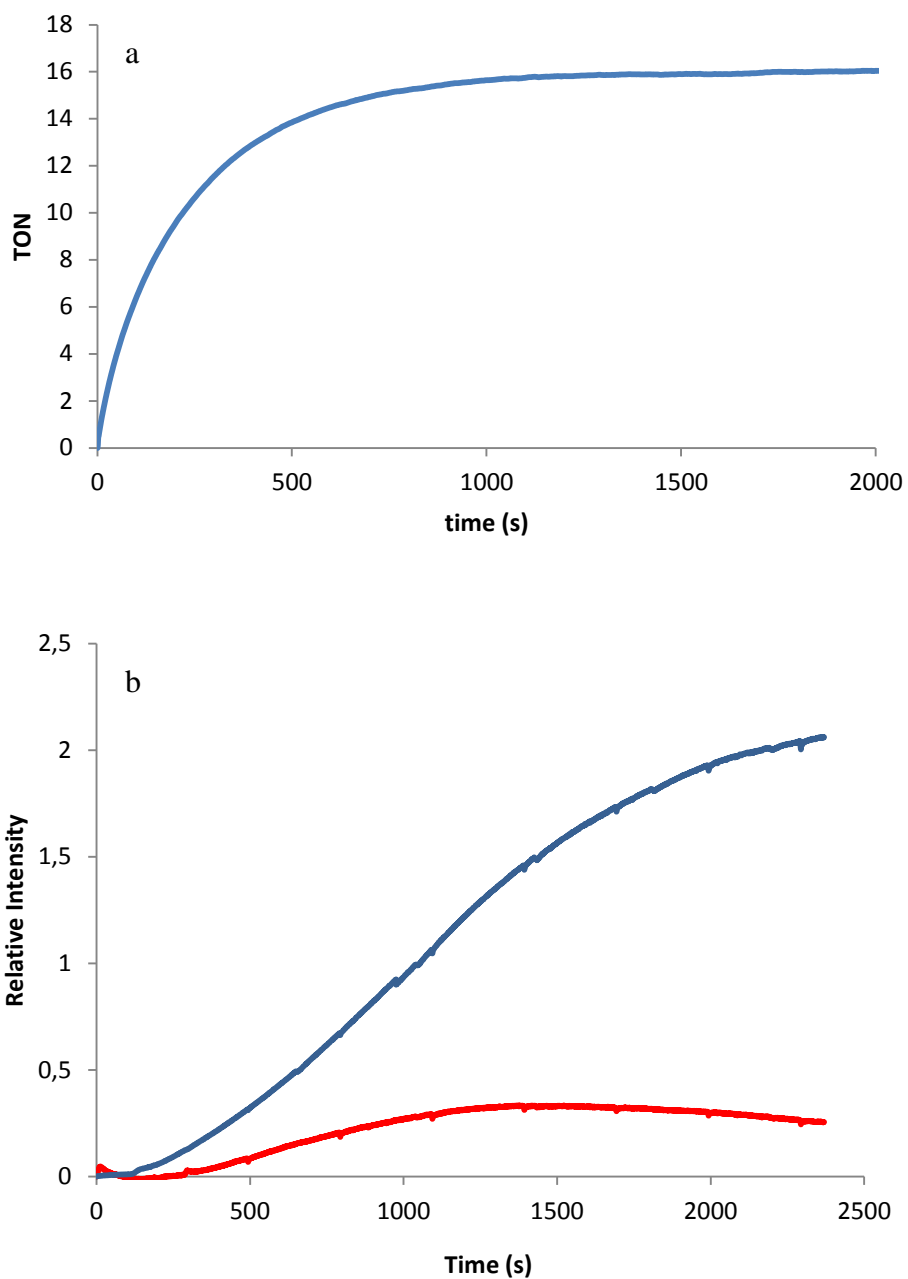


Figure 16. Chemically triggered water oxidation with Silica-8⁵⁺ (0.650 g, 1.82·10⁻³ mmol/g) at pH = 1.0 in 0.1 M triflic acid solution in the presence of (NH₄)₂Ce^{IV}(NO₃)₆ (100 mM). (a) manometric measurement (b) online Mass Spectrometry (O₂ evolution red line, CO₂ evolution blue line).

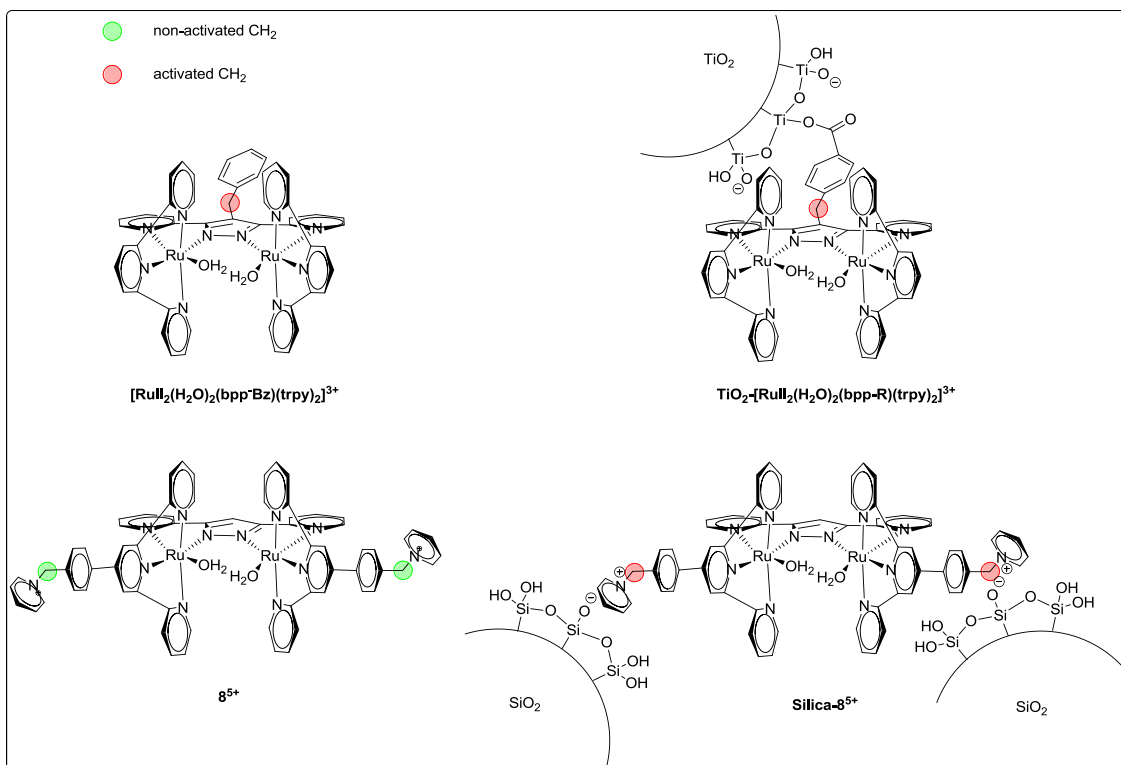
Table 3. Catalytic WO efficiencies and O₂:CO₂ ratios for **8**⁵⁺, Silica-**8**⁵⁺, FTO-Nafion-**8**⁵⁺ and other previously reported homogeneous and heterogeneous systems for purposes of comparison. Catalytic conditions: Cerium (IV) as oxidant. Ratio 1/100 Cat/Ce^{IV}.

Entry	System	[Cat]	TON	TON	[O ₂]/[CO ₂]	TON	Eff. ^c
		(mM)	O ₂	CO ₂		Total	
1	[Ru ₂ (H ₂ O) ₂ (trpy) ₂ (bpp)] ^{3+ 8}	1.0 ^a	18	-	-	16	72.0
2	[Ru ^{II} ₂ (H ₂ O) ₂ (bpp-Bz)(trpy) ₂] ^{3+ 1c}	1.0 ^a	5.8	5.8	1.0	11.7	29.2
3	8 ⁵⁺	1.0 ^a	11	-	-	11	44
4	Silica- 8 ⁵⁺	0.3 ^{a,d}	1.8	14.2	0.125	16	7.2
5	TiO ₂ -[Ru ^{II} ₂ (H ₂ O) ₂ (bpp-R _a)(trpy) ₂] ^{3+ 4}	0.5 ^b	3.5	3	1.2	6.5	55
6	FTO-Nafion- 8 ⁵⁺	0.06 ^e	1	-	-	1	4

^a Total volume of the reaction 2 ml at pH = 1.0 in 0.1 M triflic acid. ^b Total volume of the reaction 4 ml at pH = 1.0 in 0.1 M triflic acid. ^c Eff.= Efficiency. ^d 0.350 g of Silica-**7**⁴⁺ (0.3%). ^e Total volume of the reaction 3 ml at pH = 1.0 in 0.1 M triflic acid.

The co-evolution of CO₂ (together with dioxygen) during a catalytic water oxidation reaction usually arise from an intra-molecular catalyst-catalyst degradation process where the highly oxidant M-oxo species oxidize the weaker parts of the surrounding organic ligands.^{1c,4,2} That has been already reported for the [Ru^{II}₂(H₂O)₂(bpp-Bz)(trpy)₂]³⁺ and its corresponding heterogeneous TiO₂-[Ru^{II}₂(H₂O)₂(bpp-R_a)(trpy)₂]³⁺ system, which generate notorious amounts of CO₂ (Scheme 9 and Table 3, entries 2 and 5, respectively). Taking into account the absence of CO₂ evolution when the “original” [Ru₂(H₂O)₂(trpy)₂(bpp)]³⁺ complex is employed (Table 3, entry 1), the newly introduced benzylic positions, shown in red color in Scheme 9, were identified as the initial point for ligand decomposition.^{1c,4} However, despite the presence of similar methylenic moieties in **7**⁴⁺, no CO₂ is observed in this case (Figure 15b). Therefore, it looks like that the electron-withdrawing nature of the positive pyridinium moiety deactivates the CH₂ scaffold with regards to its oxidation (Scheme 9). Contrary to this,

in the Silica- $\mathbf{8}^{5+}$ system this positive charge is dislocated due to the ionic interaction with the SiO^- residues of the solid support. Consequently, the methylene in alpha to the pyridylic nitrogen atom is here again more prone to oxidation, thus decomposing and evolving CO_2 within the catalytic conditions. (Figure 16b and Scheme 9).



Scheme 9. Representation of activated (red color) and non activated (green color) methylenic moieties.

The system FTO-Nafion- $\mathbf{5}^{4+}$, after a previous 24h activation at $\text{pH} = 1.0$ in 0.1 M triflic acid to generate the aquo derivate FTO-Nafion- $\mathbf{8}^{5+}$ (as shown in previous sections), evolved the oxygen corresponding to 1 TON (Table 3, entry 6). The latest is a surprising result still under study in our laboratory to better know the possible deactivation pathways of this material.

III.2.5.2. Electrochemically triggered materials: FTO- $\text{TiO}_2\text{-}\mathbf{5}^{4+}$

The instability of FTO- $\text{TiO}_2\text{-}\mathbf{5}^{4+}$ under the usual catalytic conditions ($\text{pH}=1/\text{Ce(IV)}$) has been demonstrated in previous sections. Therefore, modified electrodes prepared by previous activation at $\text{pH} 12$ where electro-activated by means of controlled potential electrolysis in order to test their catalytic activity. As shown in Figure 18 (and Figure

S15 in the Supporting Information), the correct potential to be applied has been electrochemically evaluated.

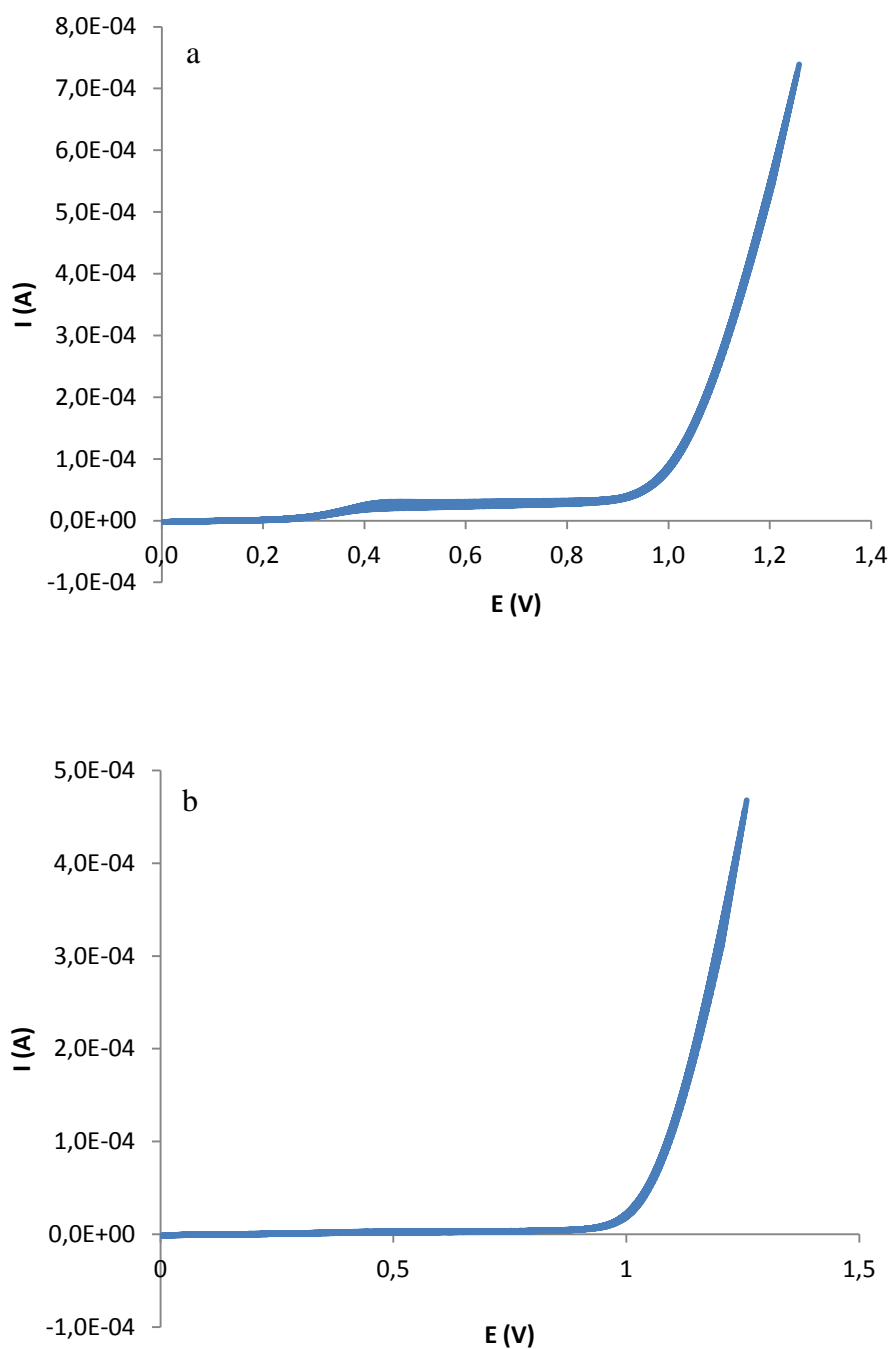


Figure 18. Differential Pulse Voltammetry for FTO-TiO₂-5⁴⁺ before (a) and after (b) CPE at pH = 12 (NaOH 0.01 M in water). FTO used as working electrode and potential measured vs. Ag/AgCl.

The catalytic reaction has been carried out in an electrochemical cell (Figure 19) formed by two different compartments (A and C) separated by a frit membrane (B). The water

oxidation process takes place in compartment A whereas proton reduction occurs in compartment C.

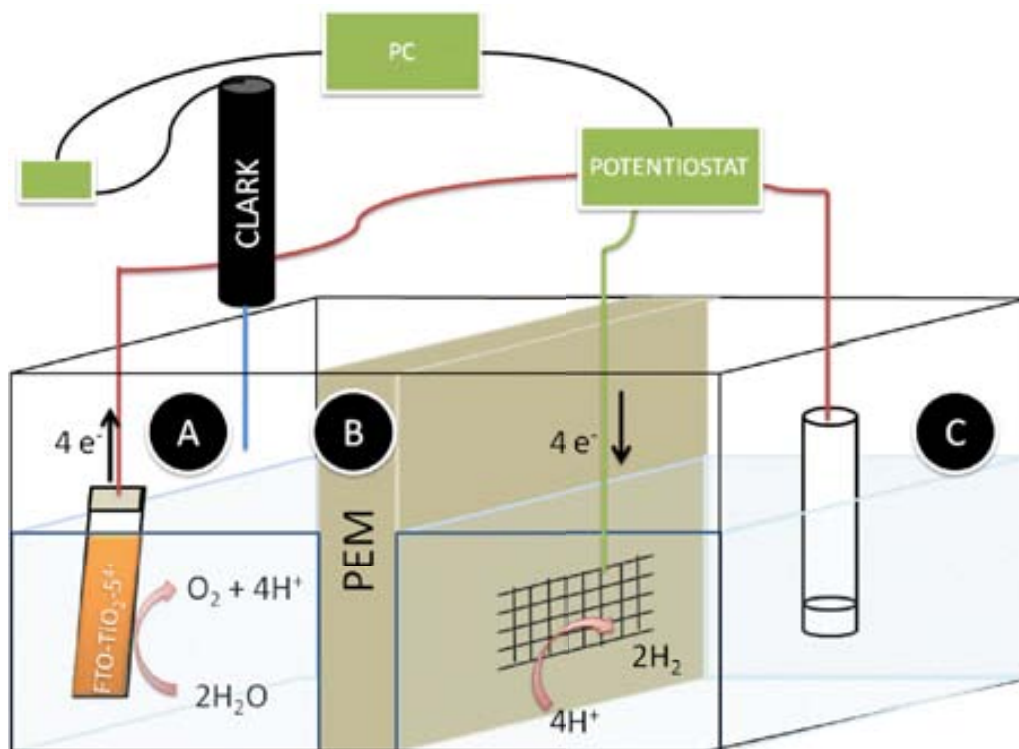


Figure 19. Electrochemical cell formed by: anode (compartment A) which contains a FTO-TiO₂-5⁴⁺ film and a Clark electrode and where the water oxidation reaction occurs; cathode (compartment C) which contains the counter and the reference electrodes and where the reduction of protons to hydrogen takes place; frit (membrane B) permeable to proton exchange.

FTO-TiO₂-5⁴⁺ was used as working electrode in the above-mentioned electrochemical cell applying a potential of 1.1 V vs. SSCE for 8h (Figure S17). Online O₂ measurement on the headspace of the cell compartment using a Clark electrode revealed that no oxygen was evolved (Figure S18). The electrochemical characterization of the electrode after the CPE experiment revealed the clear leaching of the complex from the electrode to the solution. Figure 18b displays the electrode DPV after CPE (see also Figure S16 in Supporting Information for CV) where the total disappearance of the redox waves can be appreciated. In addition to this, the UV-vis spectra of the solution after CPE (Figure S19) displayed the typical bands for 5⁴⁺, pointing out the presumed leaching of the catalyst. Both electrochemical and spectroscopic experiments have demonstrated that the major part of the current was employed in undesired processes such as the leaching of the catalyst.

III.3. Conclusions

In order to build a real device for artificial photosynthesis, accurate understanding of the limitations and consequences of anchoring WOC's onto solid surfaces is required. Therefore, research in order to explore and optimize the different types of catalyst/support interactions is a mandatory step. With this *leit motive* on mind, a new family of Ru dinuclear complexes (5^{4+} and 7^{4+}) containing the positively charged trpyPyr ligand 4'-(-p-(Pyridin-1-ylmethyl)phenyl)-2,2':6',2''-terpyridine (**L3(PF₆)**) have been synthesized and fully characterized, both in the solid state and in solution. Furthermore, the *in situ* conversion of 7^{4+} (aqueous media, pH=1) into its bis-aqua derivative 8^{5+} has been electrochemically demonstrated. The latter has been proven to be an active catalyst towards the oxidation of water, giving similar results to the ones previously reported for related complexes of the Ru-Hbpp family. The anchoring of the new catalysts onto TiO₂, SiO₂ and Nafion® has been achieved and the new hybrid materials prepared have been characterized by means of electrochemical and spectroscopic techniques.

The catalytic performance of Silica- 8^{5+} has shown a high ratio CO₂:O₂, thus revealing the oxidation of the catalyst. This result pointed out the activation of the methylene in alpha to the pyridylic residue when the positive charge is dislocated interacting with the SiO⁻ residues. The interaction between the positively charged pyridines and the TiO₂ electrode in FTO-TiO₂- 5^{4+} films is too low, thus the new material suffers a leaching process when the CPE was performed. Despite, the electrocatalytic activation of Nafion- 5^{4+} has been observed, its performance as WOC has been poor, yielding the estechiometric amount of O₂. The lack in the catalytic activation of Nafion- 7^{4+} has been attributed to the block of the Ru metal centers by the sulfonate groups. Silica and Nafion® have been demonstrated to be the best solid surfaces in terms of the interaction stability with the catalyst, meanwhile TiO₂ has shown poor results in this field. The work herein presented is a clear example of how new efforts have to be spend looking for new hybrids systems which have to be highly stable under strong oxidative conditions meanwhile increasing the catalytic activity of the units attached on them.

III.4. Experimental Section

Materials: All reagents used in the present work were obtained from Aldrich Chemical Co. and were used without further purification. Reagent-grade organic solvents were obtained from Scharlab. RuCl₃·3H₂O was supplied by Alfa Aesar and was used as received. Titanium dioxide paste (100% anatasa) used was supplied by Solaronix. Both the silica and the nafion polymer were provided by Sigma Aldrich. The starting ligands bis-(2-pyridyl)pyrazole (from now on Hbpp)¹⁶ and 4'-(-p-(bromomethyl)phenyl)-2,2':6',2''-terpyridine (**2**)¹⁷ were prepared as described in the literature. All synthetic manipulations were routinely performed under nitrogen atmosphere using Schlenk tubes and vacuum-line techniques.

Instrumentation and Measurements: UV-Vis spectroscopy was performed by a HP8453 spectrometer using 1 cm quartz cells. NMR spectroscopy was performed on a Bruker DPX 250 MHz, DPX 360 MHz or a DPX 400 MHz spectrometer. Samples were run in CD₃CN or acetone-d₆ with internal references. Elemental analyses were performed using a Carlo Erba CHMS EA-1108 instrument provided by the Chemical Analysis Service of the Universitat Autònoma de Barcelona (CAS-UAB). Electrospray ionization mass spectrometry (ESI-MS) experiments were carried out on an HP298s gas chromatography (GC-MS) system from the CAS-UAB. Cyclic voltammetry and Differential pulse voltammetry experiments were performed on an Ij-Cambria HI-660 potentiostat using a three-electrode cell. A glassy carbon electrode (2 mm diameter) was used as working electrode, platinum wire as auxiliary electrode and a SSCE as a reference electrode. Working electrodes were polished with 0.05 micron Alumina paste washed with distilled water and acetone before each measurement. The complexes were dissolved in acetone containing the necessary amount of n-Bu₄NPF₆ (TABH) as supporting electrolyte to yield 0.1 M ionic strength solution. E_{1/2} values reported in this work were estimated from CV experiments as the average of the oxidative and reductive peak potentials (E_{p,a} + E_{p,c})/2. Online manometry measurements were carried out on a Testo 521 differential pressure manometer with an operating range of 1 – 100 hPa and accuracy within 0.5% of the measurement, coupled to thermostatted reaction vessels for dynamic monitoring of the headspace pressure above each reaction. The secondary ports of the manometers were connected to thermostatically controlled reaction vessels that contained the same solvents and headspace volumes as the sample vials. Online monitoring of the gas evolution was performed on a Pfeiffer Omnistar GSD 301C mass

spectrometer. Typically, 16.04 mL degassed vials containing a suspension of the catalysts in a 0.1 M triflic acid (1.5 mL) were connected to the apparatus capillary tubing. Subsequently, the previously degassed solution of Ce(IV) (0.5 mL) at pH=1 (triflic acid, 200 equiv.) was introduced using a Hamilton gastight syringe, and the reaction was dynamically monitored. A response ratio of 1:2 was observed when equal concentrations of dioxygen and carbon dioxide, respectively, were injected and thus was used for calculation of their relative concentrations.

X-ray Crystal Structure Determination. Data collection was made on a Bruker-Nonius diffractometer equipped with an APPEX II 4K CCD area detector, a FR591 rotating anode with Mo K α radiation, Montel mirrors as a monochromatic and a Kryoflex low-temperature device (T = -173°C). Full-sphere data collection was used with ω and ϕ scans. Programs used: data collection APPEX II,¹⁸ data reduction, Bruker Saint V/.60A;¹⁹ absorption corrections, SADABS.²⁰

Structure and Refinement. For this, SHELXTL²¹ was used. The crystal data parameters are listed in Tables S1 and S2. For the structure of [Ru^{II}(μ -Cl)(bpp)(trpyPYR)₂](PF₆)₄ (**5**(PF₆)₄), the program SQUEEZE²² implemented in Platon was used in order to avoid the highly disorder imposed for 8 acetone and 13 toluene molecules that were detected.

Synthetic preparations

4'-(-*p*-(Pyridin-1-ylmethyl)phenyl)-2,2':6',2''-terpyridine (**L3**(PF₆)): 4'-(-*p*-(bromomethyl)phenyl)-2,2':6',2''-terpyridine (**2**) (0.200 g, 0.497 mmols) were dissolved in pyridine (30 ml). The mixture was allowed to react in a microwave reactor at 150 °C and 300 W for 30 minutes. The volume was reduced until dryness and the solid residue redissolved in water (30 ml). The final suspension was filtered through celite and a saturated aqueous NH₄PF₆ solution (1 mL) was added to the colorless solution to obtain a white precipitate. The mixture was filtered after two hours stirring to yield 0.2 g (85 %) of the desired powder. ¹H NMR (400MHz, [D₃]acetonitrile): δ = 8,79 (d, 2H₂₃₋₂₇, J₂₃₋₂₄= 6,40Hz) 8,73 (s, 2H₉₋₇), 8,73 (d, 2H₁₋₁₅), 8,69 (d, 2H₄₋₁₂, J₃₋₄= 8,30Hz), 8,55 (t, 1H₂₅, J₂₄₋₂₅= 8,10Hz), 8,06 (t, 2H₂₄₋₂₆, J₂₄₋₂₅= 8,10Hz, J₂₃₋₂₄= 6,40Hz), 7,99 (ddd, 2H₃₋₁₃, J₃₋₄= 8,30Hz, J₃₋₂ = 7,60Hz, J₁₋₃ = 1,46Hz), 7,99 (d, 2H₁₇₋₂₁, J₁₇₋₁₈ = 8,10Hz), 7,63 (d, 2H₁₈₋₂₀, J₁₇₋₁₈= 8,10Hz), 7,47 (t, 2H₂₋₁₄, J₂₋₃= 7,60Hz, J₁₋₂= 6,0Hz),

5,81 (s, 2H₂₂). ¹³C{¹H} NMR (400MHz, [D₃]acetonitrile): δ = 157,45 (C₆₋₁₀), 156,65 (C₅₋₁₁), 150,56 (C₁₋₁₅), 150,47 (C₈), 147,78 (C₂₅), 145,99 (C₂₃₋₂₇), 141,17 (C₁₆), 138,89 (C₃₋₁₃), 135,16 (C₁₉), 131,47 (C₁₈₋₂₀), 130,09 (C₂₄₋₂₆), 129,57 (C₁₇₋₂₁), 125,86 (C₂₋₁₄), 122,54 (C₄₋₁₂), 119,94 (C₉₋₇), 65,40 (C₂₂).

[RuCl₃(3)](PF₆) (**4**(PF₆)): **L3**(PF₆) (0.915 g, 1.617 mmol) and RuCl₃·3H₂O (0.422 g, 1.617 mmol) were dissolved in dry MeOH (130 mL). The mixture was stirred and heated at reflux temperature for 4 h. Then the solution was kept cool until appeared a brown precipitate. The solid was filtered, washed with cold water (3x5 mL) and diethyl ether (3 x 5 mL) and finally dried under vacuum to afford complex **4**(PF₆) (0.949 g, 77%). ESI-MS (MeOH): *m/z* = 610 ([M-PF₆]⁺).

[Ru^{II}₂(μ-Cl)(bpp)(trpyPyr)₂](PF₆)₄ (**5**(PF₆)₄): **4**(PF₆) (0.942 g, 1.77 mmol) and LiCl (0.113 g, 2.65mmol) were dissolved in a solution of NEt₃ (492 μl, 3.54 mmol) and dry MeOH (180 mL). The mixture was stirred at room temperature for 20 min, and then Hbpp (0.197 g, 0.884 mmol) and 0.6684 M MeONa (1.32 mL, 0.844 mmol) in dry MeOH (20 mL) were added. The resulting solution was heated for 4 h and then stirred in the presence of a 100 W Tungsten lamp for 8 h. The reaction mixture was filtered and then saturated aqueous NH₄PF₆ solution (1 mL) added to obtain a brown precipitate. The solid was collected, washed with cold water (3x5 mL) and diethyl ether (3 x 5 mL) and finally dried under vacuum to afford complex **5**(PF₆)₄ (0.860 g, 75%). ¹H NMR (400 MHz, [D₆]acetone): δ = 9.34 (d, 4H, J₂₃₋₂₄=6.08 Hz; H₂₃), 9.01 (s, 4H; H₇), 8.80 (t, 2H, J₂₅₋₂₄=7.80 Hz; H₂₅), 8.72 (d, 4H, J₃₋₄=8.00 Hz; H₄), 8.54 (s, 1H; H₈), 8.41 (d, 4H, J₁₋₂=5.76 Hz; H₁), 8.35 (t, 4H, J₂₄₋₂₅=7.80 Hz; H₂₄), 8.31 (m, 6H; H₂₈₋₁₇), 7.97 (t, 4H, J_{3-4,2}=8.00 Hz; H₃), 7.89 (d, 4H, J₁₇₋₁₈=8.20 Hz; H₁₈), 7.83 (t, 2H, J_{29-28,30}=8.00 Hz; H₂₉), 7.64 (t, 4H, J_{2-1,3}=6.57 Hz; H₂), 7.50 (d, 2H, J₃₀₋₃₁=5.90 Hz; H₃₁), 6.82 (t, 2H, J₃₀₋₃₁=5.90 Hz; H₃₀), 6.20 (s, 4H, H₂₂). ¹³C{¹H} NMR (400 MHz, [D₆]acetone): δ = 159.39 (C₆), 159.05 (C₅), 158.78 (C₃₂), 153.89 (C₃₁), 153.56 (C₁), 148.48 (C₃₃), 146.57 (C₂₅), 145.06 (C₂₃), 145.00 (C₈), 138.44 (C₁₆), 137.07 (C₃), 136.92 (C₂₉), 135.15 (C₁₉), 130.14 (C₁₈), 128.95 (C₂₄), 128.57 (C₁₇), 127.39 (C₂), 123.87 (C₄), 122.19 (C₃₀), 120.47 (C₂₈), 120.20 (C₇), 103.29 (C₃₄), 64.16 (C₂₂). UV/vis (acetone): λ_{max} (ε)= 366 (26775), 480 (19187), 509 (20235). ESI-MS (MeOH): *m/z* = 1697.2 ([M-PF₆]⁺). Elemental analysis (%) found C, 42.60; H, 2.91; N, 9.00. Calcd for C₆₇H₅₁ClF₂₄N₁₂P₄Ru₂: C, 43.70; H, 2.79; N, 9.13.

[Ru^{II}₂(μ-O₂CMe)(bpp)(trpyP_{YR})₂](PF₆)₄ (**7**(PF₆)₄): A sample of **5**(PF₆)₄ (0.225 g, 0.120 mmol), sodium acetate (0.054 g, 0.660 mmol) and AgBF₄ (0.023 g, 0.120 mmol) were dissolved in acetone/water (3:1, 40 mL), and the solution was heated at reflux overnight in the dark. The resulting solution was filtered, and saturated aqueous NH₄PF₆ solution (1 mL) added. A solid precipitated out of the solution upon reducing the volume. The solid was collected and washed with cold water (3x5 mL) and diethyl ether (3 x 5 mL) and finally dried under vacuum to afford complex **7**(PF₆)₄ (0.166 g, 73%). ¹H NMR (400 MHz, [D₆]acetone): δ = 9.35 (d, 4H, J₂₃₋₂₄=6.90 Hz; H23), 9.10 (s, 4H; H7), 8.82 (m, 6H; H25-4), 8.56 (s, 1H; H34), 8.47 (d, 4H, J₁₋₂=5.70 Hz; H1), 8.37 (t, 4H, J_{24-25,23}=6.90 Hz; H24), 8.35 (d, 4H, J₁₇₋₁₈=8.15 Hz; H17), 8.22 (d, 2H, J₂₈₋₂₉=7.97 Hz; H28), 8.05 (t, 4H, J_{3-4,2}=7.85 Hz; H3), 7.94 (d, 4H, J₁₇₋₁₈=8.15 Hz; H18), 7.76 (t, 2H, J_{29-28,30}=7.90 Hz; H29), 7.55 (t, 4H, J_{2-1,3}=6.50 Hz; H2), 7.45 (d, 2H, J₃₀₋₃₁=5.70 Hz; H31), 6.83 (t, 2H, J₃₀₋₃₁=7.73 Hz; H30), 6.23 (s, 4H, H22), 0.45 (s, 3H, H36). ¹³C{¹H} NMR (400 MHz, [D₆]acetone): δ = 191.59 (C35), 160.34 (C6), 159.77 (C5), 156.47 (C32), 153.81 (C1), 152.80 (C31), 151.89 (C33), 146.59 (C25), 145.02 (C23), 144.77 (C8), 138.83 (C16), 137.32 (C3), 135.99 (C29), 135.17 (C19), 130.19 (C18), 128.95 (C24), 128.59 (C17), 127.46 (C2), 123.89 (C4), 122.24 (C30), 120.36 (C7), 119.61 (C28), 103.89 (C34), 64.20 (C22), 25.25 (C36). UV/vis (Acetone): λ_{max} (ε)= 367 (27615), 497 (17119), 525 (15923). ESI-MS (MeOH): *m/z* = 788.09 ([M-2PF₆]²⁺). Elemental analysis (%) found C, 43.92; H, 2.75; N, 8.95. Calcd for C₆₉H₅₅F₂₄N₁₂O₂P₄Ru₂: C, 44.41; H, 2.97; N, 9.01.

Preparation of FTO-TiO₂-**5**⁴⁺: On clean FTO films, anatasa TiO₂ paste was spread uniformly. Then the films were heated for 10 min at 100 °C in order to reduce the surface irregularities. The films were calcinated following the appropriated temperature ramps (see figure S19). The anchoring process was carried out by soaking overnight every film into 5 ml of an acetone solution (0.305 mM) of **5**⁴⁺.

Preparation of FTO-Nafion-**X**⁴⁺ (X = **5**⁴⁺ or **7**⁴⁺): On clean FTO films, Nafion 5% w/w in water and low weight alcohols (50 μL) was uniformly deposited. Then the films were heated for 30 min at 100 °C in order to remove water and low weight alcohols. After cool down until room temperature the films were soaked overnight into an acetone solution of **X**⁴⁺ (10 ml, 0.0201 mM).

Preparation of Silica-7⁴⁺: Silica (3g) was poured into 10 ml of a solution of 7⁴⁺ (0.548 mM) in acetone. The mixture was stirred for some minutes until the solution became colorless. Then the pink solid was washed several times with acetone and diethyl ether and finally was air-dried.

Acknowledgements

The experiments of the stability and water oxidation catalysis of FTO films presented in sections III.2.4.2. and III.2.5.2 were developed by Dr. Laia Francàs in our research group.

III.5. References

- ¹ (a) Sala, X.; Rodríguez, M.; Romero, I.; Escriche, L.; Llobet, A. *Angew. Chem. Int. Ed.* **2009**, *48*, 2842. (b) Sala, X.; Cramer, C.J.; Gagliardi, L.; Llobet, A. et al. *Angew. Chem. Int. Ed.* **2010**, *49*(42), 7745-7747. (c) Francas, L.; Sala, X.; Escudero-Adan, E.; Benet-Buchholz, J.; Escriche, L.; Llobet, A. *Inorg. Chem.* **2011**, *50*(7), 2771-2781. (d) García-Antón, J.; Bofill, J.; Escriche, L.; Llobet, A.; Sala, X. *Eur. J. Inorg. Chem.* **2012**, 4775. (e) Romain, S.; Bozoglian, F.; Sala, X.; Llobet, A. *J. Am. Chem. Soc.* **2009**, *131*(8), 2768-2769. (f) Mola, J.; Dinoi, C.; Sala, X.; Rodríguez, M.; Romero, I.; Parella, T.; Fontrodona, X.; Llobet, A. *Dalton Trans.* **2011**, *40*(14), 3640-3646.
- ² Mola, J.; Mas-Marza, E.; Sala, X.; Romero, I.; Rodríguez, M.; Viñas, C.; Parella, T.; Llobet, A. *Angew. Chem. Int. Ed.* **2008**, *47*, 5830-5832.
- ³ Liu, F.; Cardolaccia, T.; Hornstein, B.J.; Schoonover, J.R.; Meyer, T.J. *J. Am. Chem. Soc.*, **2007**, *129*, 2446-2447.
- ⁴ Francas, L.; Sala, X.; Benet-Buchholz, J.; Escriche, L.; Llobet, A. *ChemSusChem* **2009**, *2*(4), 321-329.
- ⁵ Francàs, L.; PhD. Thesis
- ⁶ Spahni, W.; Calzaferri, G. *Helv. Chim. Acta* **1984**, *67*, 450.
- ⁷ Chakraborty, S.; Wadas, T.J.; Hester, H.; Flaschenreim, C.; Schmehl, R.; Eisenberg, R. *Inorg. Chem.* **2005**, *44*, 6284-6293.
- ⁸ Sens, C.; Romero, I.; Rodríguez M.; Llobet A.; Parella, T.; Benet-Buchholz, J. *J. Am. Chem. Soc.* **2004**, *126*, 7798-7799.
- ⁹ Dumur, F.; Mayer, C.R.; Hoang-Thi, K.; Ledoux-Rak, I.; Miomandre, F.; Clavier, G.; Dumas, E.; Méaallet-Renault, R.; Frigoli, M.; Zyss, J.; Sécheresse, F. *Inorg. Chem.* **2009**, *48*, 8120-8133.
- ¹⁰ Laurent, F.; Plantalech, E.; Donnadiou, B.; Jimenez, A.; Hernández, F.; Martínez-Ripoll, M.; Biner, M.; Llobet, A. *Polyhedron*, **1999**, *18*, 3321-3331.
- ¹¹ SQUEEZE implemented in Platon: Spek, A.L. *J. Appl. Cryst.* **2003**, *36*, 7-13
- ¹² Roeser, S.; Ertem, M.Z.; Cady, C.; Lomoth, R.; Benet-Buchholz, J.; Hammarström, L.; Sarkar, B.; Kaim, W.; Cramer, C.J.; Llobet, A. *Inorg. Chem.* **2012**, *51*, 320-327.
- ¹³ (a) Rodríguez, M.; Romero, I.; Llobet, A. *Inorg. Chem.* **2001**, *40*, 4150-4156. (b) Takeuchi, K.J.; Thompson, M.S.; Pipes, D.W.; Meyer, T.J. *Inorg. Chem.* **1984**, *23*, 1845-1851.

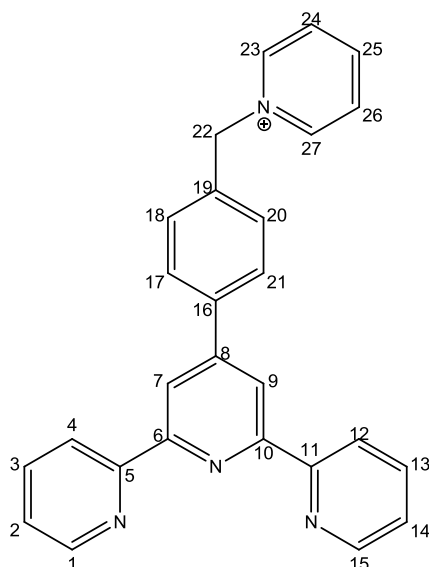
- ¹⁴ Shriver, D.F.; Atkins, P.W. *Inorganic Chemistry*; Oxford University Press, 2012.
- ¹⁵ Trammell, S.A.; Meyer, T.J. *J. Phys. Chem. B* **1999**, *103*, 104-107.
- ¹⁶ Pons, J.; Sánchez, F.J.; López, X.; Teixidor, F.; Casabó, J. *Polyhedron*, **1990**, *9*, 2839.
- ¹⁷ Pikramenou, Z. et al. *Inorg Chem.* **2001**, *40*, 3912-3921.
- ¹⁸ Data collection with: *Apex II*, versions v1.0-22, v2009.1-0 and v2009.1-02; Bruker AXS Inc.: Madison, WI, 2007.
- ¹⁹ Data reduction with : *SAINT*, versions V.2.10 (2003), V/.60A and V7.60A; Bruker AXS Inc.: Madison, WI, 2007.
- ²⁰ *SADABS*, versions V.2.10 (2003): V2008 and V2008/1 (2001); Bruker AXS Inc.: Madison, WI, 2008. Blessing, R. H. *Acta Crystallogr.* **1995**, *A51*, 33-38.
- ²¹ Sheldrick, G. M. *Acta Crystallogr.* **2008**, *A64*, 112-122 (SHELXTL, versions V6.12 and V6.14).
- ²² Spek, A.L. *J. Appl. Cryst.* **2003**, *36*, 7-13.

III.6. Supporting Information

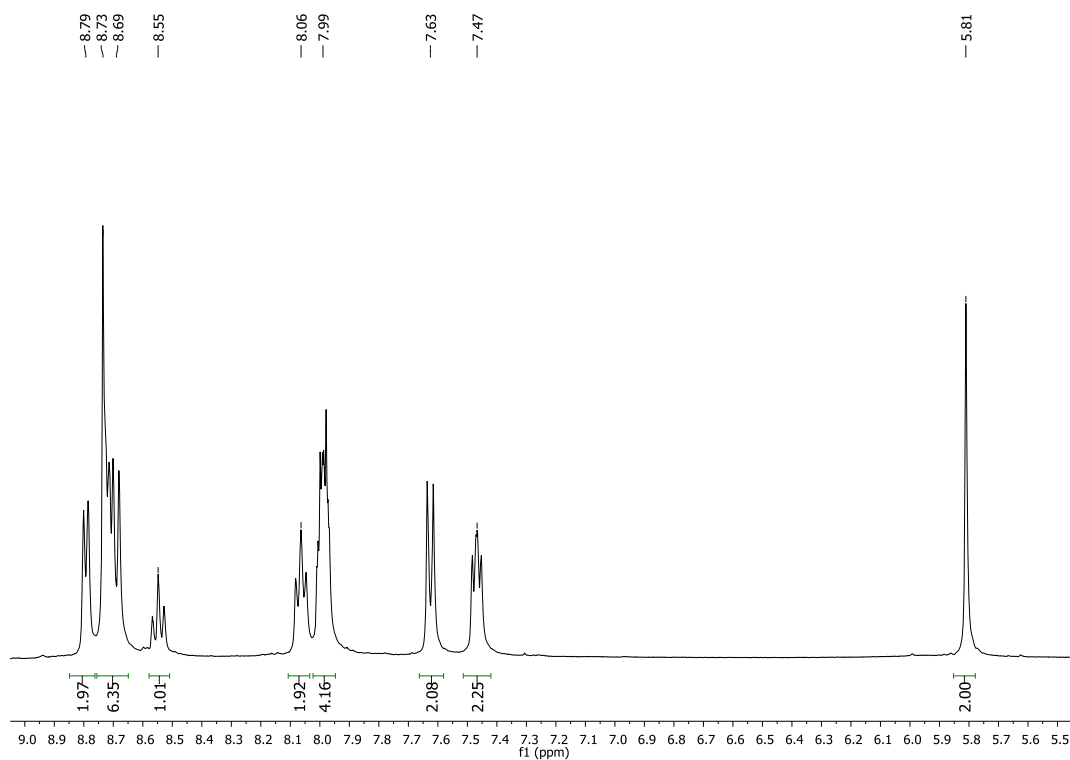
- NMR
- Electrochemistry
- ESI-MS
- X-Ray
- WOC

Figure S1. 1D and 2D NMR spectra (400 MHz, 298 K, d_3 -Acetonitrile) for 3^+ : (a) schematic representation (b) ^1H -NMR, (c) COSY, (d) ^{13}C - $\{^1\text{H}\}$ -NMR, (e) HSQC-NMR (aromatic region) (f) HMBC-NMR (aromatic region).

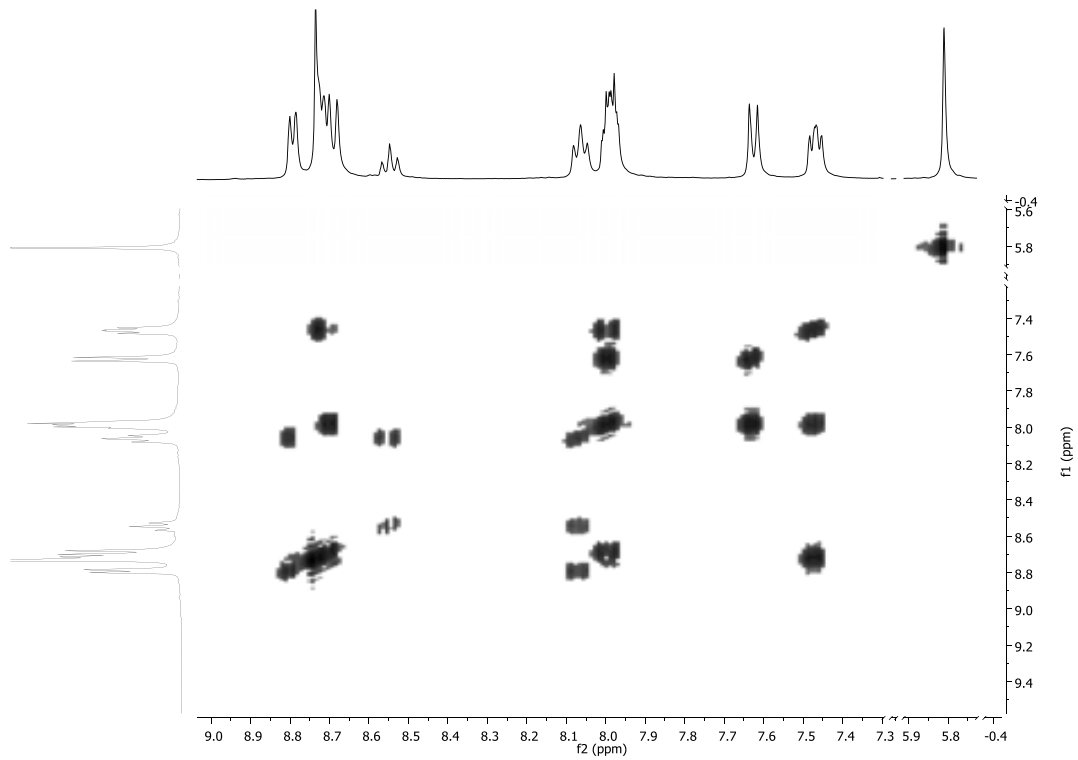
a)



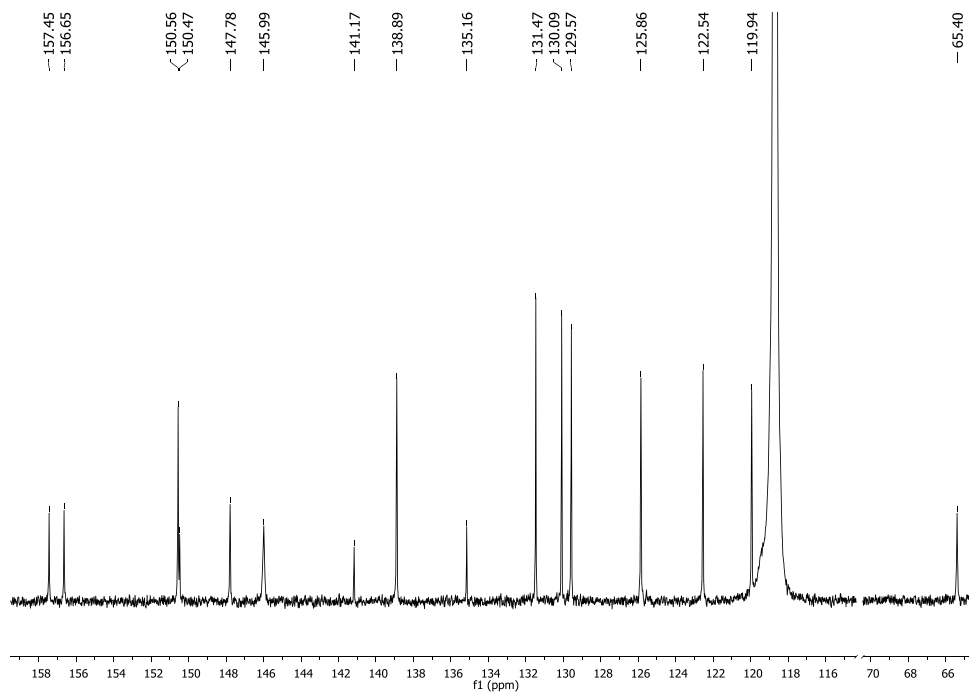
b)



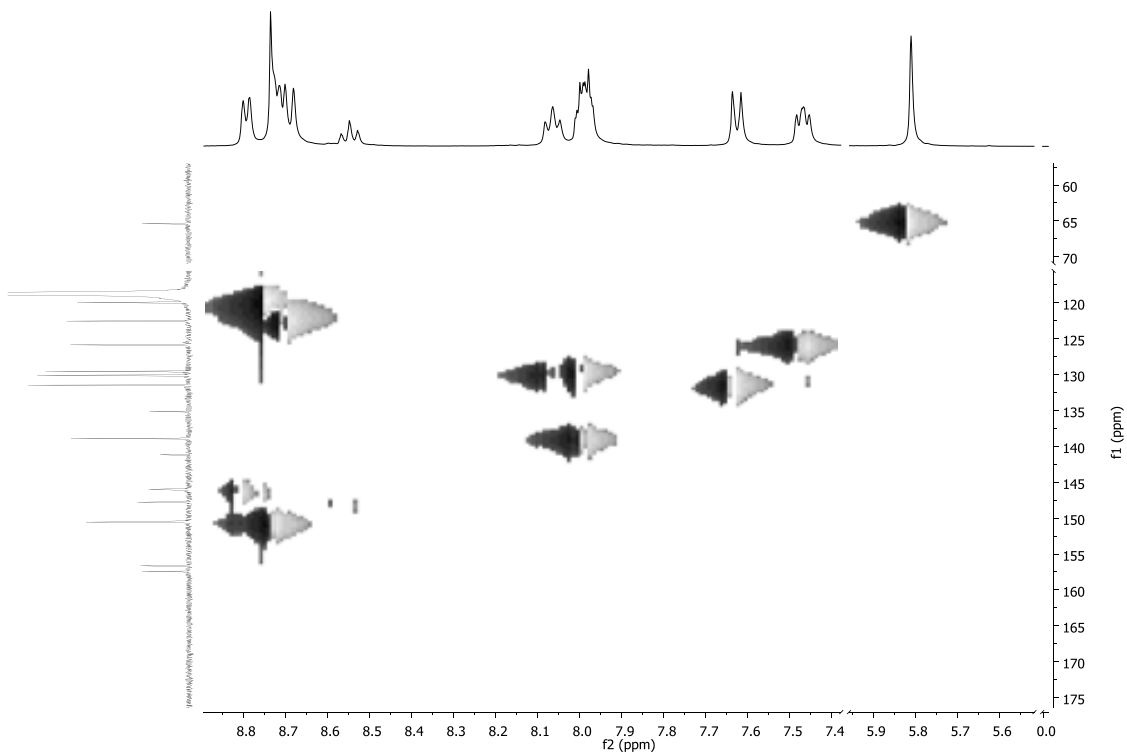
c)



d)



e)



f)

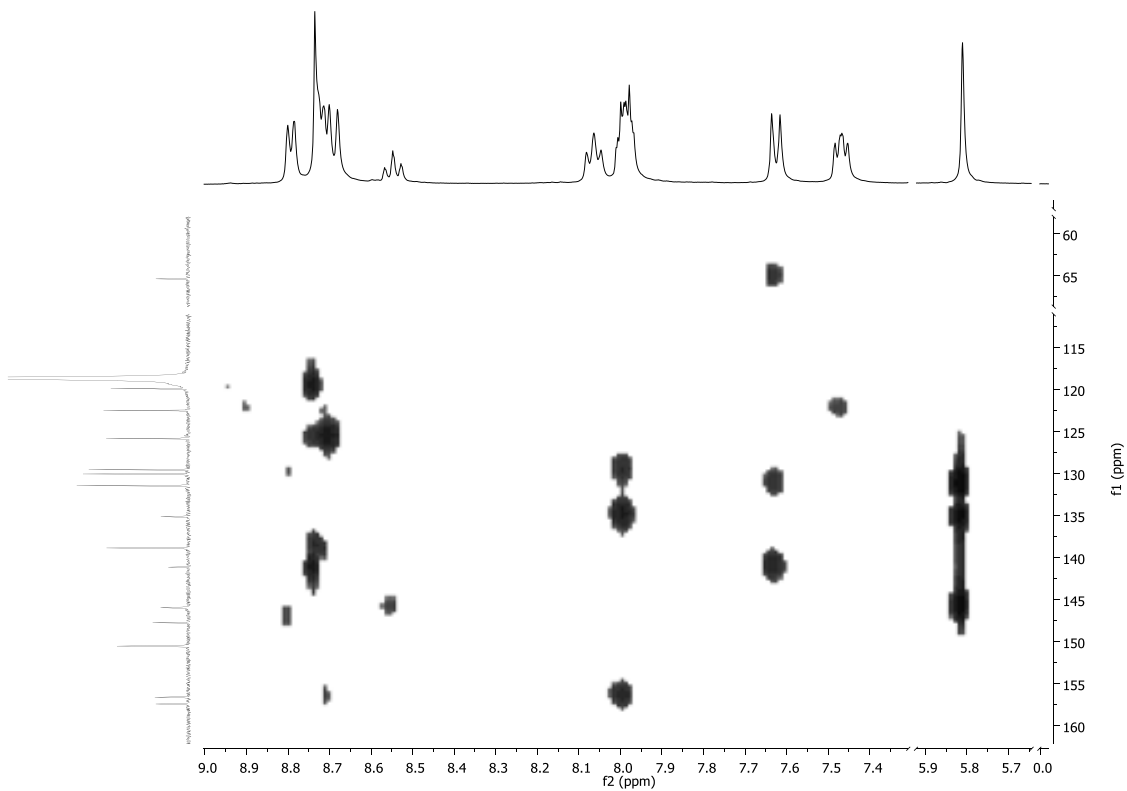
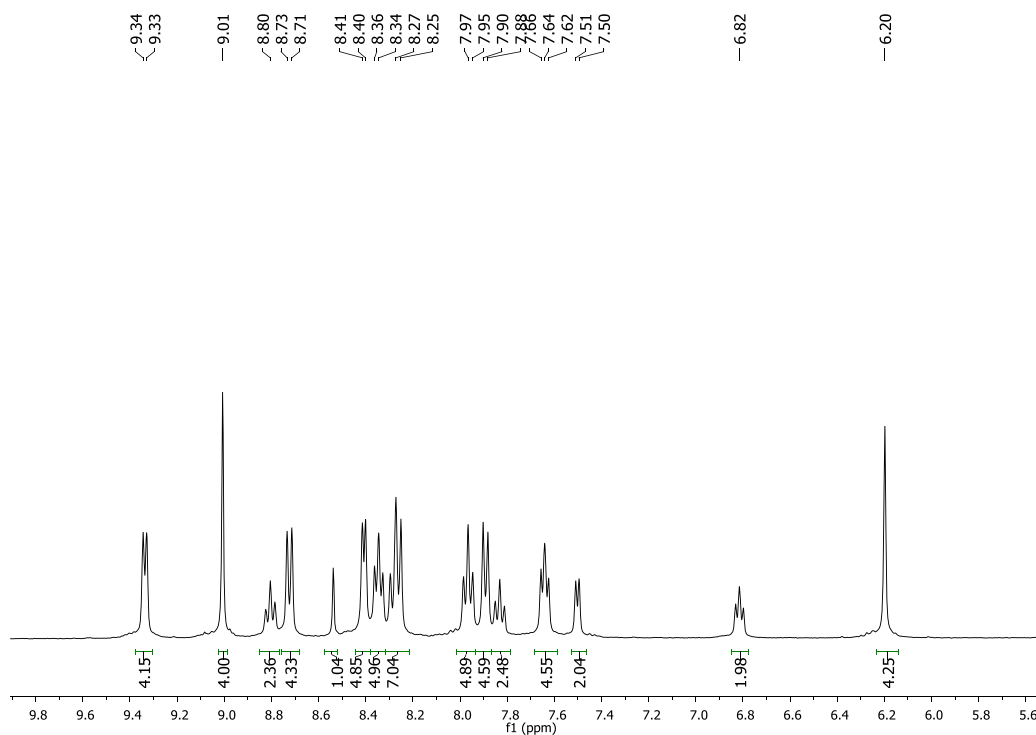
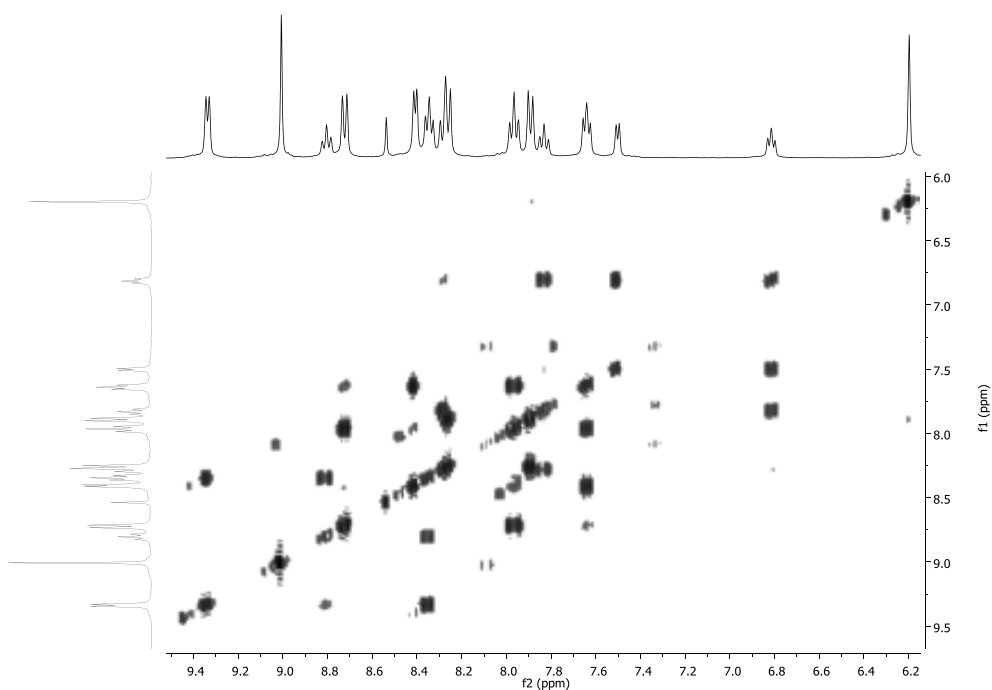


Figure S2. 1D and 2D NMR spectra (400 MHz, 298 K, d_6 -Acetone) for complex **5**⁴⁺: (a) ¹H-NMR, (b) COSY, (c) ¹³C-¹H-NMR, (d) HSQC-NMR (aromatic region) (e) HMBC-NMR (aromatic region).

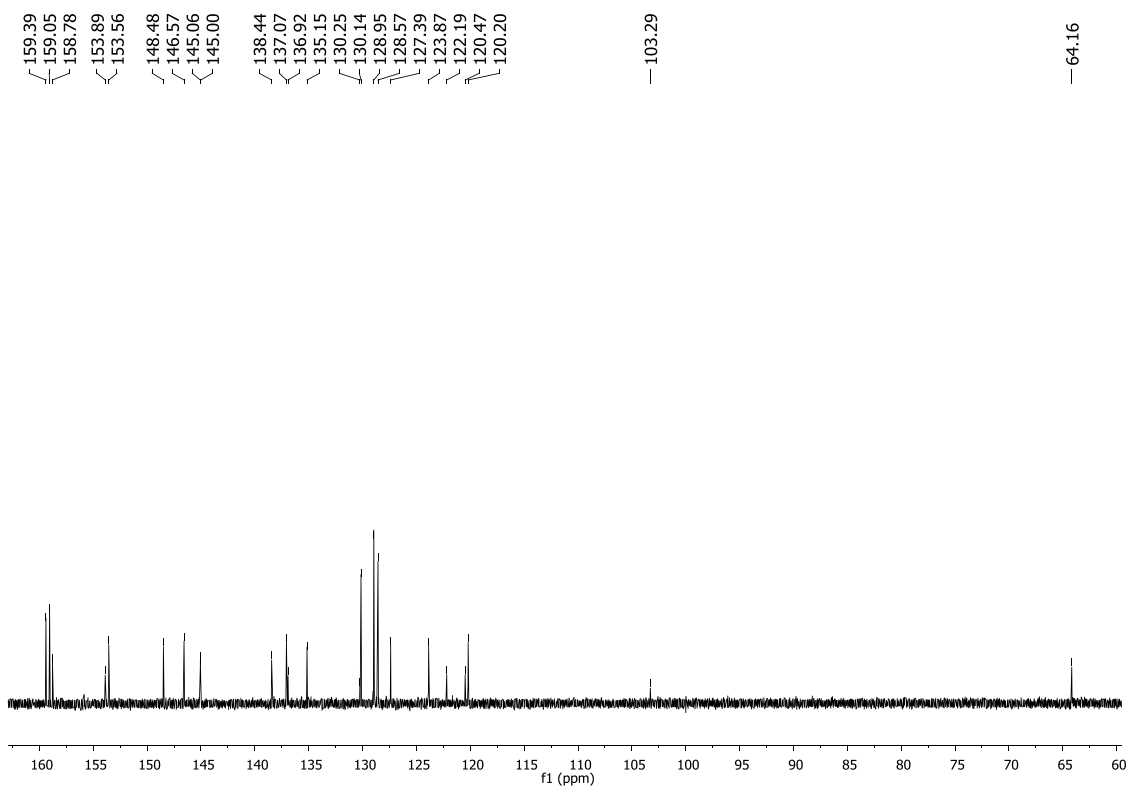
a)



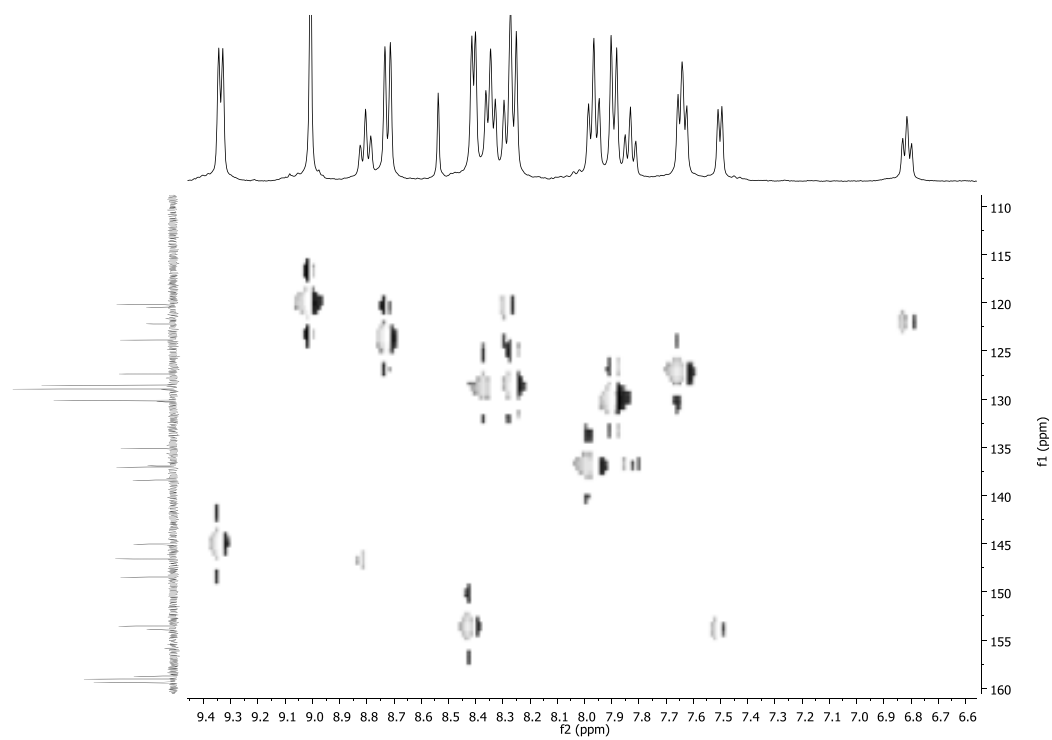
b)



c)



d)



e)

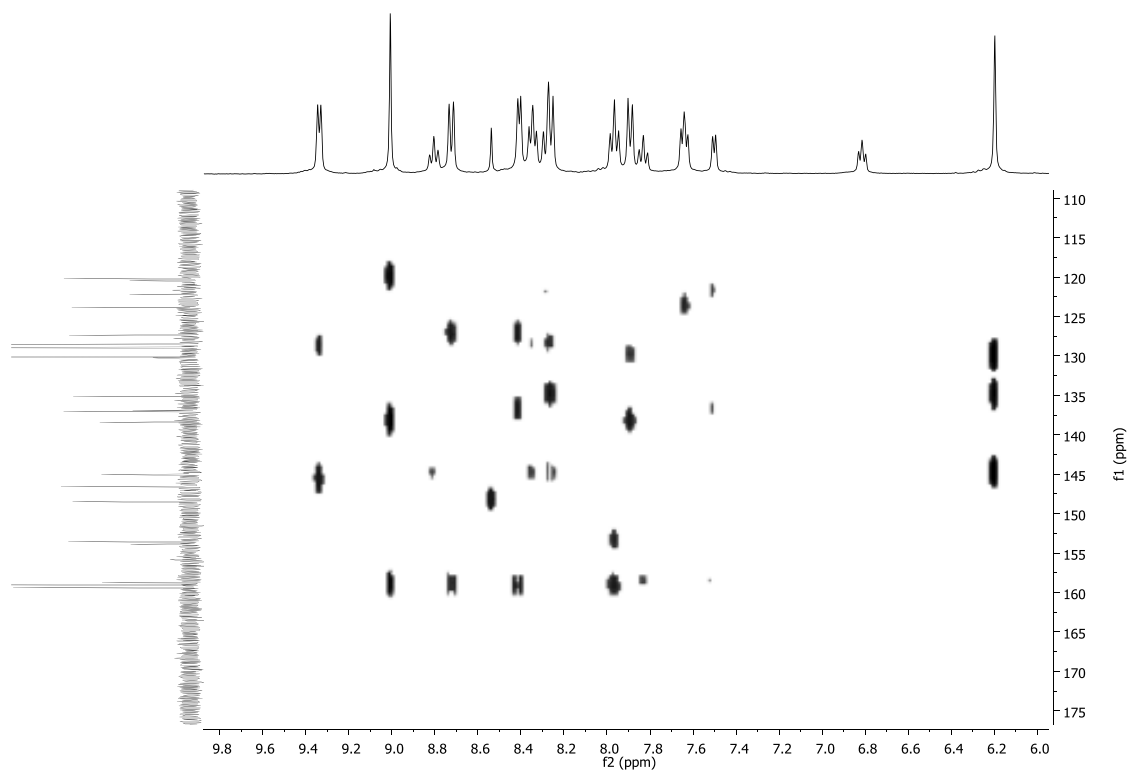
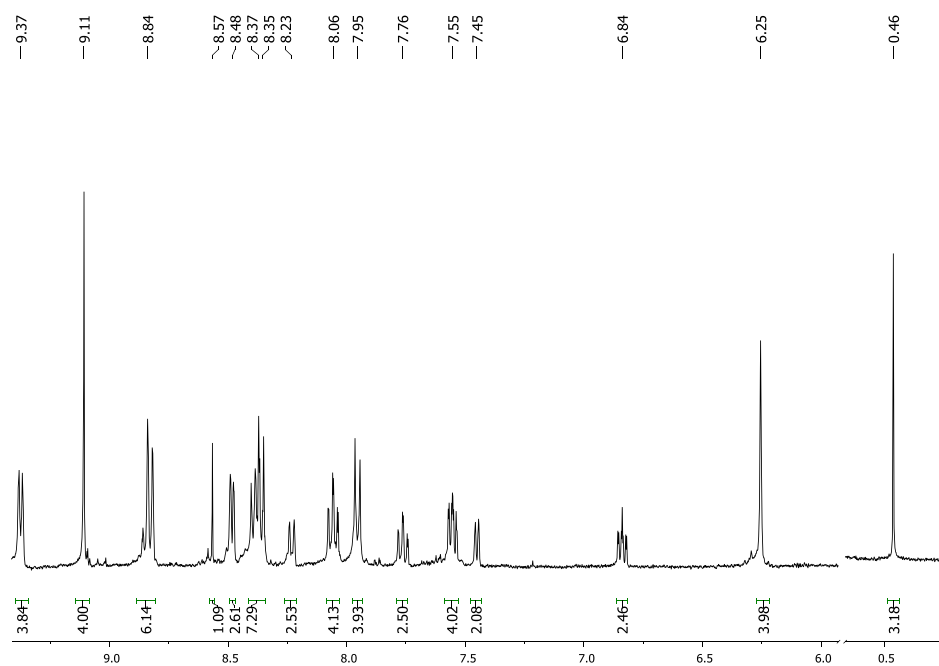
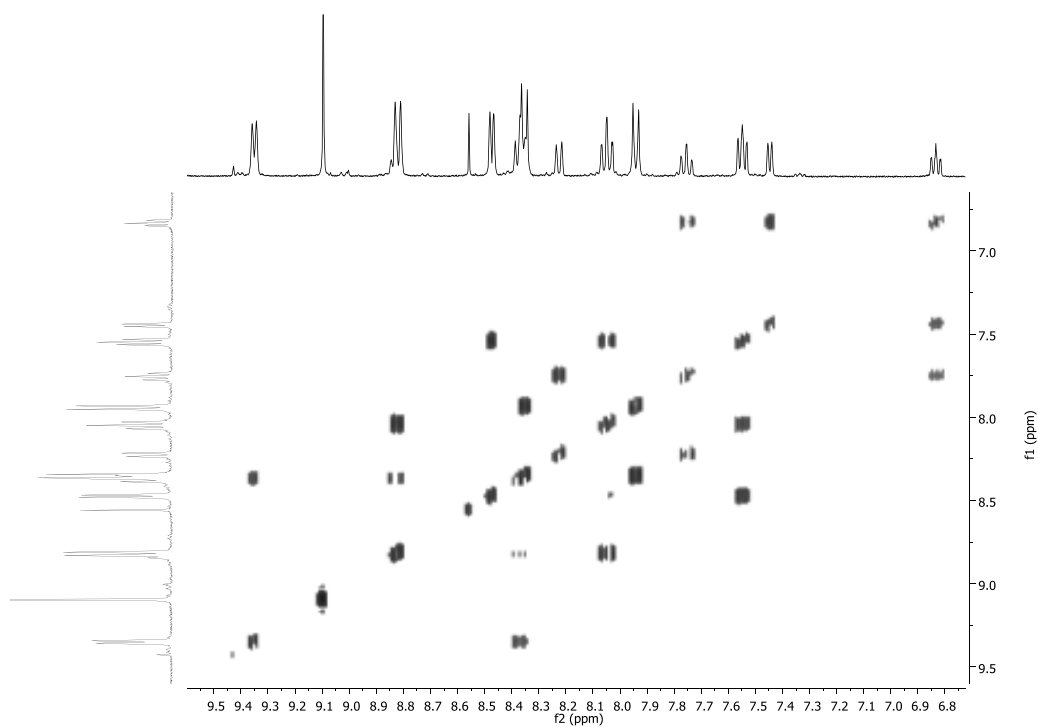


Figure S3. 1D and 2D NMR spectra (250 MHz, 298 K, d_6 -Acetone) for complex 7^{4+} : (a) ^1H -NMR, (b) COSY, (c) $^{13}\text{C}\{-^1\text{H}\}$ -NMR, (d) HSQC-NMR (aromatic region) (e) HMBC-NMR (aromatic region).

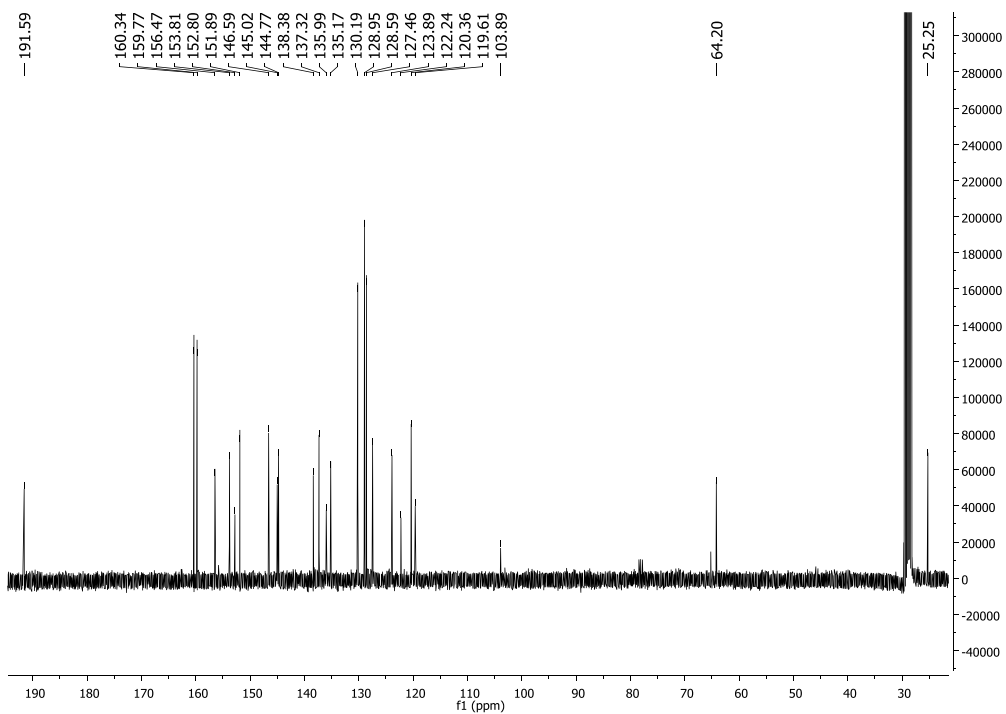
a)



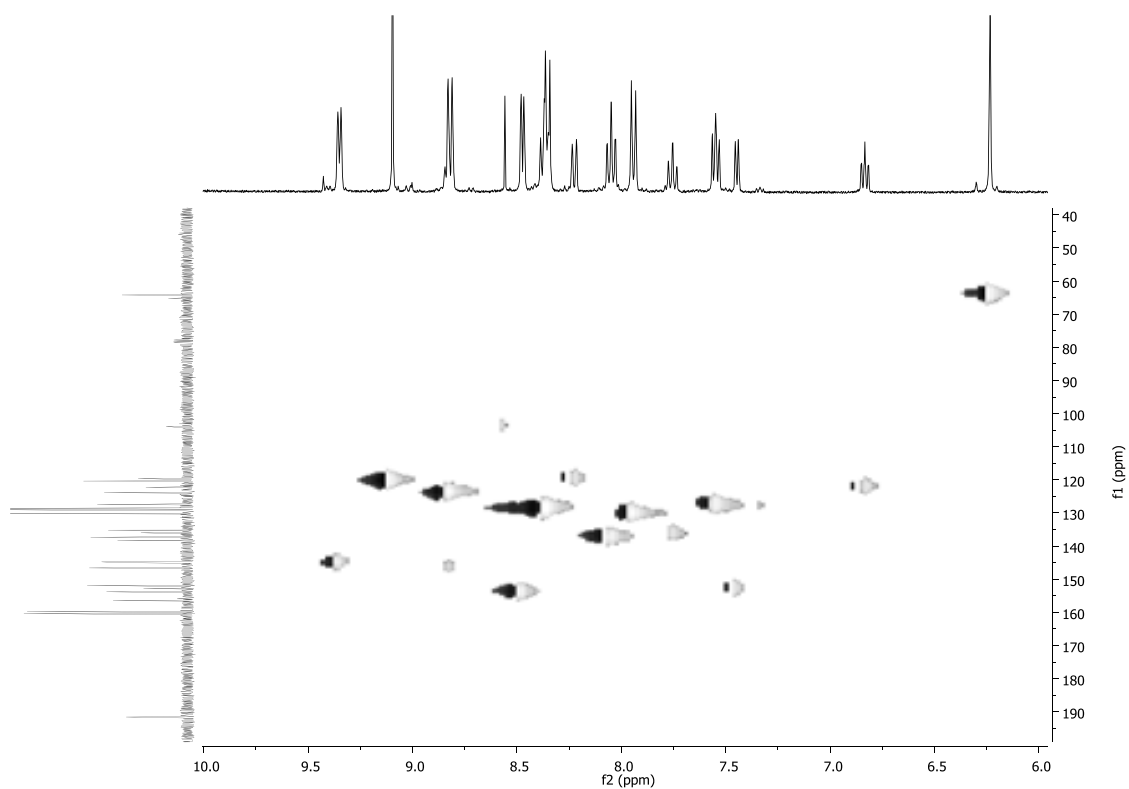
b)



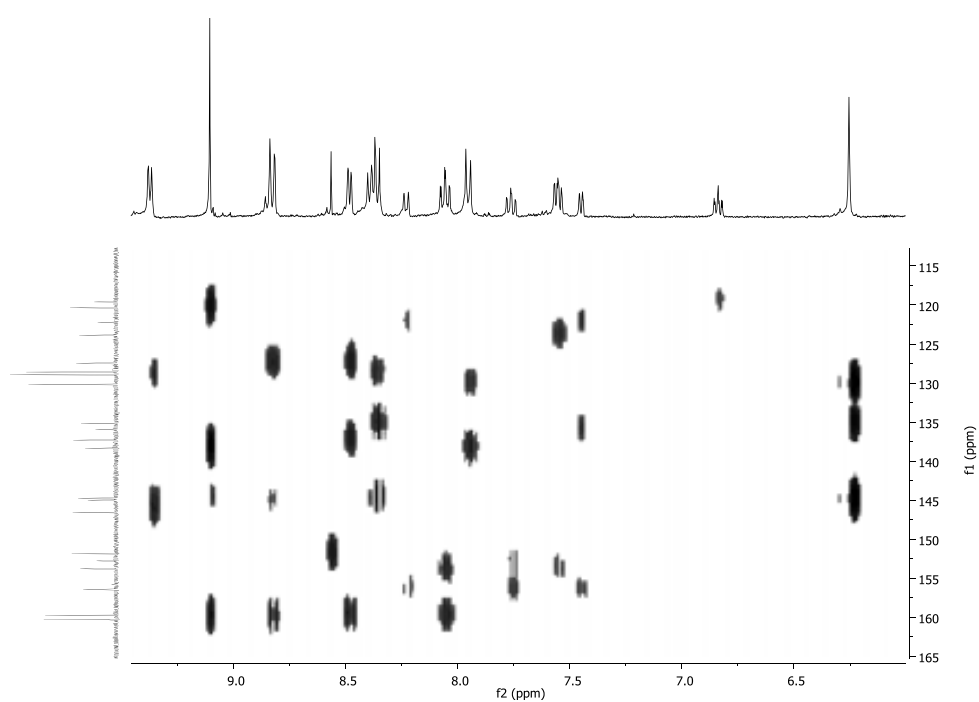
c)



d)



e)



III

Figure S4. Cyclic voltammetry for $[\text{Ru}^{\text{III}}\text{Cl}_3(\text{trpy})]$ in 0.1 M $n\text{-Bu}_4\text{NPF}_6$ in acetonitrile at 100 mV/s scan rate. Glassy carbon electrode is used as working electrode and the potential is measured vs. SSCE.

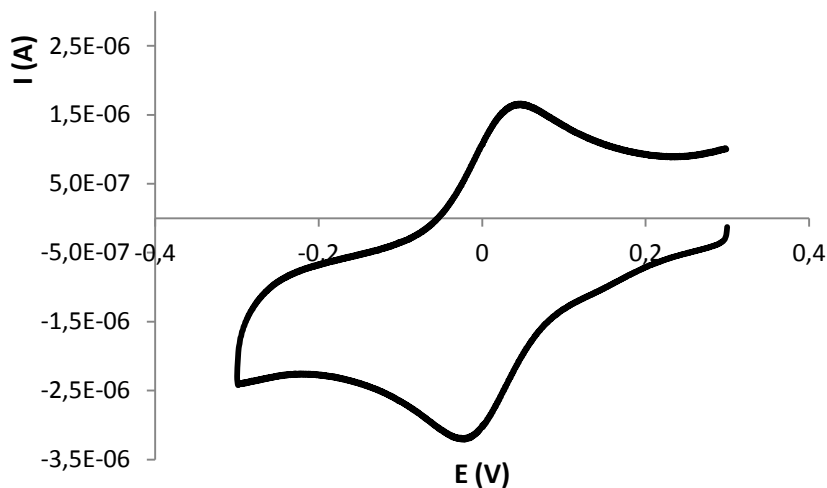


Figure S5. Cyclic voltammetry for complex 4^+ in 0.1 M $n\text{-Bu}_4\text{NPF}_6$ in acetonitrile at 100 mV/s scan rate. Glassy carbon electrode is used as working electrode and the potential is measured vs. SSCE.

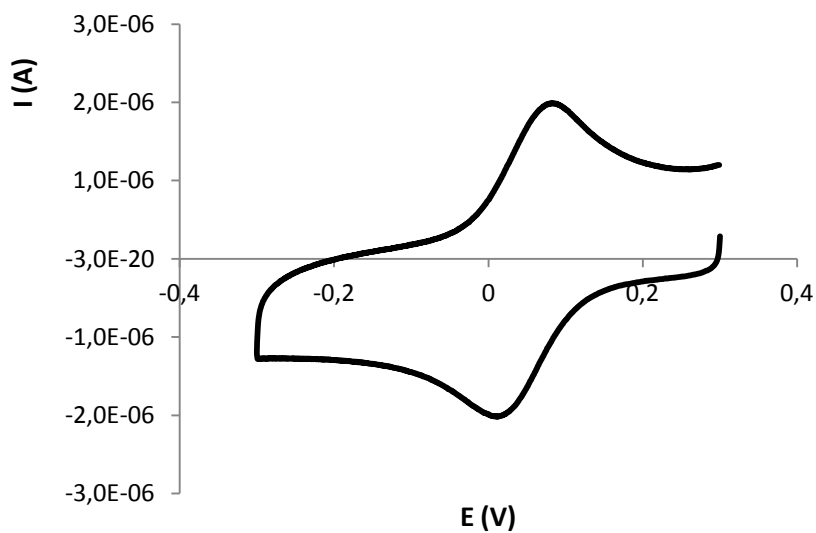


Figure S6. Cyclic voltammetry for complex 8^{5+} at pH = 1.0 in 0.1 M triflic acid aqueous solution. Glassy carbon electrode is used as working electrode and the potential is measured vs SSCE.

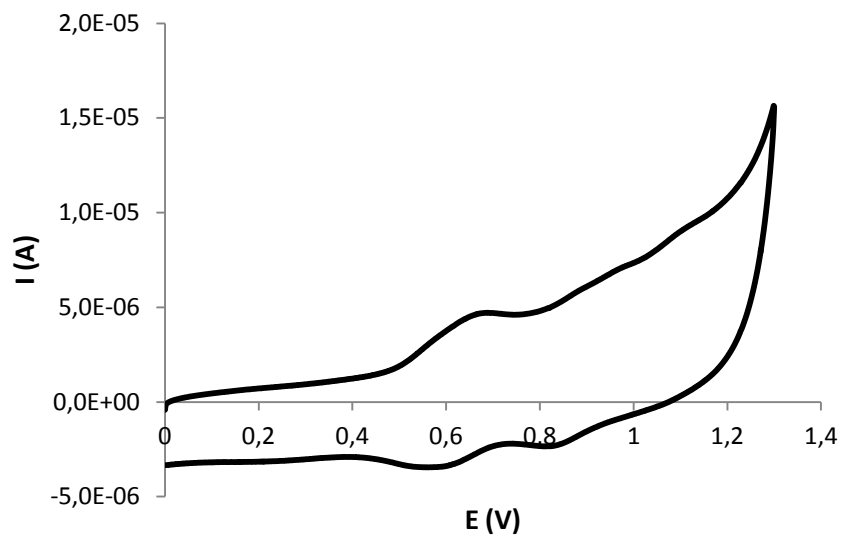


Figure S7. UV-Vis spectra for washer acetone for Silica- 7^{4+} .

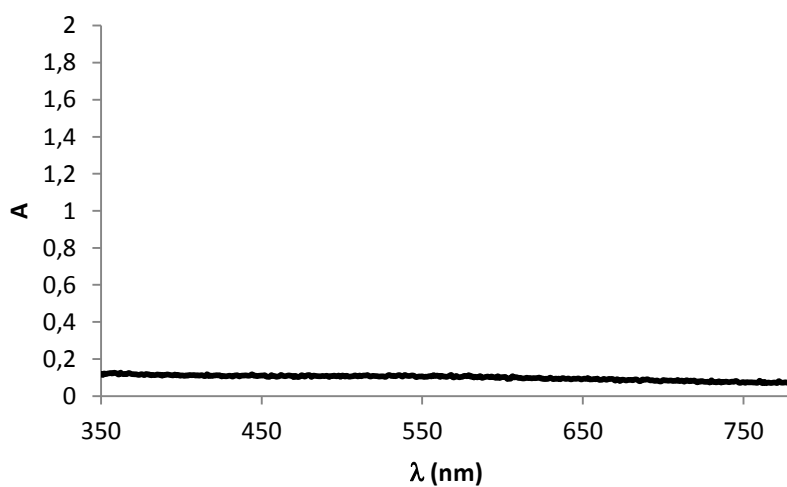


Figure S8. Experimental (right side) and theoretical zoom (left side) Mass Spectra for complex 4^+ .

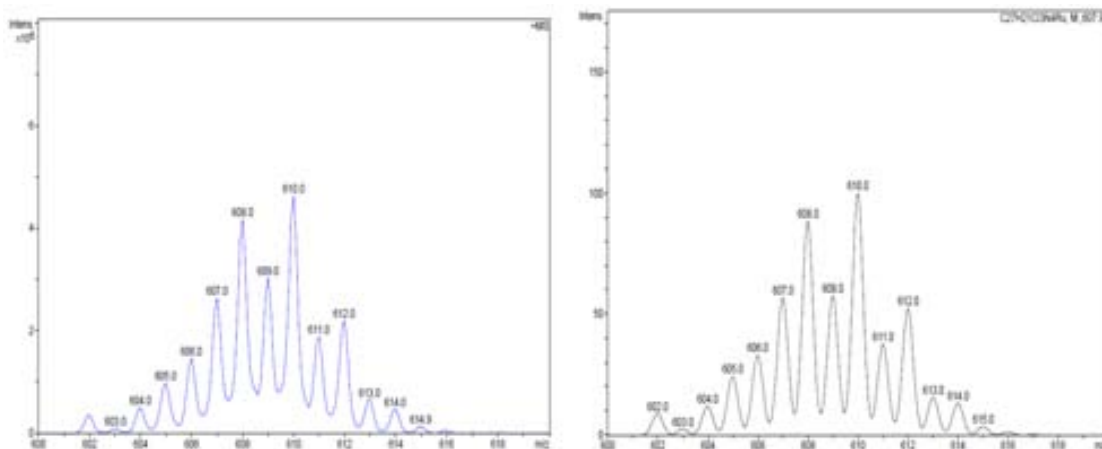


Figure S9. Mass Spectrum for complex 5^{4+}

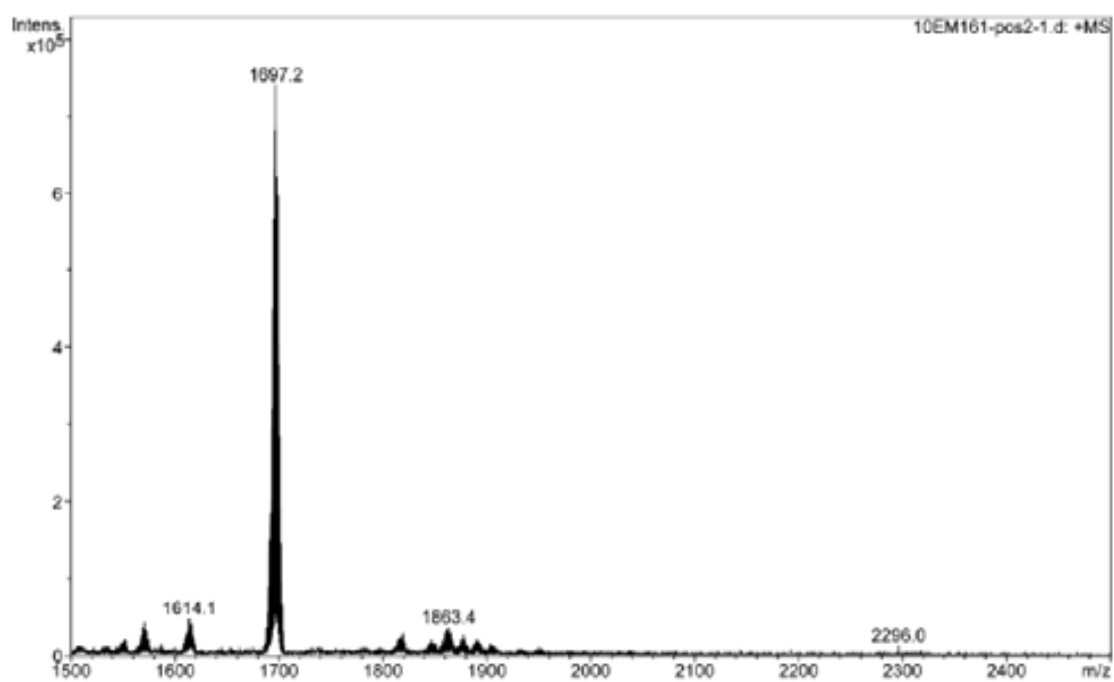


Figure S10. Experimental (right side) and theoretical zoom (left side) Mass Spectra for complex 5^{4+} .

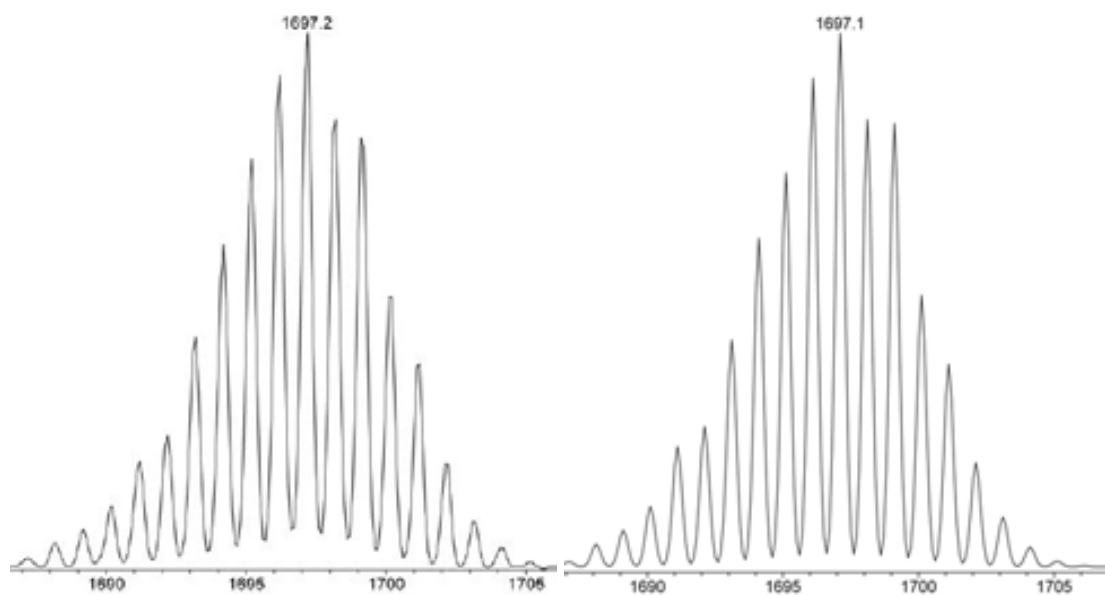
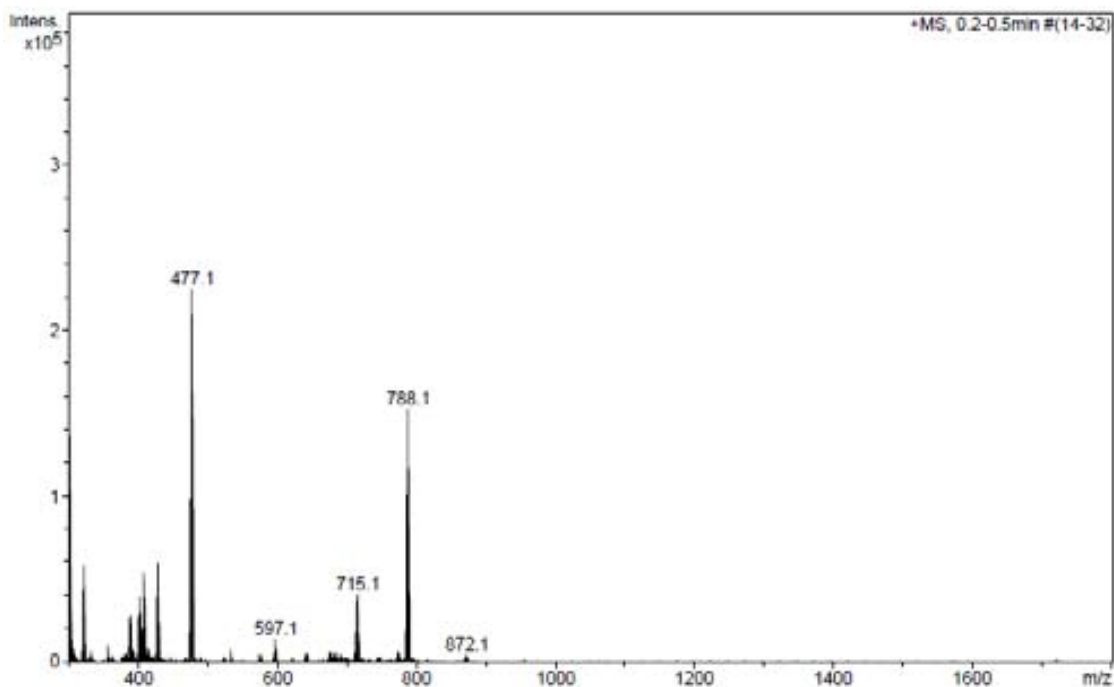


Figure S11. Mass Spectrum for complex 7^{4+}



III

Figure S12. Experimental (right side) and theoretical zoom (left side) Mass Spectra for complex 7^{4+} .

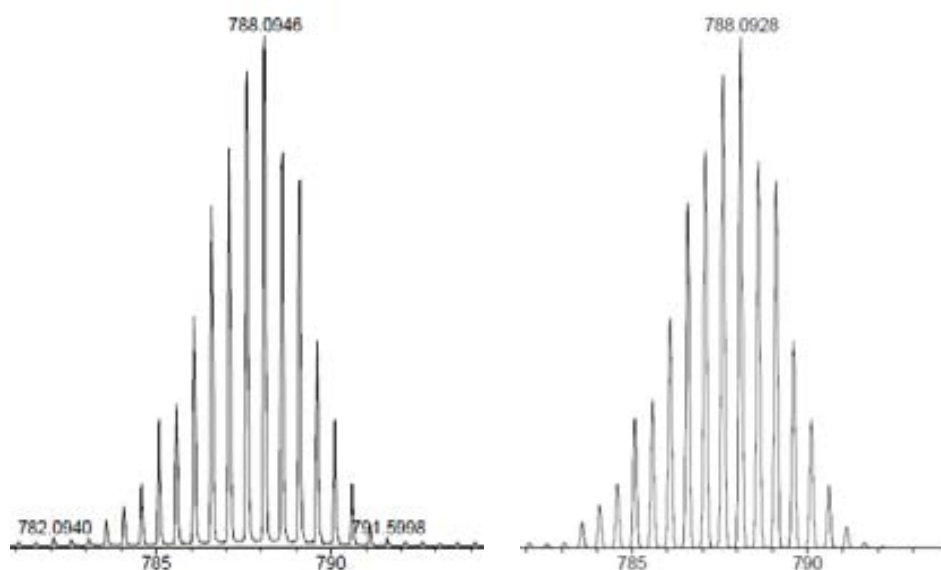


Table S1. Crystallographic data for complex 4^+

Empirical formula	C ₂₇ H ₂₂ Cl ₃ N ₆ O ₆ Ru	
Formula weight	733.93	
Temperature	100(2)K	
Wavelength	0.71073 Å	
Crystal system	Orthorhombic	
Space group	Pbca	
Unit cell dimensions	a = 19.3405(8) Å	$\alpha = 90.00^\circ$
	b = 11.3692(3) Å	$\beta = 90.00^\circ$
	c = 25.8709(8) Å	$\gamma = 90.00^\circ$
Volume	5688.6(3) Å ³	
Z	8	
Density (calculated)	1.714 Mg/m ³	
Absorption coefficient	0.887 mm ⁻¹	
F(000)	2952	
Crystal size	0.50 x 0.20 x 0.10 mm ³	
Theta range for data collection	1.89 to 33.07 °	
Index ranges	-18 ≤ h ≤ 29, -17 ≤ k ≤ 13, -21 ≤ l ≤ 36	
Reflections collected	26492	
Independent reflections	9571 [R(int) = 0.0552]	
Completeness to theta = 33.07 °	0.886 %	
Absorption correction	Empirical	
Max. and min. transmission	0.9165 and 0.6653	
Refinement method	Full-matrix least-squares on F ²	

Data / restraints / parameters	9571 / 0 / 388
Goodness-of-fit on F2	1.037
Final R indices [$I > 2\sigma(I)$]	R1 = 0.0433 , wR2 = 0.0905
R indices (all data)	R1 = 0.0752 , wR2 = 0.1038
Largest diff. peak and hole	0.924 and -0.593 e.Å ⁻³

Table S2. Crystallographic data for complex **5⁴⁺**

Empirical formula	C268 H204 Cl4 F96 N48 P16 Ru8	
Formula weight	7366.67	
Temperature	100(2)K	
Wavelength	0.71073 Å	
Crystal system	Monoclinic	
Space group	P2(1)/n	
Unit cell dimensions	a = 26.0256(14) Å b = 52.120(3) Å c = 28.8286(14) Å	$\alpha = 90.00^\circ$ $\beta = 91.920(2)^\circ$ $\gamma = 90.00^\circ$
Volume	39083(4) Å ³	
Z	4	
Density (calculated)	1.252 Mg/m ³	
Absorption coefficient	0.486 mm ⁻¹	
F(000)	14688	
Crystal size	0.35 x 0.15 x 0.15 mm ³	
Theta range for data collection	0.78 to 24.78 °	
Index ranges	-30 ≤ h ≤ 30 , -61 ≤ k ≤ 61 , -32 ≤ l ≤ 33	
Reflections collected	480821	
Independent reflections	65635 [R(int) = 0.1010]	
Completeness to theta = 24.78 °	0.977 %	
Absorption correction	Empirical	
Max. and min. transmission	0.9307 and 0.8483	
Refinement method	Full-matrix least-squares on F ²	
Data / restraints / parameters	65635 / 30 / 3961	
Goodness-of-fit on F ²	1.033	
Final R indices [$I > 2\sigma(I)$]	R1 = 0.0743 , wR2 = 0.1663	
R indices (all data)	R1 = 0.1179 , wR2 = 0.1816	
Largest diff. peak and hole	1.319 and -0.995 e.Å ⁻³	



Figure S13. Ortep plot (ellipsoid at 50 % probability) of the X-ray crystal structure of the cationic moiety of 5^{4+}

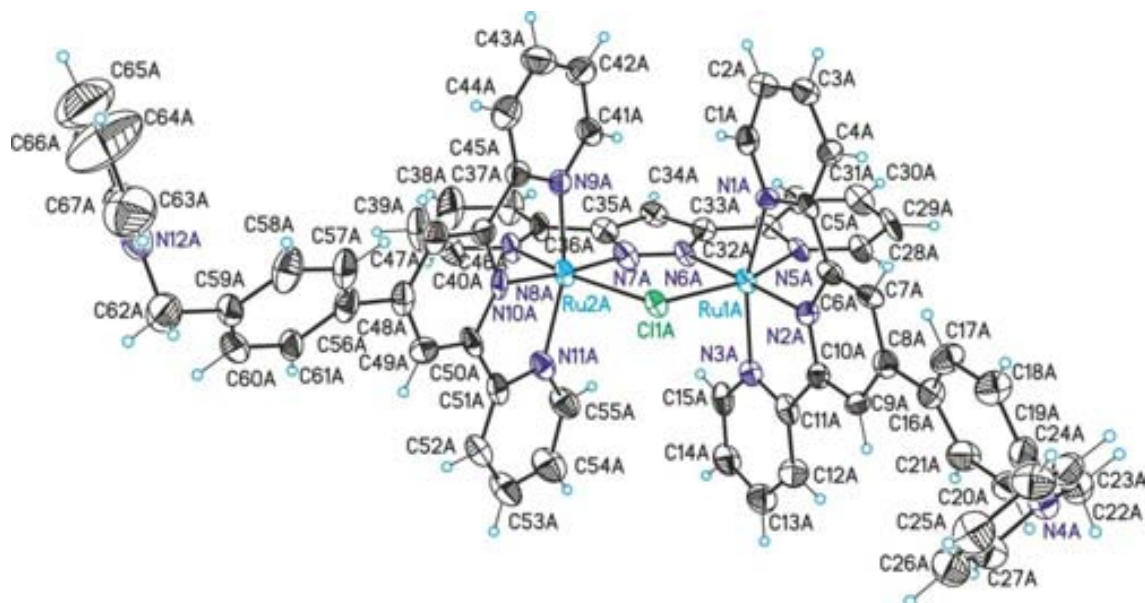


Figure S14. Chemical water oxidation with FTO-Nafion- 8^{5+} (1 mM) at pH =1.0 in 0.1M triflic acid solution in the presence of $(\text{NH}_4)_2\text{Ce}^{\text{IV}}(\text{NO}_3)_6$ (100 mM).

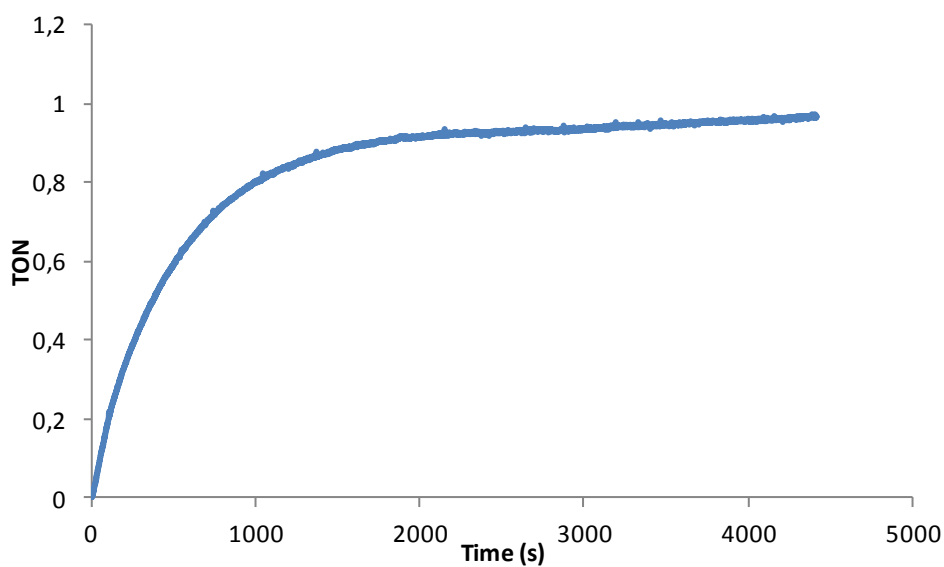
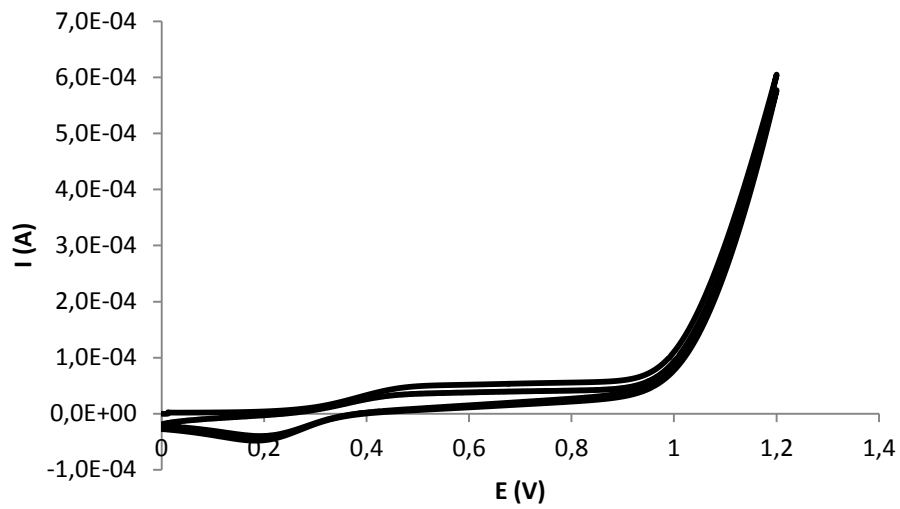


Figure S15. Cyclic voltammetry for FTO-TiO₂-5⁴⁺ before CPE at pH = 12 (NaOH 0.01 M in water). FTO used as working electrode and potential measured vs Ag/AgCl.



III

Figure 16 Cyclic voltammetry for FTO-TiO₂-5⁴⁺ after CPE at pH = 12 (NaOH 0.01 M in water). FTO used as working electrode and potential measured vs Ag/AgCl.

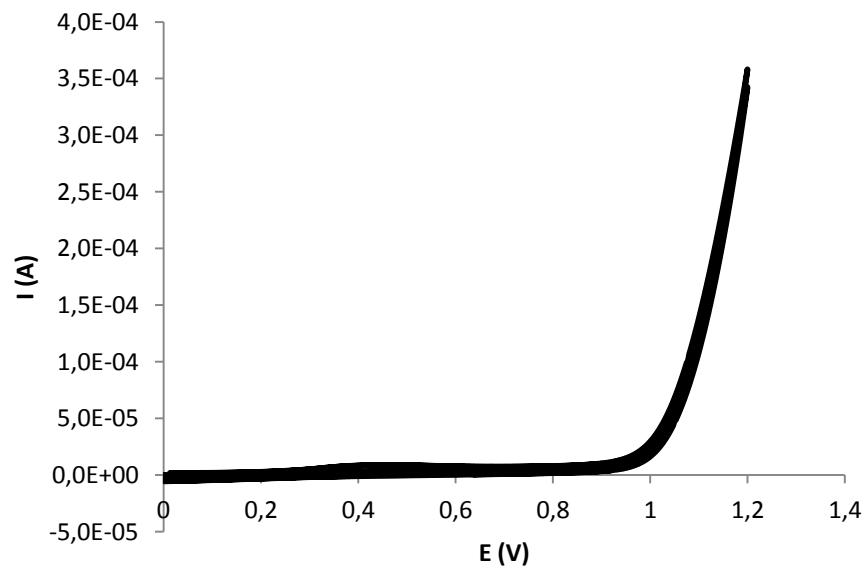


Figure S17. Controlled Potential Electrolysis for FTO-TiO₂-5⁴⁺. E = 1.1 V for 8h. FTO used as working electrode. Potential measured vs Ag/AgCl

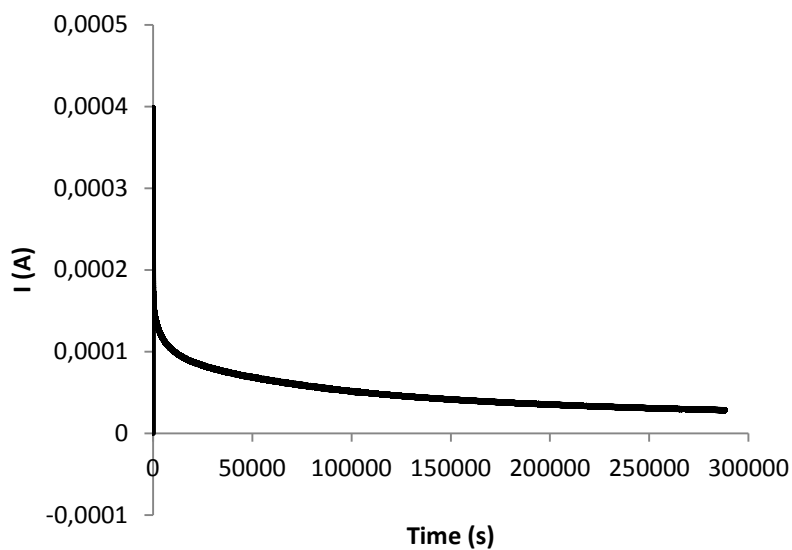


Figure S18. Clark electrode profile during the Controlled Potential Electrolysis for FTO-TiO₂-5⁴⁺. E = 1.1 V for 8h

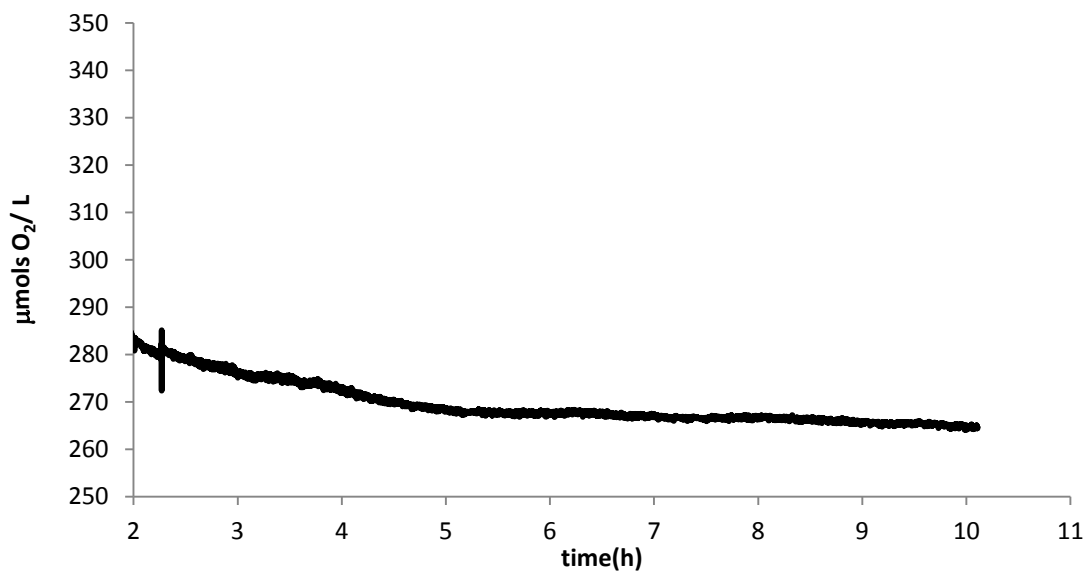


Figure S19. UV-vis spectra of the solution after CPE.

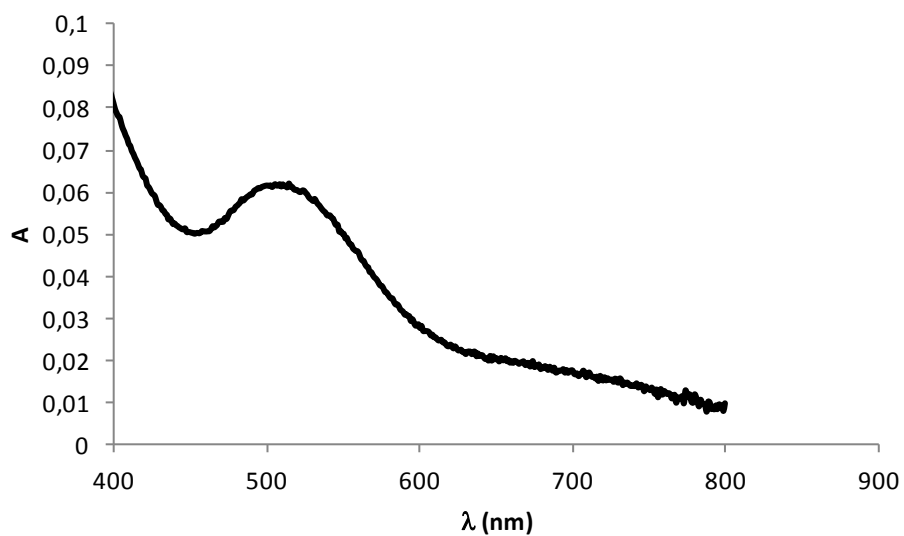
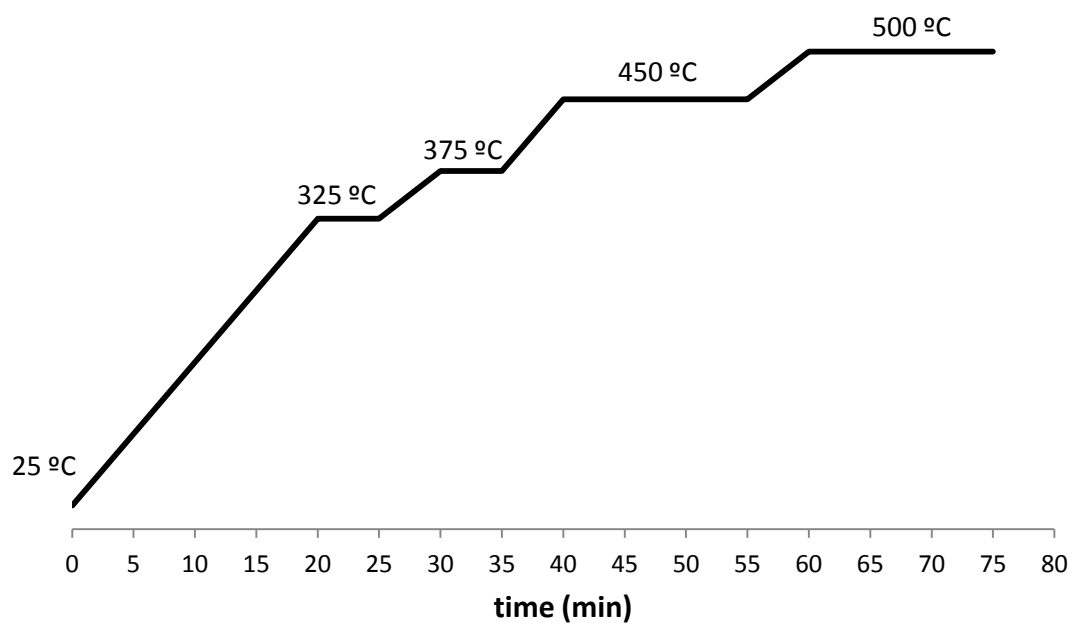
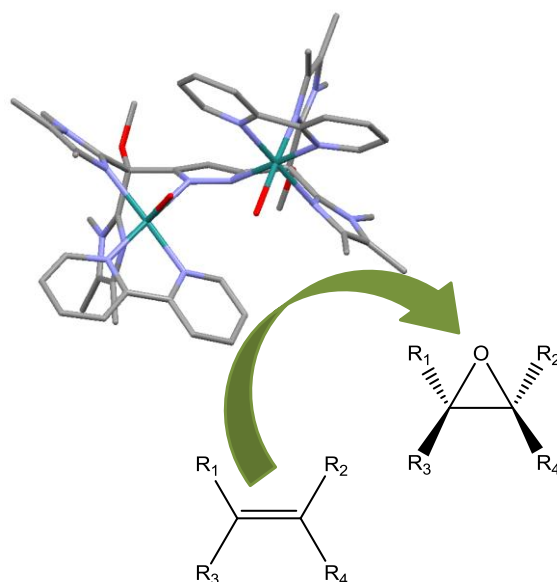


Figure S20. Temperature ramps for the calcination film process.



CHAPTER IV

Bis-facially Bridged Ru Dinuclear Complexes: Powerful Catalyst for the Epoxidation of Alkenes



In this chapter we report the synthesis and characterization of a novel diruthenium complex containing the bis-facial hexadentate bridging ligand Hbimp. Its reactivity towards the oxidation of water and olefins and the comparative discussion with the already reported family of related dinuclear complexes is reported herein.

TABLE OF CONTENTS

CHAPTER IV. *Bis-facially Bridged Ru Dinuclear Complexes: Powerful Catalyst for the Epoxidation of Alkenes*

- IV.1. Introduction
- IV.2. Results & Discussion
 - IV.2.1. Synthesis and characterization of **1**, **2(PF₆)₂** and **3³⁺**
 - IV.2.1.1. Electrochemistry
 - IV.2.1.2. UV-vis
 - IV.2.2. Water Oxidation Catalysis
 - IV.2.3. Epoxidation Catalysis
- IV.3. Conclusions
- IV.4. Experimental Section
- IV.5. References
- IV.6. Supporting Information

